

# Deep Neural Newsvendor

Jinhui Han

Rotman School of Management, University of Toronto, Toronto, Ontario, Canada M5S 3E6, jinhuizjcu@gmail.com

Ming Hu

Rotman School of Management, University of Toronto, Toronto, Ontario, Canada M5S 3E6, ming.hu@rotman.utoronto.ca

Guohao Shen

Department of Applied Mathematics, Hong Kong Polytechnic University, Hung Hom, Kowloon, Hong Kong, guohao.shen@polyu.edu.hk

We consider a data-driven newsvendor problem, where one has access to past demand data and the associated feature information. We solve the problem by estimating the target quantile function using a deep neural network (DNN). The remarkable representational power of DNN allows our framework to incorporate or approximate various extant data-driven models. We provide theoretical guarantees in terms of excess risk bounds for the DNN solution characterized by the network structure and sample size in a non-asymptotic manner, which justify the applicability of DNNs in the relevant contexts. Specifically, the convergence rate of the excess risk bound with respect to the sample size increases in the smoothness of the target quantile function but decreases in the dimension of feature variables. This rate can be further accelerated when the target function possesses a composite structure. In particular, our theoretical framework can be extended to accommodate the data-dependent scenarios, where the data-generating process could be time-dependent but not necessarily identical over time. Building on our theoretical results, we provide further managerial insights and practical guidance through simulation studies. Finally, we apply the DNN method to a real-world dataset obtained from a food supermarket. Our numerical experiments demonstrate that (1) the DNN method consistently outperforms other alternatives across a wide range of cost parameters, and (2) it exhibits good performance when the sample size is either very large or relatively limited.

---

## 1. Introduction

The newsvendor problem manages to find the optimal inventory level to serve random demand in balancing the overage or underage costs if the inventory is higher or lower than the realized demand. The accurate prediction of demand (distribution) is essential in newsvendor decision-making. In particular, the demand may be influenced by a variety of factors, such as customer demographics, seasonality, and general economic indexes. Thanks to the big data era, the availability of historical demand data and observations on associated features renders data-driven demand prediction viable and effective. Motivated by this viewpoint, we investigate the newsvendor problem in a data-driven context where the observed feature variables are deployed to better predict unknown demand.

Specifically, we propose to solve the data-driven newsvendor problem using a one-step, distribution-free, nonparametric deep neural network (DNN) method. In recent decades, DNN has

achieved tremendous success beyond the computer science community in various fields, such as medical science, engineering, and finance. However, its applications in the context of operations management (OM) are still relatively limited compared to its popularity in other areas, especially for exploring the theoretical properties that support its efficacy in solving OM problems (Feng and Shanthikumar 2018). In our setting, the inherent structure of the newsvendor problem allows us to express its solution as a conditional quantile function of demand-related features, which can be conveniently approximated by DNNs based on their remarkable representation power. In addition, the DNN method also enjoys the advantages of handling high-dimensional data over other alternatives such as the parametric two-step, estimate-then-optimize method.

Our data-driven inventory decision is made by feeding the observed feature information as inputs into a fitted DNN with the optimized inventory decision under the empirical risk minimization as an output, a process analogous to the high-dimensional quantile regression. For our nonparametric DNN model, we can properly design the network structure, such as the network depth and width, that essentially determines the model complexity and approximation power.

It is natural to ask whether the black-box DNN can produce the right solution we desire. We give a positive answer to this question by providing theoretical guarantees on bounding the excess risk of the DNN solution in terms of the network structure and sample size in a non-asymptotic manner. Here, the excess risk refers to the discrepancy in the expected newsvendor loss between any decision and the optimal one when knowing the demand distribution. In particular, we discover that the excess risk can be separated into two independent components. The first component is the *stochastic error* due to random realizations in the observed data, while the second one is the *approximation error* capturing the distance between the target quantile function and the function class represented by DNNs. If the given DNN can directly represent the target quantile function, then only the stochastic error is present, which encompasses parametric (piecewise) linear models as special cases. In such a situation, further increasing the network complexity is unnecessary, as doing so would only amplify the stochastic error bound. In general situations, the approximation error decreases with network complexity. Therefore, choosing appropriate network configurations to strike a balance between stochastic and approximation errors becomes crucial.

We analyze both the high-probability and expected excess risk bounds. Specifically, for the former, the stochastic error bound scales as  $1/\sqrt{n}$  up to a logarithm factor of the sample size  $n$ , and as  $\sqrt{\log(1/\delta)}$  for  $\delta$ , where  $1 - \delta$  denotes the probabilistic accuracy of the high-probability bound. After balancing between the stochastic and approximation errors, the excess risk scales as  $n^{-\frac{\beta}{2\beta+p}}$  for  $n$  and also as  $\sqrt{\log(1/\delta)}$  for  $\delta$ , where  $\beta$  measures the smoothness of the underlying target function and  $p$  is the dimension of feature variables. This implies that the convergence rate is faster when the target function is smoother or when the dimension of features is lower. More importantly,

we *explicitly* characterize the impact of each model parameter, such as the network width, depth, and cost parameters, on the risk bound. Building on this, practitioners can explore suitable network designs while gaining insight into how the properties of the target function influence the required sample size and network complexity. Detailed guidance on this is provided in Section 6. We further illustrate that the DNN method can achieve the minimax optimal rate in terms of the expected excess risk. This is done by showing that the excess risk can be bounded both from above and below by polynomial terms with identical orders in the sample size up to logarithmic factors. The obtained convergence rate of the expected excess risk bound is sharper than that of the high-probability bound due to technical reasons. Nevertheless, they are both state-of-the-art when respectively compared with the existing results (Ban and Rudin 2019, Schmidt-Hieber 2020). With the above results, we justify the applicability of DNNs in our data-driven newsvendor problem and anticipate that DNN models hold significant promise in addressing other OM problems.

On the technical side, we resort to the Lipschitz property of the Newsvendor loss function to decompose the excess risk into stochastic and approximation errors. The analysis of the stochastic error relies on empirical process theory (Anthony and Bartlett 1999, Bartlett et al. 2019), where concentration inequalities play a critical role in connecting the stochastic error to complexity measures of DNN function classes. We further exploit the results in Jiao et al. (2023) regarding approximation theory for DNNs to establish non-asymptotic error bounds. The lower bound for the expected excess risk can be established by formulating an equivalent multiple hypothesis testing problem and applying Fano’s inequality (Scarlett and Cevher 2019). In particular, by leveraging the new approximation theory developed in Jiao et al. (2023), all these bounds do not require special distributional conditions or network restrictions, differing themselves from those found in the literature (e.g., Schmidt-Hieber 2020).

We further consider two practically critical extensions that enhance our theoretical contributions and the applicability of our framework. First, we provide the excess risk bound of the DNN solution when the data is not independent and identically distributed (i.i.d.). This extension is relevant in practical applications as we usually deal with time series data where the feature information and past demand are collected over a certain timeline. Without any restriction on the underlying data-generating stochastic process, such as stationarity, we reveal that a similar excess risk bound as in the i.i.d. case still holds, with an additional term measuring the intrinsic discrepancy of the underlying data-generating process. As the data-generating process exhibits greater stationarity, this discrepancy diminishes, and the excess risk bound converges to the counterpart in the i.i.d. case. Our findings demonstrate that even for the weakly dependent and non-stationary data, the DNN method can still yield satisfactory results. This observation extends the existing results in the DNN theory.

Second, we explore the scenarios where the curse of dimensionality can be alleviated when using the DNN method. Notice that the convergence rate of the excess risk bound is inversely proportional to the dimension of feature variables  $p$ . When  $p$  is sufficiently large, the convergence can be extremely slow, requiring a substantial amount of data to obtain a good prediction. Nevertheless, we find that if the target function possesses a favorable composite structure, the convergence rate is affected by the intrinsic dimension of the composite function rather than the ambient dimension  $p$ . Specifically, when a generalized linear model is assumed for the target function, the intrinsic dimension is one, and we can establish an excess risk bound that scales as  $n^{-\frac{\beta}{2\beta+1}}$ , which is considerably faster than the original rate, particularly when  $p$  is large.

Related to our theoretical results, we conduct simulation studies to provide practical insights for implementation. A central argument of our theory is the need to carefully balance the stochastic and approximation errors with opposite behaviors with respect to network complexity, given a fixed amount of data. Echoing this, we observe that the excess risk does not decrease monotonically with either an increasing network depth or width; indeed, beyond a certain threshold, the excess risk turns to rise if we use a wider or deeper network. In addition, we find that a range of network configurations can achieve comparably good performance, which not only indicates the flexibility of the DNN method but also aligns with our theory regarding selecting proper network designs to attain risk minimization. In practice, we recommend starting with a sufficiently large network width and gradually increasing the depth through fine-tuning to find a good candidate network. Of course, the specific network design will depend on various factors such as the dimensionality and smoothness of the target function. We also examine the convergence of excess risk in the sample size, which is found to be polynomial with statistical significance. Consistent with our error analysis, the convergence rate is slower than that of the stochastic error of order 1, while the difference is attributed to the presence of the approximation error.

Finally, using a unique dataset from our collaborated food supermarket in China, we conduct a case study to assess the practical performance of the DNN method and compare it with several typical data-driven approaches in the literature. To address the possible concern that the DNN method may require massive data to produce a satisfactory result, we first apply it to a subset of the full dataset where the sample size is relatively small and the number of feature variables is also moderate. We then evaluate the DNN method’s performance on the complete dataset. Both sets of experiments yield consistent results, demonstrating that the DNN method outperforms other alternatives across a wide range of critical levels  $\rho$  (defined in (2)). For instance, when  $\rho = 0.65$ , the best alternative (kernel optimization) still incurs a newsvendor loss that is 11.94% greater than the DNN method. Furthermore, thanks to the well-established computational modules, such as *Adam* (Kingma and Ba 2014), the training and execution processes of DNNs are convenient.

## 2. Literature Review

Echoing the proposals put forth in [Feng and Shanthikumar \(2018, 2022\)](#), our work contributes to the advancement of the theory and practice of OM problems using state-of-the-art data-driven methods. In particular, this paper relates to three streams of the existing literature.

The first stream applies advanced machine learning techniques in OM. For example, [Oroojlooyjadid et al. \(2020\)](#) experiment using DNN algorithms to simultaneously optimize order quantities for a list of products based on features. [Qi et al. \(2023\)](#) propose a deep learning framework to address the multi-period inventory replenishment problem. [Gijsbrechts et al. \(2022\)](#) and [Oroojlooyjadid et al. \(2022\)](#) explore the application of deep reinforcement learning in solving inventory problems. [Ye et al. \(2023\)](#) combine deep learning and doubly robust estimation to conduct causal inference for large-scale experiments. [Chan et al. \(2022\)](#) employ a machine learning model to estimate objective values for out-of-sample clients based on in-sample data and solve real-world cycling infrastructure planning problems. More recently, [Gabel and Timoshenko \(2022\)](#) and [Aouad and Désir \(2022\)](#) have also incorporated neural networks into product choice modeling and assortment scheduling.

Of course, we are not among the first to embrace machine learning advances such as DNN in the OM community, but we exploit the special structure of the newsvendor problem to relate the optimization problem to the statistical quantile regression. To this end, we are able to establish theoretical guarantees that justify the DNN approach. Notably, we explicitly explain the impact of relevant parameters, such as network structures and the feature dimension, on the potential generalization error. Such detailed error analysis regarding complex neural networks is usually absent in this stream of literature, where it is typically limited to relatively simple parametric models. Moreover, we apply the DNN method on a unique real-world dataset and confirm its practical effectiveness and superiority over other alternative data-driven approaches, further complimenting previous empirical experiments as in [Oroojlooyjadid et al. \(2020\)](#).

Our work also closely relates to the second stream of literature on data-driven prescriptive analytics in inventory management. To name a few, [Levi et al. \(2007\)](#) describe a sampling-based method to reach an inventory decision that achieves near-optimal performance, while [Levi et al. \(2015\)](#) improve the analytical bounds therein. [Lin et al. \(2022\)](#) further relax their assumptions to prove upper bounds for the general and worse-case regrets. [Qi et al. \(2022\)](#) examine the conditional quantile prediction when the data is not identically distributed. [Zhang et al. \(2024\)](#) study a distributionally robust optimal policy that can generalize unseen feature values well. Other commonly used approaches in this field also include stochastic gradient descent algorithms and bandit controls, see, e.g., [Shi et al. \(2016\)](#), [Zhang et al. \(2018\)](#), [Simchi-Levi and Xu \(2022, 2023\)](#). In a general optimization framework beyond inventory management, [Bertsimas and Kallus \(2020\)](#) adopt a nonparametric method to approximate the underlying target distribution through a weighted

empirical distribution and then solve a conditional stochastic optimization problem. [Kallus and Mao \(2023\)](#) construct random forests based on a learning scheme to solve for the optimal decision and illustrate their effectiveness. [Bertsimas and Koduri \(2022\)](#) instead use the reproducing kernel Hilbert space to find the decision from covariates.

In this stream of literature, the closest work to ours is [Ban and Rudin \(2019\)](#), which solves a similar data-driven feature-based newsvendor problem using linear and kernel decision rules. Their linear policy, which is convenient to implement, accommodates both basic and nonlinearly transformed features, making it highly adaptable. Meanwhile, the developed kernel method, despite being nonlinear, offers an elegant solution that can be expressed analytically and solved efficiently via a simple ranking algorithm. The authors also provide finite-sample performance bounds for out-of-sample costs, depending on the dimensionality and sample size. In contrast, we employ a completely different DNN method to address the problem. Inspired by the seminal work of [Ban and Rudin \(2019\)](#), we establish non-asymptotic performance bounds for the excess risk, which accounts for the approximation error introduced when the target function lies outside the optimization function class. In addition to high-probability bounds, we verify that the derived rate is minimax optimal for the expected excess risk—an aspect not covered by [Ban and Rudin \(2019\)](#).

Our DNN solution also differs from the two-step predict(or estimate)-then-optimize method (see, e.g., [Hu et al. 2022](#), [Chen et al. 2022](#), [Perakis and Tsiourvas 2022](#)) in that the DNN model directly outputs the optimal decisions. In fact, as noticed in [Liyanage and Shanthikumar \(2005\)](#) and [Ban and Rudin \(2019\)](#), the two-step approach may lead to amplified errors if the first-step estimation model is misspecified. More recently, [Siegel and Wagner \(2021, 2023\)](#) identify the statistical estimation error for the expected profit in data-driven newsvendor models and explore how to correct it asymptotically. Nevertheless, the DNN method offers an additional advantage over other approaches by mitigating model misspecification errors through the use of a sufficiently large network. Moreover, the general optimization framework laid out in some previously mentioned papers, such as [Kallus and Mao \(2023\)](#) and [Chen et al. \(2022\)](#), is not specifically tailored to newsvendor analysis, which leaves much room for a more delicate treatment by exploiting the newsvendor problem’s special structure. Our theoretical and empirical results complement those related papers in this regard.

Third, our paper contributes to statistical learning and high-dimensional quantile regression theories regarding DNNs. On the one hand, DNNs are typical statistical learning vehicles that study how to summarize and generalize useful information from empirical processes ([Anthony and Bartlett 1999](#), [Mohri et al. 2018](#), [Bartlett et al. 2019](#)). On the other hand, due to the similarity in the loss function between the newsvendor problem and quantile regression, our work also contributes to the studies in the latter using DNNs. Recently, there have been many relevant papers dedicated

to establishing generalization bounds for DNNs in the context of least square or quantile regression (e.g., Schmidt-Hieber 2020, Farrell et al. 2021, Padilla et al. 2022). Compared to these papers, we explicitly characterize the prefactor of excess risk bounds as a polynomial function of the dimensionality  $p$ , significantly improving upon the extant results with an exponential prefactor. We also do not require the related restrictions on the network structure, such as the parameters should be bounded by a prescribed constant and the whole network has to be sparse in a certain level (Schmidt-Hieber 2020, Padilla et al. 2022). Finally, our paper also differs from Jiao et al. (2023) and Shen et al. (2021) in that we focus primarily on high-probability and expectation bounds with fast convergence rates corresponding to the newsvendor loss using different techniques. Specifically, Jiao et al. (2023) examine the deep least square regression problem, where the square loss function benefits from the variance-bounding trick, linking the variance of the loss difference to its expectation. However, this approach does not directly apply to the newsvendor loss, requiring us to use conditional expectations to derive new generalization bounds for the empirical process (see Theorem OA.3). Shen et al. (2021) investigate a relevant quantile regression problem, but their primary technical contribution lies in dealing with possibly unbounded response variables through truncation techniques, where the final rate depends on moment conditions. In contrast to both papers, we further validate that the obtained rate for the expected excess risk bound is indeed minimax optimal, using Fano’s inequality (Scarlett and Cevher 2019). While those two papers focus on dimensionality challenges of DNN estimation with i.i.d. data, we are mainly interested in newsvendor-related issues, such as comparisons with the classical SAA or linear models, handling dependent data, and providing practical guidance alongside real-world applications.

### 3. Deep Neural Newsvendor with Feature Data

#### 3.1. Feature-Based Newsvendor Problem

We consider a data-driven newsvendor problem where the firm needs to decide the inventory level of perishable goods to serve future random demand. Specifically, the demand distribution is unknown to the firm, but the historical demand realizations  $\mathbf{d}(n) = (d_1, d_2, \dots, d_n)^\top$  are accessible. Throughout the paper, we denote vectors or matrices using bold symbols. Besides the demand data, we assume that the firm is also able to collect feature data  $\mathbf{x}(n) = (\mathbf{x}_1, \mathbf{x}_2, \dots, \mathbf{x}_n)^\top$  consisting of observable (and not necessarily independent) features along with each demand realization. These features may include, among others, macroeconomic data such as GDP and CPI, weather conditions, and even location details (Ban and Rudin 2019). In practice, it is reasonable to imagine that the demand is influenced by various factors, and we are interested in using these factors to predict the demand. In this paper, we assume that the features have already been carefully and properly selected based on their significant relevance to the demand, and their data are available prior to decision-making. The variable selection problem falls beyond the scope of the current study.

Let  $D \in \mathbb{R}$  and  $\mathbf{X} \in \mathbb{R}^p$  denote the random demand and feature vector, respectively. The classical newsvendor problem aims to solve for the optimal ordering quantity that minimizes the expected newsvendor cost loss expressed as

$$C(q) := \mathbb{E}_D[b(D - q)^+ + h(q - D)^+], \quad (1)$$

where the expectation  $\mathbb{E}_D$  is taken with respect to  $D$ ,  $q$  is the inventory decision,  $b$  (resp.,  $h$ ) represents the unit underage (resp., overage) cost for the unsatisfied demand (resp., unsold inventory). Let  $F(\cdot)$  denote the cumulative distribution function (CDF) of the random demand  $D$ . In an oracle case with full information of  $F(\cdot)$ , the optimal quantity is then

$$q^* = \inf\{q \geq 0 : F(q) \geq \rho\}, \quad \text{where } \rho := \frac{b}{b+h}. \quad (2)$$

Obviously, the above oracle newsvendor solution cannot be directly obtained in practice since we do not know  $F(\cdot)$  in advance. Data-driven methods then come into play by using the empirical distribution of random samples to estimate the unknown  $F(\cdot)$ , and a typical example is the celebrated SAA approach (see Shapiro et al. 2021 for more details).

Alternatively, the feature-based newsvendor problem aims to find an optimal measurable mapping  $f^* : \mathbb{R}^p \rightarrow \mathbb{R}$  such that, based on the observed features  $\mathbf{X} = \mathbf{x}$ , the optimal inventory decision is determined accordingly by  $f^*(\mathbf{x})$ . In other words,

$$f^* := \arg \min_f \mathbb{E}_{D, \mathbf{X}}[b(D - f(\mathbf{X}))^+ + h(f(\mathbf{X}) - D)^+],$$

where the expectation  $\mathbb{E}_{D, \mathbf{X}}$  is taken with respect to the joint distribution of  $D$  and  $\mathbf{X}$ . Equivalently, for any given  $\mathbf{X} = \mathbf{x}$ , the optimal decision can be established with respect to the conditional distribution  $D|\mathbf{X}$  as follows

$$f^*(\mathbf{x}) := \arg \min_{f(\mathbf{x}): f \text{ measurable}} \mathbb{E}_{D|\mathbf{X}}[b(D - f(\mathbf{X}))^+ + h(f(\mathbf{X}) - D)^+ | \mathbf{X} = \mathbf{x}]. \quad (3)$$

Similar to (2), the oracle solution to (3), when knowing the joint distribution of  $\mathbf{Z} := (\mathbf{X}, D)$ , is exactly the conditional quantile function given by

$$f_\rho(\mathbf{x}) := \inf\{q \geq 0 : F(q|\mathbf{X} = \mathbf{x}) \geq \rho\}, \quad (4)$$

where  $F(\cdot|\mathbf{x})$  is the conditional CDF of  $D$  given  $\mathbf{X} = \mathbf{x}$ .

With only finite random samples  $\mathbf{S}_n = \{(\mathbf{x}_i, d_i)\}_{i=1}^n$  from the joint distribution  $\mathbf{Z}$  in hand, we then consider the data-driven, feature-based newsvendor problem by minimizing the empirical risk  $\mathcal{R}_n^\rho(\cdot)$  to obtain the empirical risk minimizer (ERM)  $\hat{f}_n$  by:

$$\hat{f}_n \in \arg \min_{f \in \mathcal{F}_n} \mathcal{R}_n^\rho(f) := \arg \min_{f \in \mathcal{F}_n} \frac{1}{n} \sum_{i=1}^n \left[ b(d_i - f(\mathbf{x}_i))^+ + h(f(\mathbf{x}_i) - d_i)^+ \right], \quad (5)$$



where  $\mathcal{F}_n$  is a suitable function class, which may depend on the sample size  $n$ . In this paper, we choose  $\mathcal{F}_n$  to be a class of functions represented by DNNs. In addition to exploring the practical performance of DNNs for our problem, we are particularly interested in establishing theoretical guarantees so that the DNN tool does not simply work as a black box. Our nonparametric DNN solution integrates the forecasting and optimization steps into one, unlike the separated estimation and optimization (SEO) approach. Moreover, we do not require prior knowledge or assumptions about the underlying demand distribution.

### 3.2. Newsvendor Solution Using DNNs

Typical multi-layer perceptrons (MLPs), the commonly used feedforward neural networks, consist of several key components: the number of layers that decides the neural network’s depth, the number of neurons in each layer that determines the network width, the connections between neurons specifying how data is processed through the network, and the activation functions in each neuron that introduce nonlinearity. Figure 1 illustrates the architecture of a two-hidden-layer network that maps the input  $(x_1, x_2)$  to the output  $y$ .

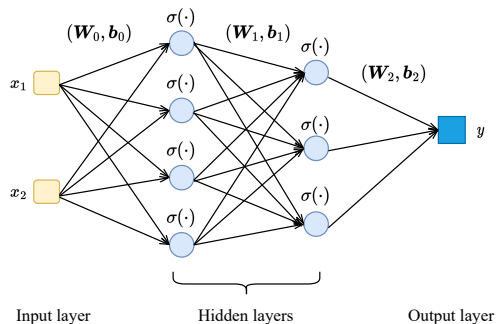


Figure 1 An illustrative fully connected feedforward neural network with two hidden layers.

Mathematically, we can also represent the MLP architecture in terms of the composition of a series of functions as follows:

$$f(\mathbf{x}; \mathbf{W}, \mathbf{b}) = \mathcal{L}_{\mathcal{D}} \circ \sigma \circ \mathcal{L}_{\mathcal{D}-1} \circ \sigma \circ \cdots \circ \sigma \circ \mathcal{L}_1 \circ \sigma \circ \mathcal{L}_0(\mathbf{x}), \quad \mathbf{x} \in \mathbb{R}^p, \quad (6)$$

where  $\mathcal{D}$  is the number of hidden layers. Throughout the paper, we consider the standard component-wise rectified linear unit (ReLU) activation function  $\sigma(x) = \max\{0, x\}$  and  $\mathcal{L}_i(\mathbf{x}) = \mathbf{W}_i \mathbf{x} + \mathbf{b}_i$ , for  $i = 0, 1, \dots, \mathcal{D}$ , in which  $\mathbf{W}_i \in \mathbb{R}^{w_{i+1} \times w_i}$ ,  $\mathbf{b}_i \in \mathbb{R}^{w_{i+1}}$ , and  $w_i$  is the number of neurons (width) of the  $i$ -th layer. Consider the network shown in Figure 1 as an example. The input  $(x_1, x_2)$  first undergoes a linear transformation with weights  $\mathbf{W}_0$  and bias  $\mathbf{b}_0$ , resulting in a 4-dimensional vector. The ReLU activation function is then applied component-wise in the first hidden layer. This

process is repeated for the subsequent hidden layer. Finally, the output  $y$  is obtained by linearly combining the activated values from the last hidden layer with weights  $\mathbf{W}_2$  and bias  $\mathbf{b}_2$ .

For a given neural network, its width, denoted by  $\mathcal{W}$ , is defined as the maximum number of neurons in any hidden layer, i.e.,  $\mathcal{W} := \max\{w_1, \dots, w_{\mathcal{D}}\}$ ; its depth  $\mathcal{D}$  refers to the number of hidden layers; its size  $\mathcal{S}$  is the total number of parameters (weights and biases) involved, given by  $\mathcal{S} := \sum_{i=0}^{\mathcal{D}} w_{i+1}(w_i + 1)$ ; and the number of neurons, denoted by  $\mathcal{U}$ , counts the neurons across all hidden layers, i.e.,  $\mathcal{U} := \sum_{i=1}^{\mathcal{D}} w_i$ . We then define the optimization function class  $\mathcal{F}_n$  as  $\mathcal{F}_{\mathcal{D}, \mathcal{W}, \mathcal{U}, \mathcal{S}, \mathcal{B}}$ , which represents a class of feedforward neural network mappings  $f_\phi: \mathbb{R}^p \rightarrow \mathbb{R}$ , parameterized by  $\phi$ , with the depth  $\mathcal{D}$ , width  $\mathcal{W}$ , size  $\mathcal{S}$ , and number of neurons  $\mathcal{U}$ , such that  $f_\phi$  satisfies  $\|f_\phi\|_\infty \leq \mathcal{B}$  for some positive constant  $\mathcal{B}$ , where  $\|\cdot\|_\infty$  denotes the sup-norm. Notably, we do not require all layers to have the same width, as imposed in [Chen et al. \(2022\)](#), nor do we need to stipulate that the network is sparse or that the parameters are uniformly bounded by 1 (see, e.g., [Schmidt-Hieber 2020](#), [Padilla et al. 2022](#)). In what follows, we write  $\mathcal{F}_{\mathcal{D}, \mathcal{W}, \mathcal{U}, \mathcal{S}, \mathcal{B}}$  as  $\mathcal{F}_{DNN}$  for brevity. Additionally, we define a DNN as any neural network with  $\mathcal{D} \geq 1$  hidden layers.

Due to the special structure of ReLU networks in (6), their outputs are piecewise linear functions. Although alternative activation functions, such as Sigmoid and Tanh, are available, ReLU networks enjoy advantages in terms of mathematical simplicity with nice theoretical properties, such as the universal approximation property ([Hornik 1991](#)). Within the context of the considered newsvendor problem, we can further demonstrate that ReLU networks attain the minimax optimal convergence rate with respect to the sample size (see [Theorems 3 and 4](#)). This result is achieved because the newsvendor loss is both Lipschitz continuous and convex in the inventory decision, and the optimal decision amounts to estimating a specific quantile of a conditional demand distribution. Meanwhile, they have gained wide popularity in deep learning applications due to their computational efficiency, ease of training, and strong generalization performance (see, e.g., [Nair and Hinton 2010](#), [Krizhevsky et al. 2012](#)). This success can be attributed, in part, to practical factors such as effective initialization strategies ([Glorot and Bengio 2010](#), [He et al. 2015](#)), which help mitigate issues like vanishing or exploding gradients in deep architectures. Given their theoretical strengths and empirical effectiveness, we focus on ReLU networks as our optimization function space.

Our feature-based, data-driven deep neural newsvendor problem aims to find a measurable function  $\hat{f}_{DNN} \in \mathcal{F}_{DNN}$  such that

$$\hat{f}_{DNN} := \arg \min_{f \in \mathcal{F}_{DNN}} \mathcal{R}_n^\rho(f), \quad (7)$$

where  $\mathcal{R}_n^\rho(f)$  is the empirical newsvendor risk defined in (5). To evaluate the theoretical performance of the deep neural newsvendor solution, we employ the oracle solution  $f_\rho$  in (4) as a

benchmark and quantify the *excess risk* bounds in terms of the sample size and network parameters in the next section. Specifically, the *excess risk* is defined as the difference in the expected newsvendor loss between  $\hat{f}_{DNN}$  and  $f_\rho$  based on the joint distribution of  $\mathbf{Z} = (\mathbf{X}, D)$ , i.e.,

$$\mathcal{R}^\rho(\hat{f}_{DNN}) - \mathcal{R}^\rho(f_\rho) := \mathbb{E}_{\mathbf{Z}}[b(D - \hat{f}_{DNN}(\mathbf{X}))^+ + h(\hat{f}_{DNN}(\mathbf{X}) - D)^+] - \mathbb{E}_{\mathbf{Z}}[b(D - f_\rho(\mathbf{X}))^+ + h(f_\rho(\mathbf{X}) - D)^+].$$

We notice that the excess risk remains a random variable, contingent upon the random samples  $\mathbf{S}_n$  and through the fitting of  $\hat{f}_{DNN}$ .

## 4. Theoretical Guarantees: Non-Asymptotic Excess Risk Bounds

Machine learning methods using neural networks are often perceived as black boxes, where outputs are produced by feeding covariates into trained networks. They have demonstrated remarkable practical performance in various tasks, e.g., image classification (Krizhevsky et al. 2012, He et al. 2015), game intelligence (Silver et al. 2016), and speech recognition (Hinton et al. 2012), given that the data amount is “adequate.” Despite these successes, several questions naturally arise: How does the performance improve as more data is available? How does the network structure, such as the network depth and width, influence prediction accuracy? Most importantly, can DNNs solve the target problem with theoretical guarantees rather than relying solely on trial and error? In this section, we address these questions in the context of the data-driven newsvendor problem by examining the theoretical non-asymptotic excess risk bounds for DNN solutions in terms of the sample size and network structure.

### 4.1. High-Probability Bound for Excess Risk

In general, the excess risk arises from two different sources: the *stochastic error*, resulting from the random realizations of observed data, and the *approximation error*, caused by the inability of the DNN with a given network structure to exactly represent the target quantile function. The former risk is inherent in data-driven problems since we aim to apply the learned decision rule from finite observed data to any future random realization. The latter one emerges when seeking the optimal rule within a prescribed set  $\mathcal{F}_{DNN}$ , rather than the general function space. However, it is expected that with more complex network structures, DNNs can represent a broader class of functions, reducing this error to a negligible level. We formally state these intuitions in the following lemma.

LEMMA 1. *The excess risk of the ERM  $\hat{f}_{DNN}$  satisfies*

$$\mathcal{R}^\rho(\hat{f}_{DNN}) - \mathcal{R}^\rho(f_\rho) \leq 2 \underbrace{\sup_{f \in \mathcal{F}_{DNN}} |\mathcal{R}^\rho(f) - \mathcal{R}_n^\rho(f)|}_{\text{stochastic error}} + \underbrace{\inf_{f \in \mathcal{F}_{DNN}} \{\mathcal{R}^\rho(f) - \mathcal{R}^\rho(f_\rho)\}}_{\text{approximation error}}.$$

As elucidated in Sections 4.1.1 and 4.1.2, on the one hand, a more complex network can result in a smaller approximation error because of the growing representation power; on the other hand, it will amplify the stochastic error due to the increased number of model parameters needing to be estimated. We first separately analyze each error and then strike a balance between them to achieve an optimal error rate with respect to the sample size.

**4.1.1. Stochastic Error: When the Fixed DNN Can Represent  $f_\rho$ .** According to Lemma 1, if the given DNN can represent  $f_\rho$ , i.e.,  $f_\rho \in \mathcal{F}_{DNN}$ , the approximation error term vanishes, and only the stochastic error remains when using this given DNN to solve for the newsvendor decision. However, it is important to note that this scenario is an ideal one, and we typically do not know the exact form of the underlying conditional quantile function  $f_\rho$  or whether it belongs to the representation class of a certain DNN. Nevertheless, we will address the general case later in Theorem 2, knowing only the target function's smoothness rather than its specific functional form.

We make the following assumption regarding the underlying distributions.

**ASSUMPTION 1.** *The random demand  $D$  has a bounded compact support, which is assumed to be  $[0, \bar{D}]$  for some  $\bar{D} > 0$  without loss of generality.*

Assumption 1 is very mild and reasonable since the demand data should be finite in values in practice. We can derive a stochastic error bound based on this assumption.

**THEOREM 1 (STOCHASTIC ERROR BOUND).** *Under Assumption 1, for any  $\delta \in (0, 1)$  and  $n \geq C \cdot \mathcal{SD} \log(\mathcal{S})$  with a large enough  $C > 0$ , with probability at least  $1 - \delta$  over the random draw of  $\mathbf{S}_n = \{(\mathbf{x}_i, d_i)\}_{i=1}^n$ , where  $(\mathbf{x}_i, d_i)$  are i.i.d. samples from the unknown joint distribution  $(\mathbf{X}, D)$ , we have*

$$\sup_{f \in \mathcal{F}_{DNN}} |\mathcal{R}^\rho(f) - \mathcal{R}_n^\rho(f)| \leq \sqrt{2}(b\bar{D} + h\mathcal{B}) \left( C_1 \sqrt{\frac{\mathcal{SD} \log(\mathcal{S}) \log(n)}{n}} + \sqrt{\frac{\log(1/\delta)}{n}} \right),$$

where  $C_1 > 0$  is an independent universal constant.

Theorem 1 is established using empirical process theory (Anthony and Bartlett 1999, Bartlett et al. 2019), and the error bound does not require restrictions on the DNN structure. As a direct consequence of Lemma 1, we obtain the excess risk bound under the assumption that  $f_\rho \in \mathcal{F}_{DNN}$ .

**COROLLARY 1.** *If  $f_\rho \in \mathcal{F}_{DNN}$ , under conditions of Theorem 1, with probability at least  $1 - \delta$  over the random draw of  $\mathbf{S}_n$ ,*

$$\mathcal{R}^\rho(\hat{f}_{DNN}) - \mathcal{R}^\rho(f_\rho) \leq 2\sqrt{2}(b\bar{D} + h\mathcal{B}) \left( C_1 \sqrt{\frac{\mathcal{SD} \log(\mathcal{S}) \log(n)}{n}} + \sqrt{\frac{\log(1/\delta)}{n}} \right).$$

When  $f_\rho \in \mathcal{F}_{DNN}$ , Theorem 1, and in particular, Corollary 1, describe the additional cost of the in-sample learned inventory policy for the out-of-sample newsvendor problem compared to the optimal oracle solution. It is reasonable to imagine that with more collected samples, the DNN can better learn the underlying distributional structure so that its performance gets better. Specifically, we notice that with a fixed DNN and given cost parameters  $b$  and  $h$ , the stochastic error (excess risk) scales in the order of  $O(\sqrt{\log(n)/n})$ . Meanwhile, the stochastic error bound increases with the network complexity. In other words, if the target function can be exactly represented by a fixed neural network (e.g., assuming it is linear as in Example 1), there is no need for a more complex and redundant configuration with additional width or depth. Of course, this assumption is not guaranteed in practice (hence referred to as the ideal case), but we will get rid of this impractical condition for the general case in the next subsection.

**EXAMPLE 1 (LINEAR DEMAND MODEL).** We consider the linear demand model with random errors  $D|\mathbf{X}=\mathbf{x}=\alpha+\boldsymbol{\beta}^\top\mathbf{x}+\epsilon$ , where  $\alpha\in\mathbb{R},\boldsymbol{\beta}\in\mathbb{R}^p$ , and  $\epsilon\sim F_\epsilon$  is independent of the random feature vector  $\mathbf{X}$ , with its  $\rho$ -th quantile being zero. Therefore, the conditional  $\rho$ -th quantile function is given by  $f_\rho(\mathbf{x})=\alpha+\boldsymbol{\beta}^\top\mathbf{x}$ , which implies that the optimal oracle inventory policy is simply a linear combination of the feature variables. In this case, the following lemma shows that a one-layer ReLU neural network suffices to represent it.

**LEMMA 2.** *The linear function  $f_\rho(\mathbf{x})=\alpha+\boldsymbol{\beta}^\top\mathbf{x}$  can be represented by the one-layer ReLU neural network architecture (6) via  $f_\rho(\mathbf{x})=\alpha+\boldsymbol{\beta}^\top\mathbf{x}=\mathbf{W}_1\sigma(\mathbf{W}_0\mathbf{x}+\mathbf{b}_0)+b_1$ , where  $\mathbf{W}_0=(\boldsymbol{\beta},-\boldsymbol{\beta})^\top\in\mathbb{R}^{2\times p}$ ,  $\mathbf{b}_0=(\alpha,-\alpha)^\top\in\mathbb{R}^2$ ,  $\mathbf{W}_1^\top=(1,-1)^\top\in\mathbb{R}^2$ , and  $b_1=0$ .*

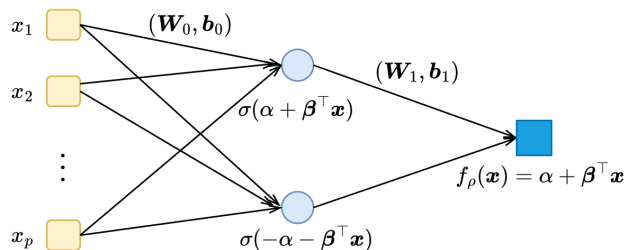


**Figure 2** Illustration of a one-layer ReLU neural network representing linear functions.

Figure 2 illustrates the one-layer ReLU neural network. In this parametric setting, we can directly apply Corollary 1 to obtain an excess risk bound that scales in the order of  $O(\sqrt{p\log(n)/n})$ , given that  $\mathcal{S}=\sum_{i=0}^1 w_{i+1}(w_i+1)=2p+5$  for the network structure shown in Figure 2. For this special case, our bound is comparable, up to a logarithm factor, to the counterparts in Ban and Rudin (2019), whether using linear or kernel decision rules. Nevertheless, beyond parametric models such as in Example 1, we are able to provide theoretical guarantees for general target functions without requiring a priori specification of their explicit functional forms.

**4.1.2. Approximation Error and Balanced Excess Risk Bounds.** The approximation error quantifies the ability of any DNN to approximate the target function, regardless of the sample size. Indeed, it is determined by the smoothness and dimensionality of the target function. For instance, if the target function is simple, say a linear function, as in Example 1, the approximation error could be extremely small. To encompass a wide range of scenarios, we here consider the general case where the target function  $f_p$  belongs to a Hölder function class.

DEFINITION 1 (HÖLDER FUNCTION CLASS). For  $\beta, B_0 > 0$ , and  $\mathcal{X} \in \mathbb{R}^p$ , the Hölder function class  $\mathcal{H}^\beta(\mathcal{X}, B_0)$  is defined by

$$\mathcal{H}^\beta(\mathcal{X}, B_0) := \left\{ f : \mathcal{X} \rightarrow \mathbb{R}, \max_{\|\alpha\|_1 \leq s} \|\partial^\alpha f\|_\infty \leq B_0, \text{ and } \max_{\|\alpha\|_1 = s} \sup_{x \neq y} \frac{|\partial^\alpha f(x) - \partial^\alpha f(y)|}{\|x - y\|_2^r} \leq B_0 \right\},$$

where  $s := \lfloor \beta \rfloor$  denotes the largest integer that is strictly smaller than  $\beta$  and  $r = \beta - \lfloor \beta \rfloor \in (0, 1]$ ;  $\alpha := (\alpha_1, \dots, \alpha_p)^\top$  is a vector of non-negative integers and  $\|\alpha\|_1 := \sum_{i=1}^p \alpha_i$ ; and  $\partial^\alpha = \partial^{\alpha_1} \dots \partial^{\alpha_p}$  denotes the partial derivative operators.

By definition, a function in  $\mathcal{H}^\beta(\mathcal{X}, B_0)$  is  $\lfloor \beta \rfloor$ -times differentiable over  $\mathcal{X}$ , with all derivatives up to order  $\lfloor \beta \rfloor$  uniformly bounded by  $B_0$ , and its  $\lfloor \beta \rfloor$ -th derivative is Hölder continuous with exponent  $\beta - \lfloor \beta \rfloor$ . For example, when  $\beta = 1$ , this class includes Lipschitz continuous functions, and when  $\beta = 2$ , it includes functions with continuous first-order derivatives. We need the following assumptions to analytically analyze the approximation error bound in terms of the network structure.

ASSUMPTION 2. (i) The support  $\mathcal{X}$  of the feature vector is a compact set in  $\mathbb{R}^p$ , and without loss of generality, we assume that  $\mathcal{X} := [0, 1]^p$ . The marginal probability measure of  $\mathbf{X}$  is absolutely continuous with respect to the Lebesgue measure; (ii) The conditional quantile function  $f_p$  belongs to the Hölder class  $\mathcal{H}^\beta([0, 1]^p, B_0)$  for a given  $\beta > 0$  and a finite constant  $B_0 > 0$  with  $B_0 \leq \mathcal{B}$ .

Assumption 2(i) imposes a mild boundedness condition on the domain of the feature data, while Assumption 2(ii) introduces a basic smoothness condition on the target function. Although the smoothness parameter may not be directly inferred in practice, this condition is rather reasonable and general because it encompasses a large subset of continuous functions. For example, by conservatively setting  $\beta = 1$ , Assumption 2(ii) implies that the target quantile function is Lipschitz continuous, a condition that already covers many frequently used demand-covariate models, such as Example 1, where we can choose  $B_0$  to be the largest absolute value of the elements in the coefficient vector.

PROPOSITION 1. Let  $\mathcal{F}_{DNN}$  be the ReLU neural network mappings with the width and depth respectively specified as

$$\mathcal{W} = 38(\lfloor \beta \rfloor + 1)^2 p^{\lfloor \beta \rfloor + 1} N \lceil \log_2(8N) \rceil \text{ and } \mathcal{D} = 21(\lfloor \beta \rfloor + 1)^2 M \lceil \log_2(8M) \rceil + 2, \quad (8)$$

where  $\lceil a \rceil$  denotes the smallest integer that is no less than  $a$ . Under Assumption 2 and for any  $N, M \in \mathbb{N}_+$ , we have

$$\inf_{f \in \mathcal{F}_{DNN}} [\mathcal{R}^\rho(f) - \mathcal{R}^\rho(f_\rho)] \leq 18 \max\{b, h\} B_0(\lfloor \beta \rfloor + 1)^2 p^{\lfloor \beta \rfloor + (\beta \vee 1)/2} (NM)^{-2\beta/p},$$

where  $a \vee b := \max\{a, b\}$ .

As opposed to Theorem 1, Proposition 1 demonstrates that the approximation error bound is decreasing in the network complexity (measured by its width  $\mathcal{W}$  and depth  $\mathcal{D}$  via  $N$  and  $M$ ). This observation is quite intuitive since a network with a larger width or depth has greater approximation power. Therefore, a careful network structure design is necessary to strike a balance between the stochastic and approximation errors since the excess risk is a sum of them, as shown in Lemma 1. Moreover, the feature dimension  $p$  also affects the approximation error, and the approximation to the target function becomes tougher if the number of covariates grows. Finally, the smoothness parameter  $\beta$  influences the approximation error because ReLU neural networks essentially use piecewise linear functions to approximate the target function.

Although the network depth and width can vary by tuning the free parameters  $N$  and  $M$ , we always treat the uniform upper bound  $\mathcal{B}$  for the network mappings as a fixed positive constant. This can be enforced by truncating the network output to ensure that  $\|f_\phi\|_\infty \leq \mathcal{B}$ , even as the network size grows. Technically, this truncation can be implemented using the following composite ReLU operations:  $y = -\max\{\mathcal{B} - \max\{x, 0\}, 0\} + \max\{\mathcal{B} - \max\{-x, 0\}, 0\}$ , which ensures that for any  $x \in \mathbb{R}$ , the output  $y$  is constrained within  $[-\mathcal{B}, \mathcal{B}]$ . Consequently, to achieve an optimal convergence rate of the excess risk bound in the sample size, we can balance the two errors in Theorem 1 and Proposition 1 by appropriately relating  $M$ ,  $N$ , or both, to the sample size  $n$ . Using any of these approaches can result in the same optimal convergence rate but would incur different total numbers of parameters in the network.

**THEOREM 2 (HIGH-PROBABILITY BOUND FOR EXCESS RISK).** *Let the network width and depth be defined according to (8) with  $NM = \lfloor n^{\frac{p}{2p+4\beta}} \rfloor$ . Under Assumptions 1 and 2, for all  $n \geq C$  with a large enough  $C > 0$ , with probability at least  $1 - \delta$  over the random draw of  $\mathbf{S}_n$ , we have*

$$\mathcal{R}^\rho(\hat{f}_{DNN}) - \mathcal{R}^\rho(f_\rho) \leq 2\sqrt{2}(b\bar{D} + h\mathcal{B}) \left( C_1(\lfloor \beta \rfloor + 1)^4 p^{\lfloor \beta \rfloor + 1} (\log(n))^2 n^{-\frac{\beta}{2\beta+p}} + \sqrt{\frac{\log(1/\delta)}{n}} \right), \quad (9)$$

where  $C_1 > 0$  is an independent universal constant.

**REMARK 1.** If the excess risk has some nice local quadratic structure (see Assumption 3), the approximation rate in Proposition 1 can be further accelerated (Proposition OA.1). As a result, the excess risk bound can also be slightly improved to  $O(n^{-\frac{2\beta}{4\beta+p}})$  (Theorem OA.2).

It is worth highlighting that the excess risk bound in Theorem 2 is established without requiring prior knowledge of the functional form of  $f_\rho$  and applies to a large class of target functions. Nevertheless, DNNs can still provide satisfactory solutions with explicit theoretical guarantees in this general setting. The DNN method itself is nonparametric, meaning that we simply need to train a DNN with sufficient data and a properly chosen network structure. In fact, Theorem 2 suggests that a wide range of network configurations can achieve a designed precision, and this flexibility is also observed numerically (see Section 6). In some sense, we “unwrap” the black box of DNNs in the data-driven newsvendor context by demonstrating that the DNN solution can be reliable in theory and should be considered a valuable candidate in the problem-solving toolbox, particularly for complex scenarios where parametric methods fall short.

The excess risk bound holds without requiring specific distributional conditions or network restrictions, exhibiting a polynomial dependence on the feature dimension  $p$ . It scales as  $O(n^{-\frac{\beta}{2\beta+p}})$  up to a logarithmic factor, which comes from the first error term in (9). This indicates that a smoother target function (i.e.,  $\beta$  is larger) leads to a faster convergence rate. Again, this is because ReLU neural networks are essentially piecewise linear functions, and they excel at approximating smooth functions. However, we also notice that the convergence rate decreases with the feature dimension, so in a high-dimensional scenario, the convergence of the error bound could be very slow. This is a commonly encountered problem in high-dimensional statistics, often referred to as the “curse of dimensionality.” To mitigate this issue in the current setting, we propose focusing on the intrinsic dimension of the prediction problem in Section 5.2. By doing so, the convergence order no longer depends on the feature dimension  $p$  but on the much smaller intrinsic dimension if the target function has a composite structure. We also remark that the second error term in (9) is a result of the concentration inequalities that bound the deviation between sample values and expected values, which is common in measuring the performance of sample-based policies.

#### 4.2. Sharper Bound in Expectation: An Optimal Rate

In this section, we show that the DNN method can attain the minimax convergence rate in that the expected excess risk can be bounded both from above and below by the same polynomial term in the sample size, up to logarithmic factors. In this sense, the derived rate is optimal.

**ASSUMPTION 3 (Local Quadratic Condition of Excess Risk).** *There exist some constants  $c_\rho^0 = c_\rho^0(\rho, D, \mathbf{X}) > 0$  and  $\delta_\rho^0 = \delta_\rho^0(\rho, D, \mathbf{X}) > 0$  such that  $\mathcal{R}^\rho(f) - \mathcal{R}^\rho(f_\rho) \leq c_\rho^0 \|f - f_\rho\|_{L^2(\nu)}^2$ , for any  $f$  satisfying  $\|f - f_\rho\|_{L^\infty(\mathcal{X}^0)} \leq \delta_\rho^0$ , where  $\mathcal{X}^0$  is any subset of  $\mathcal{X}$  with  $\mathbb{P}(\mathbf{X} \in \mathcal{X}^0) = \mathbb{P}(\mathbf{X} \in \mathcal{X})$ .*

**THEOREM 3 (UPPER BOUND FOR EXPECTED EXCESS RISK).** *Under Assumptions 1, 2, and 3, with the same network structure as in Theorem 2, we have*

$$\mathbb{E} \left[ \mathcal{R}^\rho(\hat{f}_{DNN}) - \mathcal{R}^\rho(f_\rho) \right] \leq C(\log(n))^4 n^{-\frac{2\beta}{p+2\beta}}, \quad (10)$$



for  $n$  large enough, where  $C$  is a universal constant depending on model parameters.

In fact, the technical assumption of a local quadratic structure for the excess risk is minor, which is satisfied when the density of the conditional distribution  $D|\mathbf{X}$  has an upper bound near  $f_\rho(\mathbf{X})$ . Notably, the bound on the expected excess risk in Theorem 3 is tighter than the high-probability bound in Theorem 2 in that the convergence rate with respect to the sample size almost doubles. On the one hand, this is not surprising because one may not be able to directly recover the high-probability bound (9), additive in the logarithm of  $\delta$ , from (10) via the Markov inequality. The additive form in (9) with respect to the logarithm of  $\delta$  is actually more common in statistical learning theory (Mohri et al. 2018). We also keep our main focus on the high-probability bound, as shown in Section 4.1, to facilitate the comparisons with the existing findings. On the other hand, the proofs of these two bounds are totally different, where some technical gaps may exist to improve the convergence rate in the high-probability bound. While this is out of the scope of our paper, we leave the explorations to future research. Finally, compared with the state-of-the-art results in the literature (e.g., Padilla et al. 2022), our result does not require restrictive assumptions on the network parameters, such as boundedness and sparsity, which is theoretically stronger and can be practically more relevant.

Meanwhile, we are able to establish a parallel lower bound for the expected excess risk using any sample-based policy.

**THEOREM 4 (LOWER BOUND FOR EXPECTED EXCESS RISK).** *Under Assumptions 1 and 2 and additional assumptions that (i) the density function of the conditional distribution  $D|\mathbf{X}$  is Lipschitz continuous and uniformly lower bounded by  $\kappa > 0$ ; (ii) the marginal density function of  $\mathbf{X}$  has a finite upper bound over  $\mathcal{X}$ , we have*

$$\inf_{\hat{f}_n} \sup_{f_\rho \in \mathcal{H}^\beta([0,1]^p, B_0)} \mathbb{E} \left[ \mathcal{R}^\rho(\hat{f}_n) - \mathcal{R}^\rho(f_\rho) \right] \geq cn^{-\frac{2\beta}{p+2\beta}}, \quad (11)$$

where  $c$  is some positive constant and the infimum is taken over all possible estimators based on the random samples  $\mathbf{S}_n = \{(\mathbf{x}_i, d_i)\}_{i=1}^n$  from the joint distribution  $(\mathbf{X}, D)$  with the  $\rho$ -th quantile of the conditional distribution  $D|\mathbf{X}$  being  $f_\rho(\mathbf{X})$ .

The lower bound in Theorem 4 matches the upper bound in Theorem 3, up to certain logarithm factors, indicating that the rate  $n^{-\frac{2\beta}{p+2\beta}}$  is indeed minimax optimal. It further demonstrates the effectiveness of the DNN method in dealing with the data-driven, feature-based newsvendor problem. To our knowledge, our optimal rate result is also new to the literature on DNN theories and is not restricted to special distributions and network structures (unlike, e.g., Schmidt-Hieber 2020).

## 5. Extensions and Further Discussions

We further consider two practical extensions within the general framework established earlier. The first extension focuses on accommodating a learning environment with dependent data. We then explore how to mitigate the curse of dimensionality when the target function exhibits a composite structure. Each subsection presents its background and conditions, and they stand alone without necessarily being connected.

### 5.1. Learning from Dependent Data

In practice, the sample data is usually a time series where the feature information  $\mathbf{x}_i$  and demand  $d_i$  are collected over a certain timeline. In such cases, imposing inter-independence assumptions on the data may be challenging or even unreasonable, as time series data commonly exhibits various dependence structures. Such a dependency can arise from auto-regressive effects, memory effects, or momentum patterns, where each observation at a given time point may be influenced by past observations. Consequently, it becomes necessary to extend the previously established theory when dealing with potentially dependent data.

In the following, we consider a general time series prediction problem where  $\mathbf{S}_T = \{\mathbf{Z}_i := (\mathbf{X}_i, D_i)\}_{i=1}^T$  comes from some stochastic process. We note that no specific assumptions are imposed on the data-generating stochastic process so it could be non-stationary and non-mixing. One can imagine the sample data to be the chronological features and demand over the past several weeks, months, or quarters. The objective is to predict the inventory decision in the next period ( $T+1$ ) in order to minimize the expected newsvendor loss.

Given the potential dependence of the data, we are particularly interested in the risk conditioning on the past realizations of the stochastic process  $\mathbf{S}_T$ . With a little abuse of notation, we define the *path-dependent* conditioned risk as

$$\mathcal{R}^\rho(f) = \mathbb{E}[b(D_{T+1} - f(\mathbf{X}_{T+1}))^+ + h(f(\mathbf{X}_{T+1}) - D_{T+1})^+ | \mathbf{Z}_1, \dots, \mathbf{Z}_T]$$

for any function  $f: \mathbb{R}^p \rightarrow \mathbb{R}$ , which differs from the averaged version  $\mathbb{E}[b(D_{T+1} - f(\mathbf{X}_{T+1}))^+ + h(f(\mathbf{X}_{T+1}) - D_{T+1})^+]$  in that the latter averages the newsvendor loss over all possible historical paths. Meanwhile, the path-dependent risk is considered more reasonable due to the fact that we have already observed a feature-demand time series. Similarly, we define

$$f_\rho(\mathbf{x}) := \arg \min_f \mathcal{R}^\rho(f) = \inf\{q \geq 0 : F(q | \mathbf{X}_{T+1} = \mathbf{x}, \mathbf{Z}_1, \dots, \mathbf{Z}_T) \geq \rho\},$$

which is the  $\rho$ -th quantile of the conditional CDF of  $D_{T+1}$  given  $\mathbf{X}_{T+1} = \mathbf{x}$  and past observations  $(\mathbf{Z}_1, \dots, \mathbf{Z}_T)$ . Correspondingly, the empirical risk is given by

$$\mathcal{R}_T^\rho(f) = \frac{1}{T} \sum_{i=1}^T [b(D_i - f(\mathbf{x}_i))^+ + h(f(\mathbf{x}_i) - D_i)^+], \quad (12)$$

and the minimizer within a given DNN function class is denoted by  $\hat{f}_{DNN} := \arg \min_{f \in \mathcal{F}_{DNN}} \mathcal{R}_T^\rho(f)$ .

Again, we intend to provide a non-asymptotic upper bound for the excess risk  $\mathcal{R}^\rho(\hat{f}_{DNN}) - \mathcal{R}^\rho(f_\rho)$  under this new dependent-data scenario.

**THEOREM 5 (EXCESS RISK BOUND FOR DEPENDENT DATA).** *Suppose the same network structure as in Theorem 2. Under Assumptions 1 and 2 and for  $T$  large enough, with probability at least  $1 - \delta$  over the random draw of  $\mathbf{S}_T$ , where the elements are possibly dependent, we have*

$$\mathcal{R}^\rho(\hat{f}_{DNN}) - \mathcal{R}^\rho(f_\rho) \leq 2\sqrt{2}(b\bar{D} + h\mathcal{B}) \left( C(\lfloor \beta \rfloor + 1)^4 p^{\lfloor \beta \rfloor + 1} (\log(T))^2 T^{-\frac{\beta}{2\beta+p}} + \sqrt{\frac{\log(1/\delta)}{T}} \right) + 2\Delta, \quad (13)$$

where  $C > 0$  is a universal constant and  $\Delta := \sup_{L \in \mathcal{F}_L} \left( \mathbb{E}[L(\mathbf{Z}_{T+1}) \mid \mathbf{Z}_1, \dots, \mathbf{Z}_T] - \sum_{t=1}^T \frac{1}{T} \mathbb{E}[L(\mathbf{Z}_t) \mid \mathbf{Z}_1, \dots, \mathbf{Z}_{t-1}] \right)$ , in which  $L(\mathbf{z}) := b(d - f(\mathbf{x}))^+ + h(f(\mathbf{x}) - d)^+$  and  $\mathcal{F}_L := \{L(f(\mathbf{x}), d) : f \in \mathcal{F}_{DNN}\}$ .

A few comments are in order. First, we notice that the main difference between the dependent-data excess risk bound in Theorem 5 and the counterpart in Section 4 lies in the term  $\Delta$ . By definition, it evaluates the discrepancy between the target distribution and the distribution of past observations. Specifically, it can also serve as a natural measure of non-stationarity for the stochastic process  $\mathbf{S}_t$ , which is tailored to adapt to the loss function  $L$  and the hypothesis set  $\mathcal{F}_{DNN}$  (Kuznetsov and Mohri 2015). As the network size increases, the discrepancy also increases. In particular, when the sample data is i.i.d., it is apparent that  $\Delta = 0$  and this excess risk bound reduces to the one established in Section 4. In general cases, it links to the familiar measures such as the total variation distance ( $\|\cdot\|_{TV}$ ) and relative entropy ( $D_{KL}(\cdot\|\cdot)$ ) between the conditional distribution of  $\mathbf{Z}_{T+1}$  given  $\mathbf{Z}_1, \dots, \mathbf{Z}_T$  (denoted by  $\mathbb{P}(\cdot \mid \mathbf{Z}_1, \dots, \mathbf{Z}_T)$ ) and the mixture distribution of sample margins  $\sum_{t=1}^T \frac{1}{T} \mathbb{P}(\cdot \mid \mathbf{Z}_1, \dots, \mathbf{Z}_{t-1})$  with an application of the Pinsker's inequality,

$$\Delta \leq C \left\| \mathbb{P}(\cdot \mid \mathbf{Z}_1, \dots, \mathbf{Z}_T) - \sum_{t=1}^T \frac{1}{T} \mathbb{P}(\cdot \mid \mathbf{Z}_1, \dots, \mathbf{Z}_{t-1}) \right\|_{TV} \leq \sqrt{2D_{KL} \left( \mathbb{P}(\cdot \mid \mathbf{Z}_1, \dots, \mathbf{Z}_T) \left\| \sum_{t=1}^T \frac{1}{T} \mathbb{P}(\cdot \mid \mathbf{Z}_1, \dots, \mathbf{Z}_{t-1}) \right. \right)},$$

provided that  $L(\mathbf{z}) \leq C$  holds uniformly for a positive constant  $C$ . From the inequality above, we can see more clearly that as the target distribution and the distribution of samples get closer, measured by a smaller total variation distance or relative entropy, the discrepancy measure  $\Delta$  becomes smaller, and the stochastic process is also more stationary. The excess risk bound in Theorem 5 grows with  $\Delta$ , implying that when the time series becomes more non-stationary, it is more challenging to make predictions upon past observations because they may be less informative about future outcomes.

Second, there is additional flexibility in adjusting the weights of the historical data in the prediction. Recall that we directly compute the empirical risk as the average cost for all past observations in (12). This is a natural treatment for i.i.d. data, where each sample contributes equally. However, in a dependent-data scenario, it may be the case that observations closer to the prediction date

or those occurring on the same day of the week are more informative and carry greater predictive power. Therefore, it is no longer appropriate to treat every past observation equally. Instead, assigning different weights to them can be beneficial. For example, we can assign higher weights to closer data points or samples from the same day of the week. Importantly, even with a flexible weighting scheme, the excess risk bound in Theorem 5 still holds, with a corresponding modification on the definition of the discrepancy measure  $\Delta$  (Kuznetsov and Mohri 2015).

## 5.2. Mitigating Curse of Dimensionality

Recall that the excess risk bound in Theorem 2 scales as  $O(n^{-\frac{\beta}{2\beta+p}})$  up to a logarithmic factor, where  $n$  is the sample size,  $\beta$  represents the smoothness of the target function, and  $p$  is the dimension of the feature variables. While the smoothness parameter is endogenously given, the dimensionality strongly influences the convergence rate so that a large dimension parameter  $p$  could result in an extremely slow convergence rate, commonly referred to as the *curse of dimensionality* in data science. A slow convergence rate thus requires many more samples so as to attain certain theoretical accuracy, which is usually impractical in real-world scenarios. We here discuss how to mitigate this issue by maintaining a desirable convergence rate even with a very large  $p$ .

Generally speaking, there are two main approaches in the literature that impose assumptions either on the target function or the covariate distribution to achieve effective dimension reduction (Jiao et al. 2023). For the former, it can be shown that if the target function exhibits a suitable composite structure, the effective dimension parameter appearing in the convergence rate could be much smaller than the nominal dimension  $p$ . In what follows, we use an example with a generalized linear demand (GLM) model to illustrate this.

**EXAMPLE 2 (GENERALIZED LINEAR DEMAND).** We assume that the target function  $f_\rho$  is a generalized linear function in the feature covariates:  $f_\rho(\mathbf{x}) = g(\boldsymbol{\theta}^\top \mathbf{x})$  for  $\boldsymbol{\theta}, \mathbf{x} \in \mathbb{R}^{p+1}$ , where the first element of  $\mathbf{x}$  is 1 without loss of generality and  $g: \mathbb{R} \rightarrow \mathbb{R}$  is a univariate function. This model includes the commonly used MNL model and linear demand model as special cases, and it has been widely adopted in the literature dealing with contextual information (e.g., Ban and Rudin 2019, Miao et al. 2022). With this special structure, we are able to show that the effective dimension in the convergence order is indeed only 1, indicating a faster rate without being plagued by the curse of dimensionality.

**THEOREM 6 (EXCESS RISK BOUND FOR GLM).** *Let the network width and depth be respectively  $\tilde{\mathcal{W}} = \max\{\mathcal{W}, 2p\}$  and  $\tilde{\mathcal{D}} = \mathcal{D} + 3$ , where  $\mathcal{W}$  and  $\mathcal{D}$  are defined according to (8) with  $MN = \lfloor n^{\frac{1}{4\beta+2}} \rfloor$ . Under Assumptions 1 and 2(i) and the additional assumption that the target quantile function follows  $f_\rho(\mathbf{x}) = g(\boldsymbol{\theta}^\top \mathbf{x})$ , where  $g \in \mathcal{H}^\beta([a, c], B_0)$  for a given  $\beta > 0$ , a finite constant  $B_0 > 0$ ,*

and  $-\infty < a < c < \infty$ , with probability at least  $1 - \delta$  over the random draw of  $\mathbf{S}_n$  (which consists of i.i.d. samples from the joint distribution of  $(\mathbf{X}, D)$ ), we have

$$\mathcal{R}^\rho(\hat{f}_{DNN}) - \mathcal{R}^\rho(f_\rho) \leq 2\sqrt{2}(b\bar{D} + h\mathcal{B}) \left( C(\lfloor \beta \rfloor + 1)^4 (\log(n))^2 n^{-\frac{\beta}{2\beta+1}} + \sqrt{\frac{\log(1/\delta)}{n}} \right)$$

for  $n$  large enough, where  $C > 0$  is a universal constant.

Theorem 6 demonstrates that the excess risk bound now scales as  $O(n^{-\frac{\beta}{2\beta+1}})$  under the GLM. This bound is obviously tighter, offering a much faster convergence rate, particularly when the feature dimension is large. This improvement is achieved under the additional GLM assumption, along with corresponding modifications to the proposed network design outlined in Theorem 2. The rationale behind this is quite straightforward: a composite function behaves similarly to the structure of a DNN in (6), which means that we can approximate each layer in the composition by a neural network and then stack them together. Since a linear function can be perfectly represented by a one-layer network as shown in Lemma 2, we only need to consider the approximation of the univariate function  $g$  in the outer layer, and this leads to an excess risk bound with an effective dimension of one. Theoretically, this result can be further extended to any general composite function with finite composition layers using similar reasoning, and interested readers are referred to Shen et al. (2021) for more details.

## 6. Simulation Study and Implementation Guidance

In this section, we conduct simulation experiments to examine the implementation of the DNN method, while the next section will demonstrate its effectiveness using real-world data. Our goal is to provide practical insights associated with our developed theory. The key insights are threefold. First, our numerical experiments reveal that the error of the DNN solution does not decrease monotonically with the network depth or width for a given amount of data. This finding confirms the trade-off between stochastic and approximation errors, which is central to our theoretical error analysis, and also highlights the importance of balancing these two error sources. Second, in terms of network design, it is more efficient and effective to use a deeper yet wide enough network during the tuning process to identify the optimal architecture. In fact, a wide range of network configurations can achieve comparably good performance. Third, we numerically check the convergence rate of the DNN solution's excess risk, which is statistically significant and can be explained by our theoretical predictions. The remainder of this section will elaborate on these points.

In our numerical experiments, we consider the data-generating mechanism represented by  $D = f(\mathbf{X}) + \epsilon$ , where  $\epsilon$  follows a standard normal distribution. Therefore, the target  $\rho$ -th conditional quantile function is  $f_\rho(\mathbf{x}) = f(\mathbf{x}) + \Phi^{-1}(\rho)$ , with  $\Phi(\cdot)$  denoting the CDF of the standard normal distribution. Specifically, the following scenarios are examined:

- (a) Univariate Hölder continuous (UHC) case:  $f(x) = 2x^{1/2}$ ;
- (b) Multivariate logistic (ML) model:  $f(\mathbf{x}) = \frac{2\exp(\boldsymbol{\theta}^\top \mathbf{x})}{1+\exp(\boldsymbol{\theta}^\top \mathbf{x})}$ , where  $\boldsymbol{\theta} := (4, -2, 2, -1)^\top$ ;
- (c) Multivariate additive (MA) model:  $f(\mathbf{x}) = \exp(x_1 - 0.5) + 2(x_2 + x_3 - 1)^2 + |x_4 - 0.5|$ .

These examples are carefully selected to encompass various feature dimensions and smoothness levels of the target function. The feature covariates  $\mathbf{X}$  are assumed to be uniformly distributed within the unit interval  $[0, 1]$  for the univariate case, and within  $[0, 1]^p$  for multivariate cases. To facilitate illustration, we present the numerical performance at three critical quantile levels:  $\rho = 0.25, 0.5, 0.75$ , where  $b + h$  is assumed to be 1.

For each case mentioned above, we generate training data  $(\mathbf{x}_i^{train}, d_i^{train})_{i=1}^n$  of size  $n$  to train the empirical risk minimizer at  $\rho \in \{0.25, 0.5, 0.75\}$ , denoted by  $\hat{f}_{n,\rho}$ . To estimate the excess risk of the obtained DNN solution, we also generate testing data  $(\mathbf{x}_i^{test}, d_i^{test})_{i=1}^T$  of size  $T$  from the same distribution as the training data. The testing error is then calculated in terms of the difference in average newsvendor loss between  $\hat{f}_{n,\rho}$  and  $f_\rho$  represented by

$$\frac{1}{T} \sum_{i=1}^T \left[ b(d_i^{test} - f_\rho(\mathbf{x}_i^{test}))^+ + h(f_\rho(\mathbf{x}_i^{test}) - d_i^{test})^+ \right] - \frac{1}{T} \sum_{i=1}^T \left[ b(d_i^{test} - \hat{f}_{n,\rho}(\mathbf{x}_i^{test}))^+ + h(\hat{f}_{n,\rho}(\mathbf{x}_i^{test}) - d_i^{test})^+ \right].$$

To ensure that this testing error approximates  $\hat{f}_{n,\rho}$ 's excess risk, we set  $T = 10^5$ . Additionally, we report the mean of this error over 100 replications to ensure robustness.

It is important to note that we desire to provide implementation guidance and insights that correspond to the theoretical findings established in this paper. However, this process presents certain challenges. While we have analyzed the stochastic and approximation errors associated with the DNN method, practical implementations also introduce an additional optimization error arising from the numerical solution of (7). Any practical solution based on finite samples will inevitably involve all three types of errors. Our theoretical results have tackled only the first two by assuming that  $\hat{f}_{n,\rho}$  precisely achieves the minimum empirical newsvendor loss within the given DNN function class. In practice, the optimization error can result from a variety of factors, including the choice of optimizer, initialization, and stopping criteria, making a unified theoretical analysis for this error particularly challenging. For this reason, we strive to minimize the impact of the optimization error by many trials to ensure that the numerical results align as closely as possible with our theoretical findings, though some level of error may be unavoidable. Despite these challenges, we have identified useful practical guidelines, which will be discussed in detail later.

A detailed discussion of the optimization error, including those factors mentioned above contributing to it, lies beyond the scope of the current paper, and a vast literature has discussed the relevant issues (see, e.g., [Glorot and Bengio 2010](#), [He et al. 2015](#), [Adcock and Dexter 2021](#)). In particular, we refer to [Adcock and Dexter \(2021\)](#) for a comprehensive computational framework and extensive numerical illustrations for implementing DNNs in practical situations, and we largely

follow their recommendations in our numerical experiments. Indeed, we have checked in our setting via many trials that their suggestions effectively achieve a tolerant optimization error, so we do not reiterate the related numerical experiments here. For example, the *Adam* optimizer with an adaptively decaying learning rate can contribute to smooth and stable numerical outcomes, and network parameters can be initialized using symmetric uniform or normal distributions with small variances (Adcock and Dexter 2021).

### 6.1. Trade-Off in Network Size: Bigger Isn't Always Better

As demonstrated in Section 4, there is a delicate balance between stochastic and approximation errors with respect to the network architecture. When dealing with limited data, a key observation from Theorem 1 and Proposition 1 is that stochastic error increases with network complexity, while approximation error decreases with it. In other words, our theory suggests that an appropriately chosen network architecture is essential. The architecture must provide sufficient representational capacity while keeping stochastic error at a moderate level. A network that is too deep or too wide may not automatically yield optimal outcomes, let alone the high computational cost incurred.

Figure 3 supports our claim. Using a sample size of 256, we fix the network depth and observe how the excess risk behaves as the network width increases. In the UHC and MA cases, the excess risk initially decreases. Linking to our developed theory, this reflects a dominance of approximation error over stochastic error. However, beyond a certain threshold, the excess risk stops decreasing and switches to rising as the width grows. This also aligns with our theory because the network at that point has already achieved an adequate approximation of the target function, causing the stochastic error to dominate. Interestingly, in the ML case, the excess risk keeps increasing with the network width. We hypothesize that this may be due to the high smoothness of the logistic model, where the approximation error is already minimal (negligible) even with a small network, leaving the stochastic error to dominate throughout. This phenomenon is also robust across different sample sizes (see also Figures 5, OA.1, and OA.2). Figure 4 again witnesses this trade-off, this time in terms of the network depth with a fixed width.

### 6.2. Depth vs. Width: The Efficiency Edge of Deeper Networks

Recall that in Theorems 2 and 3, we achieved an optimal balance between stochastic and approximation errors by specifying the network architecture that grows polynomially in the sample size. Intuitively, more data provides additional room for reducing the optimization error by enlarging network complexity, while keeping the stochastic error under control. We also have great flexibility in applying various combinations of network configurations. For example, one could set a fixed width and an expanding depth by setting  $N = C$  for some  $C \in \mathbb{N}_+$  and  $M = \lfloor n^{\frac{p}{2p+4\beta_0}} / C \rfloor$ . Notably, the network size  $\mathcal{S} = \sum_{i=0}^{\mathcal{D}} w_{i+1}(w_i + 1)$  grows quadratically in the width but linearly in the depth.

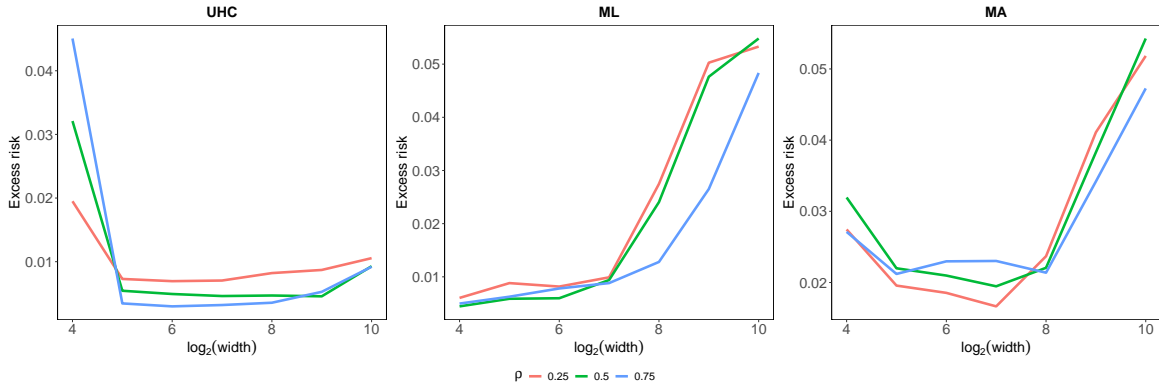


Figure 3 Excess risk against network width with a fixed depth of 4 when  $n = 256$ .

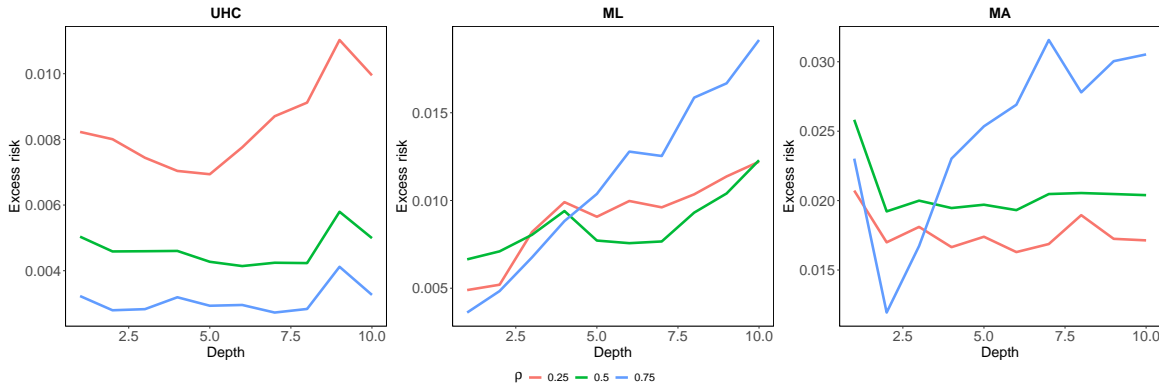


Figure 4 Excess risk against network depth with a fixed width of 128 when  $n = 256$ .

Such a special configuration can potentially save the number of parameters and also the computational cost. Moreover, as noted in [Adcock and Dexter \(2021\)](#), we observe that deep networks tend to exhibit better performance than shallower ones, provided they are sufficiently wide. We thus recommend using a network with a sufficiently large width and experimenting with different numbers of hidden layers to search for the best configuration.

We remind that Theorems 2 and 3 hold uniformly with respect to target functions within a broad Hölder function class, representing somehow a “worst-case” scenario. In practice, network configurations may deviate from those suggested in the theorems while still achieving good performance. For instance, as shown in [Example 1](#), linear functions can be effectively represented by a one-layer network with only two neurons in the hidden layer. For very smooth functions, such as linear ones, shallow networks with a moderate width may suffice. Nevertheless, our theoretical results deliver a critical message that optimal performance can be attained across a great range of network architectures, underscoring the flexibility of the DNN method.

Figure 5 validates this implication because plenty of different network configurations yield comparably good performance, evidenced by the relatively flat region corresponding to (nearly) minimum excess risk. This observation is persistent across different model setups, critical levels, and sample



sizes (see also Figures OA.1-OA.4). When comparing performances across models with varying dimensions, regularities, and sample sizes, the following general insights emerge: (1) for smoother target functions, a relatively small network can already do a decent job, and overly complex architectures may backfire, (2) as dimensionality increases, larger sample sizes are typically required to achieve a satisfactory precision, and (3) deeper or wider networks may be necessary when the target function exhibits greater nonlinearities and lower smoothness. These insights offer practical guidance, complementing the earlier recommendation. Indeed, by following the provided guidelines, practical experimentation can conveniently achieve good performance by tuning the network based on rough ideas of the target function’s regularity and dimensionality.

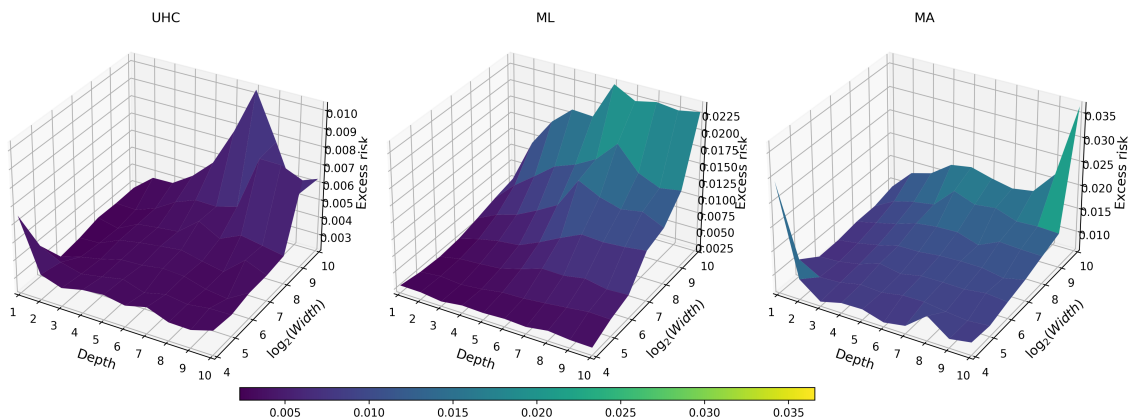


Figure 5 Excess risk against network depth and width when  $n = 1024$  and  $\rho = 0.25$ .

### 6.3. Understanding Convergence Rates in Sample Size

One of our main theoretical results is the optimal convergence rate  $2\beta/(p + 2\beta)$  of the expected excess risk in the sample size (up to logarithm factors), under properly designed network architectures. However, it is hard or even impossible to directly witness this rate in practical examples because of the presence of optimization errors, the somehow “worst-case” nature of the upper bound, and the fact that the lower bound becomes numerically significant only asymptotically (as  $c$  in (11) can be taken to be very small). Despite these challenges, we conduct a series of experiments with exponentially increasing sample sizes to investigate whether a clear convergent pattern shows up and how the rate links to our theory. To mitigate the impact of optimization errors, we explore a wide range of network configurations—varying combinations of the depth and width—for each sample size, and then select the minimum excess risk among them as the optimally balanced error for that sample size. This treatment is reasonable because the practically optimal design may deviate from the conservative plan outlined in Theorem 3, and it is stable because a variety of network designs can yield comparatively good performances, as found in Section 6.2.

Figure 6 presents the numerical convergence results. We can see clear polynomial convergence phenomena as overall, the linear regressions show a statistically significant fit to the log-transformed data points with very small  $p$ -values. As expected, the theoretically optimal rates are not directly visible. Instead, the observed rates are generally below 1 (disregarding minor random perturbations in the ML case), which is the convergence rate of the stochastic error for a fixed network design, as established in Theorem OA.3. Our findings are consistent with the theory in that the convergence rate of excess risk reflects a compromise between approximation and stochastic errors. The extent of the inferiority to the stochastic error rate depends on the degree of approximation error, which in turn is influenced by the regularity and dimensionality of the target function. Interestingly, the convergence rate approaches that of the stochastic error when the target function is very smooth, as the approximation error becomes nearly negligible (which is also consistent with our conjecture in Section 6.1); see the ML case in Figure 6. It deviates from 1 to a smaller value when the smoothness is insufficient and the dimension effect kicks in, reflecting the compromise introduced by the approximation error (see the UHC and MA cases).

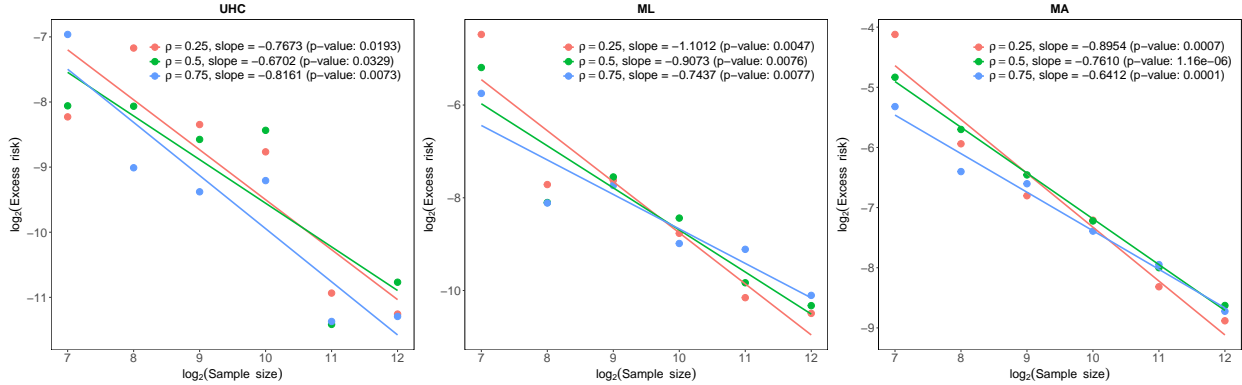


Figure 6 Excess risk against sample size under proper network architectures.

## 7. Case Study: Inventory Management for a Food Supermarket Chain

In this section, we showcase the practical application of DNNs for inventory decision-making. Specifically, we collaborate with a food company in China to collect unique sales data along with various features. Based on the empirical data, we have conducted comprehensive investigations, including testing the practical performance of DNNs and comparing it against many other data-driven benchmarks available in the literature.

### 7.1. Data Description and Candidate Methods

The dataset comprises daily sales records from our collaborated food company throughout the entire year of 2013. The firm operates 131 stores, and each store offers three types of food: processed

food, dishes, and food ingredients. While there are plenty of choices within each food type, we focus on analyzing the demand for the general food category. Given the significant variation in food choices due to availability and seasonality, we aggregate the sales within each category to represent the actual demand for that category. Figure 7 provides the summary statistics for the average daily demand of stores, categorized by food types and days of the week. Each box plot depicts the demand variability among stores. By comparing the boxes in both panels, we can observe clear dependencies of demand on these two categorical variables. For instance, the overall demand for processed food is higher than the other two types, and the food demand is relatively higher on average on Tuesdays. To facilitate our numerical experiments, we convert the categorical features into binary vectors where the length equals the number of categories, with exactly one element set to 1 and the rest to 0.

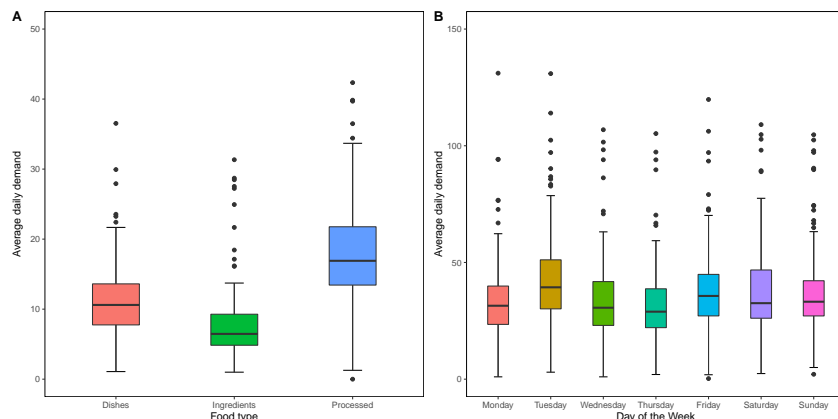


**Figure 7** Box plots of average daily demand for 131 stores versus food type and days of the week.

We also consider an additional set of features in our experiments, which consist of 14 past demands and the associated *operational statistics*. The so-called *operational statistics* refer to the sample average and the differences between consecutive pairs of order statistics of these 14 past demands. Their relevance is theoretically justified in Liyanage and Shanthikumar (2005), and their effectiveness has been observed in Ban and Rudin (2019). In particular, it is important to note that when incorporating past demands as features, one should be cautious about potential time-series dependence in practice. Nevertheless, our analysis in the dependent-data scenario, as discussed in Section 5.1, allows us to incorporate this practical consideration within our framework seamlessly.

We construct a set of feature variables to predict the demand. There are, in total, 54,780 demand records (for different food types and stores) along with their associated features. Following the common practice, we chronologically allocate 70% of the data for training and validation purposes, while the remaining 30% is reserved for testing. Specifically, the training and validation data are

used to train and fine-tune the model and hyperparameters (if any) for each data-driven method under consideration. Once calibrated, these models are then applied to predict demand in the test set, and the corresponding losses are calculated to compare the performance of different methods. To calculate the newsvendor losses, we need to set values for the unit underage and overage costs. Following the standard treatment (e.g., Ban et al. 2020), we choose the average food price of CNY 18.01 as the underage cost  $b$  without loss of generality. Since the overage cost  $h$  is hard to determine in practice, depending on various factors such as the production cost and salvaging treatment, we compute and present the newsvendor losses for various  $\rho := b/(b+h)$ , each corresponding to a unique  $h$ . These ratios implicitly relate to the product’s profitability, so we focus on the case where  $\rho > 0.5$  to reflect the practical situation.

The following set of data-driven methods are implemented on our dataset.

1. DNN method. Given our dataset with relatively simple features, we adopt a three-layer neural network with 512 neurons per layer (and justify this choice in Section F.1). The DNN model is built in Python using *Pytorch*, and the *Adam* optimization algorithm is applied with an initial learning rate of 0.001. The default coefficients  $\beta = (0.9, 0.99)$  are used for computing running averages of gradients and their squares (see Kingma and Ba 2014 for more details). We also adopt a standard early stopping rule to save computational time.

2. SAA method. We use the empirical quantile of the training data to give predictions for the demand in the test data.

3. Linear empirical risk minimization (LERM) method. We implement the linear decision rules proposed in Ban and Rudin (2019). Specifically, we investigate the performance of LERM under three different settings: one without any regularization and the remaining two with either  $\ell_1$  or  $\ell_2$  regularization.

4. Kernel optimization (KO) method. We utilize the nonparametric Gaussian kernel-based smoothing method described in Ban and Rudin (2019), which demonstrated superior performance over other alternatives on the emergency room data considered therein.

5. Reproducing Kernel Hilbert Space (RKHS) method. We conduct simulations using the RKHS approach proposed in Bertsimas and Koduri (2022). For the simulation setting, we use a radial basis function kernel  $K(x_1, x_2) = \exp(-\gamma\|x_1 - x_2\|^2)$  with  $\gamma = 10^{-6}$  and a tuning parameter  $\lambda = 10^{-4}$  for regularization. More detailed descriptions can be found in Bertsimas and Koduri (2022).

6. Separated estimation and optimization (SEO) method. A typical treatment in the literature is to assume a normal demand distribution, allowing for mean and variance estimation through linear regression with respect to feature variables. The inventory decision is then determined by the  $\rho$ -th quantile of the normal distribution.

## 7.2. Preliminary Experiments on a Small Dataset

We first carry out an experiment on a subset of the full dataset to demonstrate the effectiveness of the DNN method in dealing with small datasets. Specifically, we focus on the sales record of one selected store that provides three types of food. This subset consists of 990 daily sales records for all food types and includes a total of 38 feature variables ( $p = 38$ ), such as the day of the week, past demands, and operational statistics, as previously introduced. Following the procedure outlined in the previous section, we test the performance of each considered method on this small dataset.

**Table 1** Newsvendor loss (in CNY ¥) for the selected store across different methods. Each cell displays the average newsvendor loss on the first line, followed by the 95% interval on the second line.

$\rho$	0.6	0.65	0.7	0.75	0.8	0.85	0.9	0.95
SAA	119.2 (0, 479.1)	108.0 (0, 443.0)	97.4 (0, 425.0)	86.2 (6.0, 389.0)	74.3 (4.5, 353.0)	60.7 (3.2, 299.0)	45.5 (3.6, 194.5)	27.0 (4.2, 47.2)
SEO	90.8 (3.0, 276.3)	83.3 (6.1, 243.4)	75.2 (4.6, 217.2)	66.5 (3.7, 189.6)	51.1 (3.7, 158.9)	46.9 (3.7, 123.2)	35.1 (4.6, 78.2)	21.5 (3.1, 29.5)
LERM	90.5 (2.1, 314.0)	82.2 (3.1, 298.3)	71.9 (4.0, 258.4)	62.8 (3.0, 238.9)	53.1 (1.7, 228.2)	44.5 (1.7, 175.7)	35.8 (2.1, 148.7)	23.5 (2.0, 57.9)
LERM- $\ell_1$	86.4 (3.9, 317.8)	77.4 (2.9, 284.1)	68.0 (2.4, 259.2)	60.0 (2.4, 223.5)	50.9 (2.3, 209.7)	41.1 (2.1, 159.9)	32.3 (3.5, 123.5)	21.4 (3.8, 35.0)
LERM- $\ell_2$	99.3 (3.1, 293.8)	80.5 (2.8, 242.1)	70.7 (2.9, 214.8)	77.4 (2.6, 255.4)	55.8 (1.3, 197.7)	50.1 (1.5, 197.6)	49.5 (4.4, 154.4)	17.8 (1.8, 51.5)
KO	90.5 (2.1, 314.0)	82.2 (3.1, 298.3)	71.8 (3.8, 257.4)	62.8 (3.0, 238.9)	53.1 (1.8, 228.2)	44.5 (1.7, 175.6)	35.8 (2.1, 148.7)	23.5 (2.0, 57.9)
RKHS	119.3 (0.5, 478.8)	108.1 (0.4, 443.2)	97.6 (0.4, 424.6)	86.4 (6.0, 389.1)	74.5 (4.9, 351.5)	60.9 (3.5, 297.7)	45.5 (4.2, 206.5)	26.9 (3.7, 64.4)
DNN	91.6 (2.5, 283.3)	77.6 (4.6, 242.6)	68.3 (3.3, 205.2)	59.5 (4.5, 176.1)	46.7 (1.9, 136.2)	38.6 (1.7, 118.5)	24.8 (0.7, 88.8)	12.9 (0.9, 41.3)

Table 1 presents the average newsvendor loss along with the 95% empirical quantile interval, defined by the 0.025 and 0.975 quantiles of the losses, for each trained model on the common test dataset. We observe that the DNN method performs well across all critical levels and achieves the lowest average loss for critical levels above 0.7. This suggests that it remains effective even with limited data. In particular, as the critical level  $\rho$  increases, the overage penalty becomes less significant with a fixed underage cost, which reasonably explains the general improvement in prediction performance as the critical level grows.

From Figure OA.8, we can further see the relative advantage of the DNN method over others, which tends to expand as the critical level increases. A similar pattern is also observed in the empirical experiments in Oroojlooyjadid et al. (2020). This highlights the DNN method’s ability to predict extreme distributional quantiles. In comparison, the DNN method shows an advantage in reducing predictive newsvendor loss, outperforming several recent competitive methods, and improving upon the empirical SAA rule that is commonly used in practice.

### 7.3. Comparison of Results on the Entire Dataset

We proceed to conduct numerical experiments on the entire dataset, where predictive models corresponding to different methods are built using feature information such as store ID and past demands ( $p = 169$ ). The results are presented in Table 2. We clarify that these trained predictive models are essentially different from the ones in the preliminary experiments of the previous subsection. Therefore, the loss values in Table 2 are not necessarily smaller than their counterparts in Table 1 despite the larger sample size.

**Table 2** Newsvendor loss (in CNY ¥) across different methods for the entire dataset. Each cell displays the average newsvendor loss on the first line, followed by the 95% interval on the second line.

$\rho$	0.6	0.65	0.7	0.75	0.8	0.85	0.9	0.95
SAA	160.6 (0, 972.5)	150.4 (0, 936.5)	141.3 (0, 918.5)	130.4 (6.0, 882.5)	117.9 (4.5, 828.5)	103.7 (3.2, 756.4)	86.4 (6.0, 648.4)	61.8 (7.6, 396.2)
SEO	120.7 (5.4, 539.7)	115.1 (6.5, 502.4)	108.1 (7.9, 455.6)	99.3 (9.1, 412.2)	88.7 (9.9, 366.8)	76.0 (10.0, 309.5)	60.7 (9.4, 245.1)	41.6 (7.8, 150.2)
LERM	115.3 (2.4, 540.7)	117.0 (6.0, 481.4)	122.7 (25.0, 430.4)	77.1 (2.9, 294.9)	60.9 (3.4, 243.4)	80.9 (12.2, 232.3)	31.4 (1.3, 124.9)	27.8 (1.7, 79.9)
LERM- $\ell_1$	185.0 (28.4, 654.5)	131.3 (13.4, 511.4)	114.3 (3.2, 409.9)	108.2 (2.7, 365.3)	53.3 (1.4, 247.6)	102.8 (47.8, 272.7)	30.3 (1.0, 132.4)	26.9 (1.4, 98.7)
LERM- $\ell_2$	166.9 (20.5, 619.0)	142.5 (18.5, 519.3)	119.8 (17.3, 429.2)	91.1 (14.5, 331.1)	59.6 (2.0, 247.8)	49.5 (2.2, 200.7)	56.9 (23.3, 156.7)	25.3 (1.2, 111.3)
KO	106.3 (2.5, 579.8)	97.5 (2.6, 535.3)	88.5 (2.5, 488.0)	79.2 (2.4, 449.5)	69.6 (2.3, 400.8)	59.2 (2.3, 339.6)	47.4 (2.3, 252.1)	33.3 (2.5, 135.7)
RKHS	824.2 (578, 1707)	281.2 (45, 496)	3249.4 (2790, 3363)	467.6 (220, 1354)	325.0 (77, 1211)	1117.0 (933, 1162)	241.2 (140, 261)	62.5 (7.5, 416.1)
DNN	102.6 (2.5, 537.7)	87.1 (2.1, 441.7)	75.3 (1.6, 371.9)	61.2 (1.7, 305.9)	49.1 (1.4, 242.1)	36.9 (1.0, 181.5)	24.9 (0.7, 123.8)	12.8 (0.4, 66.2)

On the entire dataset, the DNN method consistently outperforms other data-driven models for all considered critical levels. The KO method performs closest to the DNN model among the alternative methods when  $\rho$  is relatively small, while the LERM algorithms tend to surpass it as  $\rho$  is large (see also Figure OA.9). Additionally, the RKHS method turns out to have poor performance when both the number of features and sample size are large, indicating that its applicability to large datasets requires caution and further exploration, which is beyond the scope of this paper.

Finally, it is worth noting that the training time of the DNN model is quite short, typically around 15 seconds when employing a standard early stopping rule. Furthermore, the execution time for a trained DNN model is approximately 0.01 seconds. All these findings highlight the convenience and efficiency of applying the DNN model rapidly (see Table OA.1 for further comparison details).

## 8. Conclusion

In this paper, we propose to solve the feature-based newsvendor problem using a data-driven DNN method. We provide analytical non-asymptotic excess risk bounds in terms of the sample size and network configuration. Specifically, the excess risk bound can be separated into stochastic and approximation errors, offering a trade-off when selecting the network structure to achieve the optimal convergence rate. The DNN method can effectively mitigate model misspecification errors by achieving a vanishing excess risk when sufficient data is available. Moreover, as reflected in the trade-off between two types of errors, an excessively wide or deep network does not automatically lead to optimal performance. Instead, starting with a sufficiently wide network and adjusting the depth to find the optimal configuration is found to be quite effective. In general, the DNN method is flexible, allowing a range of network designs to perform well, though a specific good design depends on the available data and the properties of the target function. In addition, it can handle dependent data, providing reliable solutions even in the presence of weak non-stationarity. The convergence of the excess risk bound is also accelerated when the underlying target function exhibits a composite structure. Besides theoretical characterizations, we implement the DNN method on a unique real-world dataset. The numerical experiments showcase its good performance in terms of accurate prediction and efficient and fast training and execution. Therefore, our work justifies the applicability of DNNs to the data-driven newsvendor problem and contributes to the advancement of theory and practice in OM problems by utilizing state-of-the-art DNN methods. Further discussions on some related topics can be found in Section G in the online appendix.

## References

- Adcock B, Dexter N (2021) The gap between theory and practice in function approximation with deep neural networks. *SIAM J. Math. Data Sci.* 3(2):624–655.
- Anthony M, Bartlett P (1999) *Neural Network Learning: Theoretical Foundations* (Cambridge).
- Aouad A, Désir A (2022) Representing random utility choice models with neural networks. arXiv:2207.12877.
- Ban GY, Gao Z, Taigel F (2020) Model mis-specification in newsvendor decisions: A comparison of frequentist parametric, Bayesian parametric and nonparametric approaches. Available at SSRN 3495733.
- Ban GY, Rudin C (2019) The big data newsvendor: Practical insights from machine learning. *Oper. Res.* 67(1):90–108.
- Bartlett PL, Harvey N, Liaw C, Mehrabian A (2019) Nearly-tight VC-dimension and pseudodimension bounds for piecewise linear neural networks. *J. Mach. Learn. Res.* 20(1):2285–2301.
- Bertsimas D, Kallus N (2020) From predictive to prescriptive analytics. *Management Sci.* 66(3):1025–1044.
- Bertsimas D, Koduri N (2022) Data-driven optimization: A reproducing kernel hilbert space approach. *Oper. Res.* 70(1):454–471.
- Chan TC, Lin B, Saxe S (2022) A machine learning approach to solving large bilevel and stochastic programs: Application to cycling network design. arXiv:2209.09404.

- Chen N, Lagzi S, Milner J (2022) Using neural networks to guide data-driven operational decisions. Available at SSRN 4217092.
- Farrell MH, Liang T, Misra S (2021) Deep neural networks for estimation and inference. *Econometrica* 89(1):181–213.
- Feng Q, Shanthikumar JG (2018) How research in production and operations management may evolve in the era of big data. *Prod. Oper. Management* 27(9):1670–1684.
- Feng Q, Shanthikumar JG (2022) Developing operations management data analytics. *Prod. Oper. Management* 31(12):4544–4557.
- Gabel S, Timoshenko A (2022) Product choice with large assortments: A scalable deep-learning model. *Management Sci.* 68(3):1808–1827.
- Gijsbrechts J, Boute RN, Van Mieghem JA, Zhang DJ (2022) Can deep reinforcement learning improve inventory management? Performance on lost sales, dual-sourcing, and multi-echelon problems. *Manufacturing & Service Oper. Management* 24(3):1349–1368.
- Glorot X, Bengio Y (2010) Understanding the difficulty of training deep feedforward neural networks. *Proceedings of the Thirteenth AISTATS*, 249–256 (JMLR Workshop and Conference Proceedings).
- He K, Zhang X, Ren S, Sun J (2015) Delving deep into rectifiers: Surpassing human-level performance on imagenet classification. *Proceedings of the 2015 IEEE ICCV*, 1026–1034.
- Hinton G, Deng L, Yu D, Dahl GE, Mohamed Ar, Jaitly N, Senior A, Vanhoucke V, Nguyen P, Sainath TN (2012) Deep neural networks for acoustic modeling in speech recognition: The shared views of four research groups. *IEEE Signal Process. Mag.* 29(6):82–97.
- Hornik K (1991) Approximation capabilities of multilayer feedforward networks. *Neural Netw.* 4(2):251–257.
- Hu Y, Kallus N, Mao X (2022) Fast rates for contextual linear optimization. *Management Sci.* 68(6):4236–4245.
- Jiao Y, Shen G, Lin Y, Huang J (2023) Deep nonparametric regression on approximately low-dimensional manifolds. *Ann. Statist.* 51(2):691–716.
- Kallus N, Mao X (2023) Stochastic optimization forests. *Management Sci.* 69(4):1975–1994.
- Kingma DP, Ba J (2014) Adam: A method for stochastic optimization. arXiv:1412.6980.
- Krizhevsky A, Sutskever I, Hinton GE (2012) Imagenet classification with deep convolutional neural networks. *Adv. Neural Inf. Process.* 25.
- Kuznetsov V, Mohri M (2015) Learning theory and algorithms for forecasting non-stationary time series. *Adv. Neural Inf. Process.* 2015:541–549.
- Levi R, Perakis G, Uichanco J (2015) The data-driven newsvendor problem: New bounds and insights. *Oper. Res.* 63(6):1294–1306.
- Levi R, Roundy RO, Shmoys DB (2007) Provably near-optimal sampling-based policies for stochastic inventory control models. *Math. Oper. Res.* 32(4):821–839.
- Lin M, Huh WT, Krishnan H, Uichanco J (2022) Data-driven newsvendor problem: Performance of the sample average approximation. *Oper. Res.* 70(4):1996–2012.
- Liyanage LH, Shanthikumar JG (2005) A practical inventory control policy using operational statistics. *Oper. Res. Lett.* 33(4):341–348.



- Miao S, Chen X, Chao X, Liu J, Zhang Y (2022) Context-based dynamic pricing with online clustering. *Prod. Oper. Management* 31(9):3559–3575.
- Mohri M, Rostamizadeh A, Talwalkar A (2018) *Foundations of Machine Learning* (MIT Press).
- Nair V, Hinton GE (2010) Rectified linear units improve restricted boltzmann machines. *Proceedings of the 27th ICML*, 807–814.
- Oroojlooyjadid A, Nazari M, Snyder LV, Takáč M (2022) A deep Q-network for the beer game: Deep reinforcement learning for inventory optimization. *Manufacturing & Service Oper. Management* 24(1):285–304.
- Oroojlooyjadid A, Snyder LV, Takáč M (2020) Applying deep learning to the newsvendor problem. *IIEE Trans.* 52(4):444–463.
- Padilla OHM, Tansey W, Chen Y (2022) Quantile regression with ReLU networks: Estimators and minimax rates. *J. Mach. Learn. Res.* 23(247):1–42.
- Perakis G, Tsiourvas A (2022) Optimizing objective functions from ReLU neural networks in revenue management applications. Working paper presented at the RMP conference 2022 (virtual format).
- Qi M, Cao Y, Shen ZJ (2022) Distributionally robust conditional quantile prediction with fixed design. *Management Sci.* 68(3):1639–1658.
- Qi M, Shi Y, Qi Y, Ma C, Yuan R, Wu D, Shen ZJ (2023) A practical end-to-end inventory management model with deep learning. *Management Sci.* 69(2):759–773.
- Scarlett J, Cevher V (2019) An introductory guide to Fano’s inequality with applications in statistical estimation. arXiv:1901.00555.
- Schmidt-Hieber AJ (2020) Nonparametric regression using deep neural networks with ReLU activation function. *Ann. Statist.* 48(4):1875–1897.
- Shapiro A, Dentcheva D, Ruszczyński A (2021) *Lectures on Stochastic Programming: Modeling and Theory*, volume 9 (SIAM, Philadelphia).
- Shen G, Jiao Y, Lin Y, Horowitz JL, Huang J (2021) Deep quantile regression: Mitigating the curse of dimensionality through composition. arXiv:2107.04907.
- Shi C, Chen W, Duenyas I (2016) Nonparametric data-driven algorithms for multiproduct inventory systems with censored demand. *Oper. Res.* 64(2):362–370.
- Siegel AF, Wagner MR (2021) Profit estimation error in the newsvendor model under a parametric demand distribution. *Management Sci.* 67(8):4863–4879.
- Siegel AF, Wagner MR (2023) Data-driven profit estimation error in the newsvendor model. *Oper. Res.* 71(6):2146–2157.
- Silver D, Huang A, Maddison CJ, Guez A, Sifre L, Van Den Driessche G, Schrittwieser J, Antonoglou I, Panneershelvam V, Lanctot M (2016) Mastering the game of Go with deep neural networks and tree search. *Nature* 529(7587):484–489.
- Simchi-Levi D, Xu Y (2022) Bypassing the monster: A faster and simpler optimal algorithm for contextual bandits under realizability. *Math. Oper. Res.* 47(3):1904–1931.
- Simchi-Levi D, Xu Y (2023) Phase transitions in bandits with switching constraints. *Management Sci.* 69(12):7182–7201.

- Ye Z, Zhang Z, Zhang D, Zhang H, Zhang RP (2023) Deep learning based causal inference for large-scale combinatorial experiments: Theory and empirical evidence. Available at SSRN 4375327.
- Zhang H, Chao X, Shi C (2018) Perishable inventory systems: Convexity results for base-stock policies and learning algorithms under censored demand. *Oper. Res.* 66(5):1276–1286.
- Zhang L, Yang J, Gao R (2024) Optimal robust policy for feature-based newsvendor. *Management Sci.* 70(4):2315–2329.

## Online Appendix to “Deep Neural News vendor”

### A. Auxiliary Results

To prove the non-asymptotic error bounds in Section 4, we first present some preliminary concepts and theorems that will be used later regarding complexity theory (Chapter 3 of Mohri et al. 2018) and network learning (Chapters 11 and 12 of Anthony and Bartlett 1999).

DEFINITION OA.1 (COVERING NUMBER). Let  $\mathcal{F}$  be a class of functions from  $\mathcal{X}^p$  to  $\mathbb{R}$ . For any given sequence  $\mathbf{x} = (x_1, \dots, x_p) \in \mathcal{X}^p$ , let

$$\mathcal{F}|_{\mathbf{x}} := \{(f(x_1), \dots, f(x_p)) : f \in \mathcal{F}\} \subset \mathbb{R}^p.$$

For a positive constant  $\delta$ , the covering number  $\mathcal{N}(\delta, \mathcal{F}|_{\mathbf{x}}, \|\cdot\|)$  is the smallest positive integer  $N$  such that there exist  $f_1, \dots, f_N \in \mathcal{F}|_{\mathbf{x}}$  and  $\mathcal{F}|_{\mathbf{x}} \subset \bigcup_{i=1}^N \{f : \|f - f_i\| \leq \delta\}$ , i.e.,  $\mathcal{F}|_{\mathbf{x}}$  is fully covered by  $N$  spherical balls centered at  $f_i$  with radius  $\delta$  under the norm  $\|\cdot\|$ . Moreover, the uniform covering number  $\mathcal{N}_n(\delta, \mathcal{F}, \|\cdot\|)$  is defined to be the maximum covering number over all  $\mathbf{x}$  in  $\mathcal{X}^p$ , i.e.,

$$\mathcal{N}_n(\delta, \mathcal{F}, \|\cdot\|) := \max\{\mathcal{N}(\delta, \mathcal{F}|_{\mathbf{x}}, \|\cdot\|) : \mathbf{x} \in \mathcal{X}^p\}.$$

DEFINITION OA.2 (PSEUDO-DIMENSION). The pseudo-dimension of  $\mathcal{F}$ , denoted as  $\text{Pdim}(\mathcal{F})$ , is defined as the largest integer  $m$  for which there exist  $(\mathbf{x}_1, y_1), \dots, (\mathbf{x}_m, y_m) \in \mathcal{X}^p \times \mathbb{R}$  such that for all  $\boldsymbol{\eta} \in \{0, 1\}^m$ , there exists  $f \in \mathcal{F}$  so that the following two arguments are equivalent:

$$f(\mathbf{x}_i) > y_i \iff \eta_i, \quad \text{for } i = 1, \dots, m.$$

Both the covering number and pseudo-dimension quantify the complexity of a given function class from different aspects. Indeed, the following results are available to establish the connections between them.

THEOREM OA.1 (THEOREM 12.2 IN ANTHONY AND BARTLETT 1999). *If  $\mathcal{F}$  is a set of real functions from a domain to a bounded interval  $[0, B]$  and the pseudo-dimension of  $\mathcal{F}$  is  $\text{Pdim}(\mathcal{F})$ , then*

$$\mathcal{N}_n(\delta, \mathcal{F}, \|\cdot\|_{\infty}) \leq \sum_{i=1}^{\text{Pdim}(\mathcal{F})} \binom{n}{i} \left(\frac{B}{\delta}\right)^i < \left(\frac{enB}{\delta \cdot \text{Pdim}(\mathcal{F})}\right)^{\text{Pdim}(\mathcal{F})},$$

for  $n \geq \text{Pdim}(\mathcal{F})$ .

## B. Supplementary Materials in Section 4

### B.1. Section 4.1: High-Probability Bound

*Proof of Lemma 1.* Define the “best” estimator  $f^*$  in the function class  $\mathcal{F}_{DNN}$  as

$$f^* = \arg \min_{f \in \mathcal{F}_{DNN}} \mathcal{R}^\rho(f).$$

We have

$$\begin{aligned} & \mathcal{R}^\rho(\hat{f}_{DNN}) - \mathcal{R}^\rho(f_\rho) \\ &= \left[ \mathcal{R}^\rho(\hat{f}_{DNN}) - \mathcal{R}_n^\rho(\hat{f}_{DNN}) \right] + \left[ \mathcal{R}_n^\rho(\hat{f}_{DNN}) - \mathcal{R}_n^\rho(f^*) \right] + [\mathcal{R}_n^\rho(f^*) - \mathcal{R}^\rho(f^*)] + [\mathcal{R}^\rho(f^*) - \mathcal{R}^\rho(f_\rho)] \\ &\leq \left[ \mathcal{R}^\rho(\hat{f}_{DNN}) - \mathcal{R}_n^\rho(\hat{f}_{DNN}) \right] + [\mathcal{R}_n^\rho(f^*) - \mathcal{R}^\rho(f^*)] + [\mathcal{R}^\rho(f^*) - \mathcal{R}^\rho(f_\rho)] \\ &\leq 2 \sup_{f \in \mathcal{F}_{DNN}} |\mathcal{R}^\rho(f) - \mathcal{R}_n^\rho(f)| + \mathcal{R}^\rho(f^*) - \mathcal{R}^\rho(f_\rho) \\ &= 2 \sup_{f \in \mathcal{F}_{DNN}} |\mathcal{R}^\rho(f) - \mathcal{R}_n^\rho(f)| + \inf_{f \in \mathcal{F}_{DNN}} [\mathcal{R}^\rho(f) - \mathcal{R}^\rho(f_\rho)], \end{aligned}$$

where the first inequality follows from the definition of  $\hat{f}_{DNN}$  as the minimizer of  $\mathcal{R}_n^\rho(f)$  in  $\mathcal{F}_{DNN}$ , the second inequality holds due to the fact that both  $\hat{f}_{DNN}$  and  $f^*$  belong to the function class  $\mathcal{F}_{DNN}$ , and the last equality is valid by the definition of  $f^*$ .  $\square$

*Proof of Theorem 1.* By definition, we know that the function space  $\mathcal{F}_{DNN}$  contains networks with the parameter  $\phi$ , depth  $\mathcal{D}$ , width  $\mathcal{W}$ , size  $\mathcal{S}$ , and number of neurons  $\mathcal{U}$  so that  $\|f_\phi\|_\infty \leq \mathcal{B}$ . Since the demand variable has a bounded domain as specified in Assumption 1, the newsvendor loss is also bounded:

$$L(f(\mathbf{x}), d) := b(d - f(\mathbf{x}))^+ + h(f(\mathbf{x}) - d)^+ \leq b\bar{D} + h\mathcal{B},$$

for any  $f \in \mathcal{F}_{DNN}$ . We can further obtain that

$$|L(f(\mathbf{X}), D) - \mathbb{E}L(f(\mathbf{X}), D)| \leq 2(b\bar{D} + h\mathcal{B}). \quad (\text{OA.1})$$

Meanwhile, it is obvious that the newsvendor loss function  $L(y, y')$  is  $\max\{b, h\}$ -Lipschitz in its both two arguments.

For any given  $\epsilon > 0$ , let  $f_1, f_2, \dots, f_{\mathcal{N}}$  be the anchor points of an  $\epsilon$ -covering for the function class  $\mathcal{F}_{DNN}$ , and we denote  $\mathcal{N} := \mathcal{N}_n(\epsilon, \mathcal{F}_{DNN}, \|\cdot\|_\infty)$  as the covering number of  $\mathcal{F}_{DNN}$  with radius  $\epsilon$  under the norm  $\|\cdot\|_\infty$ . By definition, for any  $f \in \mathcal{F}_{DNN}$ , there exists an anchor  $f_j$  for  $j \in \{1, \dots, \mathcal{N}\}$  such that  $\|f_j - f\|_\infty \leq \epsilon$ . The Lipschitz property of  $L(y, y')$  then implies  $|L(f(x), d) - L(f_j(x), d)| \leq \max\{b, h\}\epsilon$ , based on which an application of triangular inequality gives

$$\begin{aligned} |\mathcal{R}^\rho(f) - \mathcal{R}_n^\rho(f)| &\leq |\mathcal{R}^\rho(f_j) - \mathcal{R}_n^\rho(f_j)| + |\mathcal{R}^\rho(f) - \mathcal{R}^\rho(f_j)| + |\mathcal{R}_n^\rho(f_j) - \mathcal{R}_n^\rho(f)| \\ &= |\mathcal{R}^\rho(f_j) - \mathcal{R}_n^\rho(f_j)| \\ &\quad + |\mathbb{E}_{\mathbf{Z}}[L(f(\mathbf{X}), D) - L(f_j(\mathbf{X}), D)]| + \left| \frac{1}{n} \sum_{i=1}^n [L(f(\mathbf{X}_i), D_i) - L(f_j(\mathbf{X}_i), D_i)] \right| \\ &\leq |\mathcal{R}^\rho(f_j) - \mathcal{R}_n^\rho(f_j)| + 2 \max\{b, h\}\epsilon. \end{aligned} \quad (\text{OA.2})$$

Therefore, with a fixed  $t > 0$ ,

$$\begin{aligned}
\mathbb{P}\left(\sup_{f \in \mathcal{F}_{DNN}} |\mathcal{R}^\rho(f) - \mathcal{R}_n^\rho(f)| \geq t + 2 \max\{b, h\} \epsilon\right) &\stackrel{(a)}{\leq} \mathbb{P}\left(\exists j \in \{1, \dots, \mathcal{N}\} : |\mathcal{R}^\rho(f_j) - \mathcal{R}_n^\rho(f_j)| \geq t\right) \\
&\stackrel{(b)}{\leq} \mathcal{N}_n(\epsilon, \mathcal{F}_{DNN}, \|\cdot\|_\infty) \max_{j \in \{1, \dots, \mathcal{N}\}} \mathbb{P}\left(|\mathcal{R}^\rho(f_j) - \mathcal{R}_n^\rho(f_j)| \geq t\right) \\
&= \mathcal{N}_n(\epsilon, \mathcal{F}_{DNN}, \|\cdot\|_\infty) \max_{j \in \{1, \dots, \mathcal{N}\}} \mathbb{P}\left(\left|\sum_{i=1}^n L(f_j(\mathbf{X}_i), D_i) - \mathbb{E}[L(f_j(\mathbf{X}), D)]\right| \geq nt\right) \\
&\stackrel{(c)}{\leq} 2\mathcal{N}_n(\epsilon, \mathcal{F}_{DNN}, \|\cdot\|_\infty) \exp\left(-\frac{nt^2}{2(b\bar{D} + h\mathcal{B})^2}\right), \tag{OA.3}
\end{aligned}$$

where (a) holds due to (OA.2); notice that we have denoted  $\mathcal{N} := \mathcal{N}_n(\epsilon, \mathcal{F}_{DNN}, \|\cdot\|_\infty)$  in (b); and (c) comes from the Hoeffding's inequality and (OA.1).

For any  $\delta > 0$ , let  $\epsilon = 1/n$  and  $t = \sqrt{2(b\bar{D} + h\mathcal{B})} \sqrt{\log\left(2\mathcal{N}_n(1/n, \mathcal{F}_{DNN}, \|\cdot\|_\infty)/\delta\right)}/n$  so that the right-hand side of (OA.3) equals to  $\delta$ , we have

$$\mathbb{P}\left(\sup_{f \in \mathcal{F}_{DNN}} |\mathcal{R}^\rho(f) - \mathcal{R}_n^\rho(f)| \geq t + 2(b+h)\epsilon\right) \leq \delta.$$

In other words, with probability at least  $1 - \delta$ ,

$$\begin{aligned}
&\sup_{f \in \mathcal{F}_{DNN}} |\mathcal{R}^\rho(f) - \mathcal{R}_n^\rho(f)| \leq t + 2(b+h)\epsilon \\
&\stackrel{(a)}{\leq} \frac{\sqrt{2}(b\bar{D} + h\mathcal{B}) \sqrt{\log 2\mathcal{N}_n(1/n, \mathcal{F}_{DNN}, \|\cdot\|_\infty)}}{\sqrt{n}} + \frac{\sqrt{2}(b\bar{D} + h\mathcal{B}) \sqrt{\log(1/\delta)}}{\sqrt{n}} + \frac{2(b+h)}{n},
\end{aligned}$$

where we have used the inequality  $\sqrt{c+d} \leq \sqrt{c} + \sqrt{d}$  for any  $c, d \geq 0$  in (a). Furthermore, we know from Theorem OA.1 that

$$\begin{aligned}
\sup_{f \in \mathcal{F}_{DNN}} |\mathcal{R}^\rho(f) - \mathcal{R}_n^\rho(f)| &\leq \frac{\sqrt{2}(b\bar{D} + h\mathcal{B})}{\sqrt{n}} \left( C \sqrt{\log\left(\frac{en^2\bar{D}}{\text{Pdim}(\mathcal{F}_{DNN})}\right)^{\text{Pdim}(\mathcal{F}_{DNN})}} + \sqrt{\log(1/\delta)} \right) + \frac{2(b+h)}{n} \\
&\leq \frac{\sqrt{2}(b\bar{D} + h\mathcal{B})}{\sqrt{n}} \left( C \sqrt{\text{Pdim}(\mathcal{F}_{DNN}) \log(en^2\bar{D})} + \sqrt{\log(1/\delta)} \right) + \frac{2(b+h)}{n},
\end{aligned}$$

for  $n \geq \text{Pdim}(\mathcal{F}_{DNN})$ , where  $\text{Pdim}(\mathcal{F}_{DNN})$  is the pseudo-dimension of  $\mathcal{F}_{DNN}$  stated in Definition OA.2; and  $C$  is a generic constant that may have different values from time to time.

For the piecewise linear neural networks such as the ReLU network we consider in the current paper, Theorems 3 and 6 of Bartlett et al. (2019) show that there exist two universal constants  $c$  and  $C$  so that

$$c \cdot \mathcal{SD} \log(\mathcal{S}/\mathcal{D}) \leq \text{Pdim}(\mathcal{F}_{DNN}) \leq C \cdot \mathcal{SD} \log(\mathcal{S}), \tag{OA.4}$$

where  $\mathcal{S}$  and  $\mathcal{D}$  are the size and depth of the given  $\mathcal{F}_{DNN}$ , respectively; see Section 3.2 for more description. Then, with a probability of at least  $1 - \delta$ , we have

$$\begin{aligned}
\sup_{f \in \mathcal{F}_{DNN}} |\mathcal{R}^\rho(f) - \mathcal{R}_n^\rho(f)| &\leq \frac{\sqrt{2}(b\bar{D} + h\mathcal{B})}{\sqrt{n}} \left( C \sqrt{\mathcal{SD} \log(\mathcal{S}) \log(n)} + \sqrt{\log(1/\delta)} \right) + \frac{2(b+h)}{n} \\
&\stackrel{(a)}{\leq} \frac{\sqrt{2}(b\bar{D} + h\mathcal{B})}{\sqrt{n}} \left( C \sqrt{\mathcal{SD} \log(\mathcal{S}) \log(n)} + \sqrt{\log(1/\delta)} \right),
\end{aligned}$$

for  $n \geq C_1 \cdot \mathcal{SD} \log(\mathcal{S})$ , where both  $C$  and  $C_1$  are universal constants; and (a) is valid since  $\sqrt{\log(n)/n}$  decays slower than  $1/n$  and  $C$  represents a universal constant.  $\square$

*Proof of Lemma 2.* We observe the simple identity that  $x = \max\{x, 0\} - \max\{-x, 0\} =: \sigma(x) - \sigma(-x)$  for any  $x \in \mathbb{R}$ , where  $\sigma(\cdot)$  denotes the ReLU activation function. This observation leads to the result in Lemma 2.  $\square$

*Proof of Proposition 1.* For the approximation of functions in  $\mathcal{H}^\beta([0, 1]^p, B_0)$  using ReLU neural networks with the width  $\mathcal{W}$  and depth  $\mathcal{D}$  specified as below

$$\mathcal{W} = 38(\lfloor \beta \rfloor + 1)^2 p^{\lfloor \beta \rfloor + 1} N \lceil \log_2(8N) \rceil \quad \text{and} \quad \mathcal{D} = 21(\lfloor \beta \rfloor + 1)^2 M \lceil \log_2(8M) \rceil,$$

we know from Theorem 3.3 in Jiao et al. (2023) that there exists a ReLU network function  $f \in \mathcal{F}_{\mathcal{D}, \mathcal{W}, \mathcal{U}, \mathcal{S}, \mathcal{B}_{N, M}}$  so that

$$|f(\mathbf{x}) - f_\rho(\mathbf{x})| \leq 18B_0(\lfloor \beta \rfloor + 1)^2 p^{\lfloor \beta \rfloor + (\beta \vee 1)/2} (NM)^{-2\beta/p},$$

for  $\mathbf{x} \in [0, 1]^p$  except for a small set  $\Omega$  with Lebesgue measure  $\delta K p$  and  $\delta$  can be arbitrarily small, where we have added a subscript to  $\mathcal{B}_{N, M}$  to indicate the dependence of the uniform upper bound of the network function on the free parameters in the network depth and width. This is reasonable because a larger network may result in a higher upper bound for the network function. To ensure that the output is uniformly bounded within  $[-\mathcal{B}, \mathcal{B}]$ , we apply an additional truncation for  $f(\mathbf{x})$ . In fact, we observe that the function  $y = -\max\{\mathcal{B} - \max\{x, 0\}, 0\} + \max\{\mathcal{B} - \max\{-x, 0\}, 0\}$  maps any  $x \in \mathbb{R}$  to a value  $y \in [-\mathcal{B}, \mathcal{B}]$ , which corresponds a two-hidden-layer network with two neurons in each hidden layer. Therefore, we assert that there exists a ReLU network function  $\tilde{f} \in \mathcal{F}_{DNN}$ , stacked by  $f$  and this two-hidden-layer network, such that the network width remains  $\mathcal{W}$ , the network depth becomes  $\mathcal{D} + 2$ , and  $\|\tilde{f}\|_\infty \leq \mathcal{B}$ . Meanwhile, since Assumption 2 states that  $\|f_\rho\|_\infty \leq B_0 \leq \mathcal{B}$ , we can still have

$$|\tilde{f}(\mathbf{x}) - f_\rho(\mathbf{x})| \leq 18B_0(\lfloor \beta \rfloor + 1)^2 p^{\lfloor \beta \rfloor + (\beta \vee 1)/2} (NM)^{-2\beta/p},$$

for  $\mathbf{x} \in [0, 1]^p$  except a small set  $\Omega$ . Therefore, we get

$$\mathbb{E}|\tilde{f}(\mathbf{x}) - f_\rho(\mathbf{x})| \leq 18B_0(\lfloor \beta \rfloor + 1)^2 p^{\lfloor \beta \rfloor + (\beta \vee 1)/2} (NM)^{-2\beta/p} + \mathbb{P}(\Omega) \cdot \sup_{\mathbf{x} \in \Omega} \{|\tilde{f}(\mathbf{x}) - f_\rho(\mathbf{x})|\}. \quad (\text{OA.5})$$

By Assumption 2(i), the marginal distribution of  $\mathbf{X}$  is absolutely continuous with respect to the Lebesgue measure, which means that  $\liminf_{\delta \rightarrow 0} \mathbb{P}(\Omega) = 0$ .

Furthermore, since both  $\|\tilde{f}\|_\infty$  and  $\|f_\rho\|_\infty$  are bounded, taking limit infimum with respect to  $\delta$  on both sides of (OA.5) leads to

$$\mathbb{E}|\tilde{f}(\mathbf{x}) - f_\rho(\mathbf{x})| \leq 18B_0(\lfloor \beta \rfloor + 1)^2 p^{\lfloor \beta \rfloor + (\beta \vee 1)/2} (NM)^{-2\beta/p}.$$

As the newsvendor loss function is  $\max\{b, h\}$ -Lipschitz, it holds that

$$\mathcal{R}^\rho(\tilde{f}) - \mathcal{R}^\rho(f_\rho) \leq \max\{b, h\} \mathbb{E}|\tilde{f}(\mathbf{x}) - f_\rho(\mathbf{x})| \leq 18 \max\{b, h\} B_0(\lfloor \beta \rfloor + 1)^2 p^{\lfloor \beta \rfloor + (\beta \vee 1)/2} (NM)^{-2\beta/p}.$$

The conclusion in Proposition 1 is then valid since

$$\inf_{f \in \mathcal{F}_{DNN}} [\mathcal{R}^\rho(f) - \mathcal{R}^\rho(f_\rho)] \leq \mathcal{R}^\rho(\tilde{f}) - \mathcal{R}^\rho(f_\rho),$$

and we finish the proof.  $\square$

In fact, the approximation rate in Proposition 1 can be further accelerated once the excess risk has a desirable local quadratic structure.

**PROPOSITION OA.1.** *Let  $\mathcal{F}_{DNN}$  be the class of ReLU neural networks with the width and depth, respectively, specified as*

$$\mathcal{W} = 38(\lfloor \beta \rfloor + 1)^2 p^{\lfloor \beta \rfloor + 1} N \lceil \log_2(8N) \rceil \text{ and } \mathcal{D} = 21(\lfloor \beta \rfloor + 1)^2 M \lceil \log_2(8M) \rceil,$$

where  $\lceil a \rceil$  denotes the smallest integer that is no less than  $a$ . Under Assumption 2 and 3, for any  $M, N \in \mathbb{N}_+$ , we have

$$\inf_{f \in \mathcal{F}_{DNN}} [\mathcal{R}^\rho(f) - \mathcal{R}^\rho(f_\rho)] \leq 324\tilde{c} \max\{b, h\}^2 B_0^2(\lfloor \beta \rfloor + 1)^4 p^{2\lfloor \beta \rfloor + \beta \vee 1} (NM)^{-4\beta/p},$$

where  $a \vee b = \max\{a, b\}$  and  $\tilde{c} = \max\{\max\{b, h\}/\delta_\rho^0, c_\rho^0\}$ .

*Proof of Proposition OA.1.* The key observation is that

$$\inf_{f \in \mathcal{F}_{DNN}} [\mathcal{R}^\rho(f) - \mathcal{R}^\rho(f_\rho)] \leq \max\left\{\frac{\max\{b, h\}}{\delta_\rho^0}, c_\rho^0\right\} \inf_{f \in \mathcal{F}_{DNN}} \|f - f_\rho\|_{L^2(\nu)}^2, \quad (\text{OA.6})$$

and the remaining proof can be similarly conducted as in the proof of Proposition 1.

To prove (OA.6), we first notice that

$$\mathcal{R}^\rho(f) - \mathcal{R}^\rho(f_\rho) = \mathbb{E}[L(f(\mathbf{X}), D) - L(f_\rho(\mathbf{X}), D)] \leq \max\{b, h\} \mathbb{E}[|f(\mathbf{X}) - f_\rho(\mathbf{X})|],$$

where  $L(f(\mathbf{x}), d) := b(d - f(\mathbf{x}))^+ + h(f(\mathbf{x}) - d)^+$  is  $\max\{b, h\}$ -Lipschitz. Therefore, if  $\|f - f_\rho\|_{L^\infty(\mathcal{X}^0)} > \delta_\rho^0$ , we have

$$\mathcal{R}^\rho(f) - \mathcal{R}^\rho(f_\rho) \leq \max\{b, h\} \mathbb{E}[|f(\mathbf{X}) - f_\rho(\mathbf{X})|] \leq \max\{b, h\} \mathbb{E}\left[\frac{|f(\mathbf{X}) - f_\rho(\mathbf{X})|^2}{\delta_\rho^0}\right]$$

On the other hand, if  $\|f - f_\rho\|_{L^\infty(\mathcal{X}^0)} \leq \delta_\rho^0$ , Assumption 3 tells that  $\mathcal{R}^\rho(f) - \mathcal{R}^\rho(f_\rho) \leq c_\rho^0 \|f - f_\rho\|_{L^2(\nu)}^2$ . Combining these two cases, we have (OA.6).  $\square$

*Proof of Theorem 2.* Combining Lemma 1, Theorem 1, and Proposition OA.1, the following inequality holds for at least probability  $1 - \delta$ ,

$$\mathcal{R}^\rho(\hat{f}_{DNN}) - \mathcal{R}^\rho(f_\rho) \leq 2\sqrt{2}(b\bar{D} + h\mathcal{B}) \left( C_1 \sqrt{\frac{\mathcal{SD} \log(\mathcal{S}) \log(n)}{n}} + \sqrt{\frac{\log(1/\delta)}{n}} \right) \quad (\text{OA.7})$$

$$+ 18 \max\{b, h\} B_0(\lfloor \beta \rfloor + 1)^2 p^{\lfloor \beta \rfloor + (\beta \vee 1)/2} (NM)^{-2\beta/p}, \quad (\text{OA.8})$$

where  $n \geq C \cdot \mathcal{SD} \log(\mathcal{S})$  for a large enough  $C > 0$  and  $M, N \in \mathbb{N}_+$ . To balance these two error terms, we choose proper tuning parameters  $M$  and  $N$  to optimize the convergence rate in the sample size. We assume that  $M = \lfloor n^{t_1} \rfloor$  and  $N = \lfloor n^{t_2} \rfloor$  with  $t_1, t_2 \geq 0$  to be determined later. Then, we have

$$\mathcal{W} = 38(\lfloor \beta \rfloor + 1)^2 p^{\lfloor \beta \rfloor + 1} N \lceil \log_2(8N) \rceil = O(n^{t_2}),$$

$$\mathcal{D} = 21(\lfloor \beta \rfloor + 1)^2 M \lceil \log_2(8M) \rceil = O(n^{t_1}),$$

and

$$\begin{aligned} \mathcal{S} &= w_1(w_0 + 1) + \sum_{i=1}^{\mathcal{D}-1} w_{i+1}(w_i + 1) + w_{\mathcal{D}+1}(w_{\mathcal{D}} + 1) \\ &\leq \mathcal{W}(p+1) + (\mathcal{W}^2 + \mathcal{W})(\mathcal{D}-1) + \mathcal{W} + 1 \\ &= O(\mathcal{W}^2 \mathcal{D}) = O(n^{2t_2 + t_1}), \end{aligned}$$

where we have deliberately neglected those  $\log(n)$  factors here since we are mainly interested in the convergence order in  $n$ , and Schmidt-Hieber (2020) also pointed out that they are more likely artifacts in the proofs related to the high-dimensional statistics. We then check the orders of the two error terms (neglecting those  $\log(n)$  factors) in the excess risk bound:

$$(\text{OA.7}) = O\left(\sqrt{\frac{\mathcal{SD}}{n}}\right) = O(n^{t_1 + t_2 - 1/2}) \quad \text{and} \quad (\text{OA.8}) = O((MN)^{-2\beta/p}) = O(n^{-2(t_1 + t_2)\beta/p}).$$

Let  $t_1 + t_2 - 1/2 = -2t\beta/p$ , we obtain  $t_1 + t_2 = \frac{p}{2p+4\beta}$ . Plugging it back into the relevant expressions above and letting  $C$  be a generic constant whose value may change in different scenarios, we get

$$\begin{aligned} \mathcal{SD} &\leq C\mathcal{W}^2 \mathcal{D}^2 \leq C t_1^2 t_2^2 (\lfloor \beta \rfloor + 1)^8 p^{2(\lfloor \beta \rfloor + 1)} n^{\frac{p}{p+2\beta}} \log_2(n) \\ &\leq C \left(\frac{p}{2p+4\beta}\right)^2 (\lfloor \beta \rfloor + 1)^8 p^{2(\lfloor \beta \rfloor + 1)} n^{\frac{p}{p+2\beta}} \log_2(n) \\ &\leq C (\lfloor \beta \rfloor + 1)^8 p^{2(\lfloor \beta \rfloor + 1)} n^{\frac{p}{p+2\beta}} \log_2(n). \end{aligned}$$

Therefore, with probability  $1 - \delta$ ,

$$\begin{aligned} \mathcal{R}^\rho(\hat{f}_{DNN}) - \mathcal{R}^\rho(f_\rho) &\leq 2\sqrt{2}(b\bar{D} + h\mathcal{B}) \left( C(\lfloor \beta \rfloor + 1)^4 p^{\lfloor \beta \rfloor + 1} (\log(n))^2 n^{-\frac{\beta}{2\beta+p}} + \sqrt{\frac{\log(1/\delta)}{n}} \right) \\ &\quad + 18 \max\{b, h\} B_0(\lfloor \beta \rfloor + 1)^2 p^{\lfloor \beta \rfloor + 1} n^{-\frac{\beta}{2\beta+p}} \\ &\leq 2\sqrt{2}(b\bar{D} + h\mathcal{B}) \left( C(\lfloor \beta \rfloor + 1)^4 p^{\lfloor \beta \rfloor + 1} (\log(n))^2 n^{-\frac{\beta}{2\beta+p}} + \sqrt{\frac{\log(1/\delta)}{n}} \right), \end{aligned}$$



for  $n$  large enough. Finally, we notice that the stochastic error bound is valid only when  $n \geq C \cdot \mathcal{SD} \log(\mathcal{S})$ . Under the current setting of  $\mathcal{S}$  and  $\mathcal{D}$ , we know that  $\mathcal{SD} \log(\mathcal{S})$  grows slower than  $n$ . This condition then holds when  $n$  is large enough.  $\square$

Using similar arguments, the rate can be slightly improved to  $O(n^{-\frac{2\beta}{4\beta+p}})$  with the addition of Assumption 3.

**THEOREM OA.2.** *Let the network width and depth be defined according to (8) with  $NM = \lfloor n^{\frac{p}{2p+4\beta}} \rfloor$ . Under Assumptions 1, 2, and 3 and for all  $n \geq C \cdot \mathcal{SD} \log(\mathcal{S})$ , where  $C > 0$  is sufficiently large, with probability at least  $1 - \delta$  over the random draw of  $\mathbf{S}_n$ , we have*

$$\mathcal{R}^\rho(\hat{f}_{DNN}) - \mathcal{R}^\rho(f_\rho) \leq 2\sqrt{2}(b\bar{D} + h\mathcal{B}) \left( C_1(\lfloor \beta \rfloor + 1)^4 p^{3\lfloor \beta \rfloor + 1} (\log(n))^2 n^{-\frac{2\beta}{4\beta+p}} + \sqrt{\frac{\log(1/\delta)}{n}} \right),$$

where  $C_1 > 0$  is an independent universal constant.

## B.2. Section 4.2: Sharper Bound in Expectation

To prove Theorem 3, we need to resort to a different risk decomposition to that in Lemma 1. Nevertheless, the general rationale and procedure are similar to the proofs in Theorem 1, Proposition 1, and Theorem 2.

**LEMMA OA.1.** *The expected excess risk of the ERM  $\hat{f}_{DNN}$  satisfies*

$$\mathbb{E} \left[ \mathcal{R}^\rho(\hat{f}_{DNN}) - \mathcal{R}^\rho(f_\rho) \right] \leq \underbrace{\mathbb{E} \left[ \mathcal{R}^\rho(\hat{f}_{DNN}) - 2\mathcal{R}_n^\rho(\hat{f}_{DNN}) + \mathcal{R}^\rho(f_\rho) \right]}_{\text{stochastic error}} + 2 \underbrace{\inf_{f \in \mathcal{F}_{DNN}} \{ \mathcal{R}^\rho(f) - \mathcal{R}^\rho(f_\rho) \}}_{\text{approximation error}}.$$

*Proof of Lemma OA.1.* For any  $f \in \mathcal{F}_{DNN}$ ,

$$\begin{aligned} \mathbb{E}[\mathcal{R}^\rho(\hat{f}_{DNN}) - \mathcal{R}^\rho(f_\rho)] &\stackrel{(a)}{\leq} \mathbb{E}[\mathcal{R}^\rho(\hat{f}_{DNN}) - \mathcal{R}^\rho(f_\rho)] + 2\mathbb{E}[\mathcal{R}_n^\rho(f) - \mathcal{R}_n^\rho(\hat{f}_{DNN})] \\ &= \mathbb{E}[\mathcal{R}^\rho(\hat{f}_{DNN}) - 2\mathcal{R}_n^\rho(\hat{f}_{DNN}) + \mathcal{R}^\rho(f_\rho)] + 2\mathbb{E}[\mathcal{R}_n^\rho(f) - \mathcal{R}^\rho(f_\rho)] \\ &= \mathbb{E}[\mathcal{R}^\rho(\hat{f}_{DNN}) - 2\mathcal{R}_n^\rho(\hat{f}_{DNN}) + \mathcal{R}^\rho(f_\rho)] + 2(\mathcal{R}^\rho(f) - \mathcal{R}^\rho(f_\rho)), \end{aligned}$$

where (a) holds due to the definition of the empirical risk minimizer  $\hat{f}_{DNN}$  so that  $\mathcal{R}_n^\rho(\hat{f}_{DNN}) \leq \mathcal{R}_n^\rho(f)$  for any  $f \in \mathcal{F}_{DNN}$ ; and (b) is true because  $(\mathbf{X}_i, D_i)$  for  $i = 1, \dots, n$  are i.i.d.. Since the inequality holds for any  $f \in \mathcal{F}_{DNN}$ , we have

$$\mathbb{E}[\mathcal{R}^\rho(\hat{f}_{DNN}) - \mathcal{R}^\rho(f_\rho)] \leq \mathbb{E} \left[ \mathcal{R}^\rho(\hat{f}_{DNN}) - 2\mathcal{R}_n^\rho(\hat{f}_{DNN}) + \mathcal{R}^\rho(f_\rho) \right] + 2 \inf_{f \in \mathcal{F}_{DNN}} \{ \mathcal{R}^\rho(f) - \mathcal{R}^\rho(f_\rho) \}.$$

This completes the proof.  $\square$

Although the risk decomposition in Lemma OA.1 differs from Lemma 1, we choose to use the same terminologies with a slight abuse of notation. Still, the stochastic error is mainly incurred by random realizations, and the approximation error is caused by the representation of the target function using a DNN.

**THEOREM OA.3.** *Under Assumption 1, for  $n \geq C \cdot \mathcal{SD} \log(\mathcal{S})$  for a large enough  $C > 0$ , the ERM  $\hat{f}_{DNN}$  satisfies*

$$\mathbb{E} \left[ \mathcal{R}^\rho(\hat{f}_{DNN}) - 2\mathcal{R}_n^\rho(\hat{f}_{DNN}) + \mathcal{R}^\rho(f_\rho) \right] \leq \frac{C \log(n) \mathcal{SD} \log(\mathcal{S})}{n},$$

where  $C > 0$  is a universal constant.

*Proof of Theorem OA.3.* We first notice that the expectation operator in the stochastic error  $\mathbb{E} \left[ \mathcal{R}^\rho(\hat{f}_{DNN}) - 2\mathcal{R}_n^\rho(\hat{f}_{DNN}) + \mathcal{R}^\rho(f_\rho) \right]$  is taken with respect to the random samples  $\mathbf{S} = \{(\mathbf{X}_i, D_i)\}_{i=1}^n$ , based on which the ERM  $\hat{f}_{DNN}$  is obtained within the function class  $\mathcal{F}_{DNN}$ . Let  $\mathbf{S}' = \{(\mathbf{X}'_i, D'_i)\}_{i=1}^n$  be another set of samples independent of  $\mathbf{S}$ . For any  $f \in \mathcal{F}_{DNN}$  and  $\mathbf{X}_i \in \mathcal{X}$ , define

$$g(f, \mathbf{X}_i) := \mathbb{E}_{D|\mathbf{X}} \left[ L(f(\mathbf{X}_i), D_i) - L(f_\rho(\mathbf{X}_i), D_i) \middle| \mathbf{X}_i \right], \quad (\text{OA.9})$$

where  $L(f(\mathbf{x}), d) := b(d - f(\mathbf{x}))^+ + h(f(\mathbf{x}) - d)^+$ . By definition, we can rewrite the stochastic error in terms of the newly defined function  $g$  as below:

$$\begin{aligned} & \mathbb{E} \left[ \mathcal{R}^\rho(\hat{f}_{DNN}) - 2\mathcal{R}_n^\rho(\hat{f}_{DNN}) + \mathcal{R}^\rho(f_\rho) \right] \\ &= \mathbb{E}_{\mathbf{S}} \left[ \mathbb{E}_{\mathbf{S}'} [L(\hat{f}_{DNN}(\mathbf{X}'), D')] - \frac{2}{n} \sum_{i=1}^n [L(\hat{f}_{DNN}(\mathbf{X}_i), D_i)] + L(f_\rho(\mathbf{X}), D) \right] \\ &\stackrel{(a)}{=} \mathbb{E}_{\mathbf{S}} \left[ \mathbb{E}_{\mathbf{S}'} [L(\hat{f}_{DNN}(\mathbf{X}'), D')] - \mathbb{E}_{\mathbf{S}'} [L(f_\rho(\mathbf{X}'), D')] - \frac{2}{n} \sum_{i=1}^n \left( L(\hat{f}_{DNN}(\mathbf{X}_i), D_i) - L(f_\rho(\mathbf{X}_i), D_i) \right) \right] \\ &= \mathbb{E}_{\mathbf{S}} \left[ \frac{1}{n} \sum_{i=1}^n \left( \mathbb{E}_{\mathbf{S}'} [g(\hat{f}_{DNN}, \mathbf{X}'_i)] - 2g(\hat{f}_{DNN}, \mathbf{X}_i) \right) \right], \end{aligned} \quad (\text{OA.10})$$

where in (a), we have used the facts that  $\mathcal{R}^\rho(f_\rho)$  is not sample-dependent (so that  $\mathcal{R}^\rho(f_\rho) = \mathbb{E}_{\mathbf{S}}[\mathcal{R}^\rho(f_\rho)] = \mathbb{E}_{\mathbf{S}}\mathbb{E}_{\mathbf{S}'}[\mathcal{R}^\rho(f_\rho)]$ ) and  $\mathbf{S}_i := (\mathbf{X}_i, D_i)$  are i.i.d..

To bound (OA.10), we notice the fact that for any random variable  $W$ , it holds that  $\mathbb{E}[W] \leq \mathbb{E}[\max\{W, 0\}] = \int_0^\infty \mathbb{P}(W > t) dt$ . Therefore, it suffices to derive the upper bound for its tail probability. In fact, since  $\hat{f}_{DNN} \in \mathcal{F}_{DNN}$ , we have

$$\begin{aligned} & \mathbb{P} \left( \frac{1}{n} \sum_{i=1}^n \left( \mathbb{E}_{\mathbf{S}'} [g(\hat{f}_{DNN}, \mathbf{X}'_i)] - 2g(\hat{f}_{DNN}, \mathbf{X}_i) \right) > t \right) \\ & \leq \mathbb{P} \left( \exists f \in \mathcal{F}_{DNN} : \frac{1}{n} \sum_{i=1}^n \left( \mathbb{E}_{\mathbf{S}'} [g(f, \mathbf{X}'_i)] - 2g(f, \mathbf{X}_i) \right) > t \right) \\ & \stackrel{(a)}{=} \mathbb{P} \left( \exists f \in \mathcal{F}_{DNN} : \mathbb{E}[g(f, \mathbf{X})] - \frac{2}{n} \sum_{i=1}^n [g(f, \mathbf{X}_i)] > t \right), \end{aligned} \quad (\text{OA.11})$$

where (a) holds because  $\mathbf{S}$  and  $\mathbf{S}'$  are i.i.d.. Since  $L(y, y')$  is a  $\max\{b, h\}$ -Lipschitz function, we know from (OA.9) that

$$g(f, \mathbf{X}_i) \leq \max\{b, h\} \|f - f_\rho\|_\infty \leq \max\{b, h\} (\mathcal{B} + \bar{D}),$$

where the last inequality is valid since  $f_\rho$  is a conditional quantile function, which has the same range as  $D$ , i.e.,  $0 \leq f_\rho \leq \bar{D}$ . On the other hand, given any  $\mathbf{X}_i$ , the conditional quantile function  $f_\rho$  should minimize  $\mathbb{E}_{D|\mathbf{X}}[L(f(\mathbf{X}), D)]$  by the definitions in (3) and (4), implying that  $g(f, X_i) \geq 0$ . Consequently, we have  $g(f, \cdot) \in [0, \max\{b, h\}(\mathcal{B} + \bar{D})]$  for all  $f \in \mathcal{F}_{DNN}$ . Then, one can exactly follow the proof of Theorem 11.6 in Györfi et al. (2002) to derive the inequality below, whose tedious proof is omitted here but can be provided upon request:

$$\mathbb{P}\left(\sup_{f \in \mathcal{F}_{DNN}} \frac{\mathbb{E}[g(f, \mathbf{X})] - \frac{1}{n} \sum_{i=1}^n [g(f, \mathbf{X}_i)]}{s + \mathbb{E}[g(f, \mathbf{X})] + \frac{1}{n} \sum_{i=1}^n [g(f, \mathbf{X}_i)]} > \epsilon\right) \leq 4\mathcal{N}_n\left(\frac{s\epsilon}{16}, \mathcal{G}, \|\cdot\|_\infty\right) \exp\left(-\frac{\epsilon^2 sn}{15 \max\{b, h\}(\mathcal{B} + \bar{D})}\right), \quad (\text{OA.12})$$

where the function class  $\mathcal{G}$  is induced by  $\mathcal{F}_{DNN}$  via  $\mathcal{G} := \{g(f, \mathbf{x}) : f \in \mathcal{F}_{DNN}\}$ . We then have

$$\begin{aligned} & \mathbb{P}\left(\exists f \in \mathcal{F}_{DNN} : \mathbb{E}[g(f, \mathbf{X})] - \frac{2}{n} \sum_{i=1}^n [g(f, \mathbf{X}_i)] > t\right) \\ & \stackrel{(a)}{\leq} \mathbb{P}\left(\sup_{f \in \mathcal{F}_{DNN}} \left\{ \frac{\mathbb{E}[g(f, \mathbf{X})] - \frac{1}{n} \sum_{i=1}^n [g(f, \mathbf{X}_i)]}{2t + \mathbb{E}[g(f, \mathbf{X})] + \frac{1}{n} \sum_{i=1}^n [g(f, \mathbf{X}_i)]} \right\} > \frac{1}{3}\right) \\ & \stackrel{(b)}{\leq} 4\mathcal{N}_n\left(\frac{t}{24}, \mathcal{G}, \|\cdot\|_\infty\right) \exp\left(-\frac{2tn}{135 \max\{b, h\}(\mathcal{B} + \bar{D})}\right), \end{aligned} \quad (\text{OA.13})$$

where (a) holds since when an event A implies an event B,  $\mathbb{P}(A) \leq \mathbb{P}(B)$ ; and (b) is valid by choosing  $\epsilon = 1/3$  and  $s = 2t > 0$  in (OA.12).

Combining (OA.11) and (OA.13), for any truncating sequence  $a_n > 1/n$ , we have

$$\begin{aligned} & \mathbb{E}_{\mathbf{S}} \left[ \frac{1}{n} \sum_{i=1}^n \left( \mathbb{E}_{\mathbf{S}'} [g(\hat{f}_{DNN}, \mathbf{X}'_i)] - 2g(\hat{f}_{DNN}, \mathbf{X}_i) \right) \right] \\ & \leq \int_0^\infty \mathbb{P}\left(\frac{1}{n} \sum_{i=1}^n \left( \mathbb{E}_{\mathbf{S}'} [g(\hat{f}_{DNN}, \mathbf{X}'_i)] - 2g(\hat{f}_{DNN}, \mathbf{X}_i) \right) > t\right) dt \\ & \leq \int_0^{a_n} 1 dt + \int_{a_n}^\infty 4\mathcal{N}_n\left(\frac{t}{24}, \mathcal{G}, \|\cdot\|_\infty\right) \exp\left(-\frac{2tn}{135 \max\{b, h\}(\mathcal{B} + \bar{D})}\right) dt \\ & \stackrel{(a)}{\leq} a_n + 4\mathcal{N}_n\left(\frac{1}{24n}, \mathcal{G}, \|\cdot\|_\infty\right) \int_{a_n}^\infty \exp\left(-\frac{2tn}{135 \max\{b, h\}(\mathcal{B} + \bar{D})}\right) dt \\ & = a_n + 4\mathcal{N}_n\left(\frac{1}{24n}, \mathcal{G}, \|\cdot\|_\infty\right) \exp\left(-\frac{2a_n n}{135 \max\{b, h\}(\mathcal{B} + \bar{D})}\right) \frac{135 \max\{b, h\}(\mathcal{B} + \bar{D})}{2n}, \end{aligned}$$

where (a) holds because  $\mathcal{N}_n(\delta, \mathcal{G}, \|\cdot\|_\infty)$  is decreasing in  $\delta$  and  $a_n > \frac{1}{n}$ . We can then choose  $a_n := \log\left(4\mathcal{N}_n(1/(24n), \mathcal{G}, \|\cdot\|_\infty)\right) \frac{135 \max\{b, h\}(\mathcal{B} + \bar{D})}{2n}$  to obtain

$$\begin{aligned} \mathbb{E}_{\mathbf{S}} \left( \frac{1}{n} \sum_{i=1}^n \left[ \mathbb{E}_{\mathbf{S}'} \{g(\hat{f}_{DNN}, X'_i)\} - 2g(\hat{f}_{DNN}, X_i) \right] \right) & \leq a_n + \frac{135 \max\{b, h\}(\mathcal{B} + \bar{D})}{2n} \\ & = \frac{135 \max\{b, h\}(\mathcal{B} + \bar{D}) \log\left(4e\mathcal{N}_n\left(\frac{1}{24n}, \mathcal{G}, \|\cdot\|_\infty\right)\right)}{2n}. \end{aligned}$$

For any  $f_1, f_2 \in \mathcal{F}_{DNN}$ , by the definition of  $g$  in (OA.9) and its Lipschitz property, one can easily see that  $\|g(f_1, \cdot) - g(f_2, \cdot)\|_\infty \leq \max\{b, h\}\|f_1 - f_2\|_\infty$  and therefore,  $\mathcal{N}_n(1/(24n), \mathcal{G}, \|\cdot\|_\infty) \leq \mathcal{N}_n(1/(24 \max\{b, h\}n), \mathcal{F}_{DNN}, \|\cdot\|_\infty)$ . By Theorem OA.1 and (OA.4), we then have

$$\begin{aligned} & \mathbb{E}_{\mathbf{S}} \left[ \frac{1}{n} \sum_{i=1}^n \left( \mathbb{E}_{\mathbf{S}'} [g(\hat{f}_{DNN}, \mathbf{X}'_i)] - 2g(\hat{f}_{DNN}, \mathbf{X}_i) \right) \right] \\ & \leq \frac{135 \max\{b, h\}(\mathcal{B} + \bar{D}) \log \left( 4e \mathcal{N}_n \left( \frac{1}{24 \max\{b, h\}n}, \mathcal{F}_{DNN}, \|\cdot\|_\infty \right) \right)}{2n} \\ & \leq \frac{135 \max\{b, h\}(\mathcal{B} + \bar{D}) \left[ \log(4e) + \text{Pdim}(\mathcal{F}_{DNN}) \log(24en^2 \bar{D} \max\{b, h\}) \right]}{n} \\ & \leq \frac{135 \max\{b, h\}(\mathcal{B} + \bar{D}) \left[ \log(4e) + C \mathcal{S} \mathcal{D} \log(\mathcal{S}) \log(24en^2 \bar{D} \max\{b, h\}) \right]}{n} \\ & \leq \frac{C \log(n) \mathcal{S} \mathcal{D} \log(\mathcal{S})}{n}, \end{aligned}$$

for  $n \geq \text{Pdim}(\mathcal{F}_{DNN})$ , where  $\text{Pdim}(\mathcal{F}_{DNN})$  is the pseudo-dimension of  $\mathcal{F}_{DNN}$ ,  $\mathcal{S}$  and  $\mathcal{D}$  are the size and depth of the given  $\mathcal{F}_{DNN}$ , and  $C$  is a universal constant.

To conclude, we have established that for  $n \geq \text{Pdim}(\mathcal{F}_{DNN})$ ,

$$\mathbb{E} \left[ \mathcal{R}^\rho(\hat{f}_{DNN}) - 2\mathcal{R}_n^\rho(\hat{f}_{DNN}) + \mathcal{R}^\rho(f_\rho) \right] \leq \frac{C \log(n) \mathcal{S} \mathcal{D} \log(\mathcal{S})}{n},$$

where  $C > 0$  is a universal constant. This completes the proof.  $\square$

The upper bound for the approximation error is the same as that in Proposition OA.1 since they share the same definition. Therefore, we can prove Theorem 3 as follows.

*Proof of Theorem 3.* Under Assumption 3, we know from Proposition OA.1 that

$$\inf_{f \in \mathcal{F}_{DNN}} [\mathcal{R}^\rho(f) - \mathcal{R}^\rho(f_\rho)] \leq 324\tilde{c} \max\{b, h\}^2 B_0^2(\lfloor \beta \rfloor + 1)^4 p^{2\lfloor \beta \rfloor + \beta \vee 1} (NM)^{-4\beta/p},$$

where  $\tilde{c} = \max\{\max\{b, h\}/\delta_\rho^0, c_\rho^0\}$ ,  $N$  and  $M$  are two positive integers, and  $\mathcal{W} = 38(\lfloor \beta \rfloor + 1)^2 p^{\lfloor \beta \rfloor + 1} N \lceil \log_2(8N) \rceil$  and  $\mathcal{D} = 21(\lfloor \beta \rfloor + 1)^2 M \lceil \log_2(8M) \rceil$ . Therefore, Lemma OA.1 and Theorem OA.3 imply that

$$\mathbb{E} \left[ \mathcal{R}^\rho(\hat{f}_{DNN}) - \mathcal{R}^\rho(f_\rho) \right] \leq \frac{C \log(n) \mathcal{S} \mathcal{D} \log(\mathcal{S})}{n} + 648\tilde{c} \max\{b, h\}^2 B_0^2(\lfloor \beta \rfloor + 1)^4 p^{2\lfloor \beta \rfloor + \beta \vee 1} (NM)^{-4\beta/p}.$$

We want to find the optimal convergence rate in the sample size  $n$  by tuning parameters  $N$  and  $M$ . Following a similar argument as in the proof of Theorem 2, we can choose  $NM = \lfloor n^{\frac{p}{2p+4\beta}} \rfloor$  to reach the optimal rate. Under this setting, we also have

$$\mathcal{S} \mathcal{D} \leq C n^{\frac{p}{p+2\beta}} (\log(n))^2.$$

Therefore,

$$\begin{aligned} \mathbb{E} \left[ \mathcal{R}^\rho(\hat{f}_{DNN}) - \mathcal{R}^\rho(f_\rho) \right] &\leq \frac{C(\log(n))^4 n^{\frac{p}{p+2\beta}}}{n} + Cn^{-\frac{2\beta}{p+2\beta}} \\ &\leq C(\log(n))^4 n^{-\frac{2\beta}{p+2\beta}}, \end{aligned}$$

where  $C$  is a universal constant depending on the model parameters.  $\square$

*Proof of Theorem 4.* The proof is conducted in the following way. We first construct a finite subset of the target function space, then reduce the problem to multiple hypothesis testing, and finally establish the lower bound by applying Fano's inequality (Scarlett and Cevher 2019). We can rewrite the demand-feature model as a nonparametric quantile regression problem  $D = f_\rho(\mathbf{X}) + \epsilon$ , where  $D \in \mathbb{R}$  is the response (demand),  $\mathbf{X} \in \mathcal{X}$  is a  $p$ -dimensional vector of predictors (features), and  $\epsilon$  is an unobservable random variable that may depend on  $\mathbf{X}$ . Moreover, it satisfies that  $\mathbb{E}\{|\epsilon| \mid \mathbf{X}\} < \infty$  and its  $\rho$ -th conditional quantile given  $\mathbf{X}$  is zero. According to Assumption 2, the function  $f_\rho : \mathcal{X} \rightarrow \mathbb{R}$  is Hölder continuous of order  $\beta > 0$ , namely,  $f_\rho \in \mathcal{H}^\beta([0, 1]^p, B_0)$ . Indeed, this consists of our target function space.

The first step can be conducted using the Varshamov-Gilbert lemma (see, e.g., Lemma D.2 of Lu et al. 2021). Specifically, for any positive integer  $m$  satisfying  $m^p \geq 8$ , there exists a subset  $\mathcal{V} = \{v^{(0)}, \dots, v^{(2^{m^p/8})}\}$  of  $m^p$ -dimensional hypercube  $\{0, 1\}^{m^p}$  such that  $v^{(0)} = (0, \dots, 0)$  and the  $\ell_1$  distance between every two elements is larger than  $m^p/8$ , i.e.,

$$\sum_{i=1}^{m^p} \|v_i^{(j)} - v_i^{(k)}\|_1 \geq \frac{m^p}{8}, \quad \text{for all } 0 \leq j \neq k \leq 2^{m^p/8}.$$

In a similar vein to the proof of Theorem D.1 in Lu et al. (2021), we consider a simple  $C^\infty$  bump function supported on  $[0, 1]^d$  defined by

$$g(\mathbf{x}) = \prod_{i=1}^p h(x_i), \quad \text{for } \mathbf{x} = (x_1, \dots, x_p),$$

where  $h : \mathbb{R} \rightarrow \mathbb{R}$  is a positive integrable function in  $C^\infty(\mathbb{R})$ . We then construct multiple hypotheses on the regular grid  $(\mathbf{x}^{(j)}, j \in [m]^p)$  by

$$f_k(\mathbf{x}) = \sum_{j \in [m]^p} v_j^{(k)} \frac{\omega}{m^{\beta+p/2}} g(m(\mathbf{x} - \mathbf{x}^{(j)})), \quad k = 1, 2, \dots, 2^{m^p/8},$$

where  $\omega$  is a constant to be determined later. One can easily check that  $f_k$  is  $\beta$ -Hölder smooth and

$$\frac{C_1 \cdot \omega}{m^{2\beta}} \leq \|f_i - f_k\|_2^2 = \frac{C \cdot \omega}{m^{2\beta+p}} \sum_{j \in [m]^p} |v_j^{(i)} - v_j^{(k)}|_1 \leq \frac{C_2 \cdot \omega}{m^{2\beta}}, \quad \text{for } 1 \leq i \neq k \leq 2^{m^p/8}, \quad (\text{OA.14})$$

where  $C, C_1$  and  $C_2$  are universal constants.

Next, we reduce the problem to multiple hypothesis testing. Let  $V$  be a random index uniformly drawn from the set  $\{1, \dots, 2^{m^p/8}\}$ , and  $\mathbf{S}_n = \{(\mathbf{X}_i, D_i)\}_{i=1}^n$  be the random samples drawn from the distribution  $P_V$  associated with the model  $D = f_V(\mathbf{X}) + \epsilon$  for  $V \in \{1, \dots, 2^{m^p/8}\}$ . We remark that although the data-generating process could be different depending on the realization of  $V$ , the random variable  $\epsilon$  is fixed so that the distributional properties assumed in Theorem 4 are shared among these models. For any estimator  $\hat{f}_n$  based on the sample  $\mathbf{S}_n = \{(\mathbf{X}_i, D_i)\}_{i=1}^n$ , we further denote  $\hat{V}$  as the index corresponding to the closest  $f_j$  to  $\hat{f}_n$  in terms of the metric  $\|\cdot\|_2$ , i.e.,  $\hat{V} = \arg \min_{v=1, \dots, 2^{m^p/8}} \|f_v - \hat{f}_n\|_2$ . Using the triangle inequality and (OA.14), if  $\|f_V - \hat{f}_n\|_2^2 < \epsilon/2$  with  $\epsilon := C_1 \cdot \omega/m^{2\beta}$ , we can claim that  $\hat{V} = V$  because for any  $j \neq V$ ,

$$\|f_j - \hat{f}_n\|_2^2 \geq \|f_j - f_V\|_2^2 - \|f_V - \hat{f}_n\|_2^2 \geq \epsilon - \epsilon/2 = \epsilon/2.$$

Therefore, we have  $\mathbb{P}(\|f_V - \hat{f}_n\|_2^2 < \epsilon/2) \leq \mathbb{P}(\hat{V} = V)$ , implying that

$$\mathbb{P}(\|f_V - \hat{f}_n\|_2^2 \geq \epsilon/2) \geq \mathbb{P}(\hat{V} \neq V).$$

We then know that

$$\begin{aligned} \sup_{f_\rho \in \mathcal{H}^\beta([0,1]^p, B_0)} \mathbb{E} \|\hat{f}_n - f_\rho\|_2^2 &\stackrel{(a)}{\geq} \sup_{f_\rho \in \mathcal{H}^\beta([0,1]^p, B_0)} \epsilon \times \mathbb{P}(\|\hat{f}_n - f_\rho\|_2^2 \geq \epsilon) \\ &\stackrel{(b)}{\geq} \epsilon \times \max_{v=1, \dots, 2^{m^p/8}} \mathbb{P}(\|\hat{f}_n - f_v\|_2^2 \geq \epsilon) \\ &\geq \epsilon \times \max_{v=1, \dots, 2^{m^p/8}} \mathbb{P}(\hat{V} \neq v) \\ &\stackrel{(c)}{\geq} \epsilon \times \frac{1}{2^{m^p/8}} \sum_{v=1}^{2^{m^p/8}} \mathbb{P}(\hat{V} \neq v) \\ &\stackrel{(d)}{\geq} \epsilon \times \left(1 - \frac{I(V; \mathbf{S}_n) + \log 2}{\log(2^{m^p/8})}\right) \\ &= \frac{C_1 \cdot \omega}{m^{2\beta}} \times \left(1 - \frac{I(V; \mathbf{S}_n) + \log 2}{m^p \log(2)/8}\right), \end{aligned}$$

where (a) follows from taking supremum after an application of the Markov inequality; (b) is valid because  $\{f_v\}_{v=1}^{2^{m^p/8}} \subset \mathcal{H}^\beta([0,1]^p, B_0)$ ; (c) is due to the fact that the maximum value of a real sequence is larger than its average; and (d) follows from the Fano's inequality (Theorem 1 in [Scarlett and Cevher 2019](#)), where  $I(V; \mathbf{S}_n)$  denotes the mutual information of  $V$  and  $\mathbf{S}_n$  representing how much information  $V$  reveals about  $\mathbf{S}_n$  ([Scarlett and Cevher 2019](#)).

To obtain the lower bound, we then need to bound the mutual information  $I(V; \mathbf{S}_n)$ . Recall that  $\mathbf{S}_n = \{(\mathbf{X}_i, D_i)\}_{i=1}^n$  contains  $n$  i.i.d. random samples, then we can tensorize the mutual information

$I(V; \mathbf{S}_n)$  through a sum of  $n$  separate mutual information terms. Indeed, Lemma 2 in [Scarlett and Cevher \(2019\)](#) tells that

$$I(V; \mathbf{S}_n) \leq \sum_{i=1}^n I(V; (\mathbf{X}_i, D_i)) = n \times I(V; (\mathbf{X}, D)).$$

By the KL divergence-based bounds (see, e.g., Lemma 4 in [Scarlett and Cevher 2019](#)), we further have

$$I(V; (\mathbf{X}, D)) \leq \max_{v, v' \in \{1, \dots, 2^{mp}/8\}} D_{\text{KL}}(P_v \parallel P_{v'}),$$

where  $D_{\text{KL}}(P_v \parallel P_{v'})$  denotes the KL divergence between two distributions  $P_v$  and  $P_{v'}$ , and  $P_v$  stands for the joint distribution of  $(\mathbf{X}, D)$  under the model  $D = f_v(\mathbf{X}) + \epsilon$ . For convenience, we respectively let  $p_v$  and  $p_{v'}$  be the density function of the joint distribution  $P_v$  and  $P_{v'}$ , and denote  $p_\epsilon$  as the conditional density of  $\epsilon$  given  $\mathbf{X}$ . By definition of the  $\chi^2$  divergence, we get

$$\begin{aligned} D_{\text{KL}}(P_v \parallel P_{v'}) &\stackrel{(a)}{\leq} D_{\chi^2}(P_v \parallel P_{v'}) \\ &= \mathbb{E}_{(\mathbf{X}, D) \sim P_{v'}} \left[ \frac{(p_v(\mathbf{X}, D) - p_{v'}(\mathbf{X}, D))^2}{p_{v'}^2(\mathbf{X}, D)} \right] \\ &= \mathbb{E}_{(\mathbf{X}, D) \sim P_{v'}} \left[ \frac{(p_v(D | \mathbf{X}) - p_{v'}(D | \mathbf{X}))^2}{p_{v'}^2(D | \mathbf{X})} \right] \\ &= \mathbb{E}_{(\mathbf{X}, D) \sim P_{v'}} \left[ \frac{(p_\epsilon(D - f_v(\mathbf{X})) - p_\epsilon(D - f_{v'}(\mathbf{X})))^2}{p_{v'}^2(D | \mathbf{X})} \right] \\ &\stackrel{(b)}{\leq} \frac{L_\epsilon}{\kappa^2} \mathbb{E}_{(\mathbf{X}, D) \sim P_{v'}} |f_v(\mathbf{X}) - f_{v'}(\mathbf{X})|^2 \\ &\stackrel{(c)}{\leq} \frac{L_\epsilon C_X}{\kappa^2} \|f_v - f_{v'}\|_2^2 \\ &\stackrel{(d)}{\leq} \frac{L_\epsilon C_X}{\kappa} \times \left[ \frac{C_2 \cdot \omega}{m^{2\beta}} \right] \\ &\leq \frac{C_2 \cdot \omega}{m^{2\beta}}, \end{aligned}$$

where (a) is a standard relationship between KL and  $\chi^2$  divergence measures (see, e.g., Lemma 6 of [Scarlett and Cevher 2019](#)); (b) holds because the density function of the conditional distribution  $D|\mathbf{X}$  is uniformly bounded below by  $\kappa$ , which is  $L_\epsilon$ -Lipschitz continuous (and therefore,  $p_\epsilon$  is also  $L_\epsilon$ -Lipschitz continuous); (c) comes from the fact that the marginal density distribution of  $\mathbf{X}$  is bounded above by  $C_X$ ; (d) is valid by [\(OA.14\)](#).

Combining the obtained bounds, for any estimator  $\hat{f}_n$  based on the sample  $\mathbf{S}_n = \{(\mathbf{X}_i, D_i)\}_{i=1}^n$ , we have

$$\sup_{f_\rho \in \mathcal{H}^\beta([0,1]^p, B_0)} \mathbb{E} \|\hat{f}_n - f_\rho\|_2^2 \geq \frac{C_1 \cdot \omega}{m^{2\beta}} \times \left( 1 - \frac{C_2 \cdot \omega \cdot n}{m^{p+2\beta}} \right),$$

where we have left those finite numbers to the universal constants. By choosing  $m = \lfloor n^{1/(p+2\beta)} \rfloor$  and a proper  $\omega$ , we can reach the following conclusion:

$$\inf_{\hat{f}_n} \sup_{f_\rho \in \mathcal{H}^\beta([0,1]^p, B_0)} \mathbb{E} \|\hat{f}_n - f_\rho\|_2^2 \geq C \times n^{-2\beta/(p+2\beta)}.$$

Finally, we can apply Theorem OA.4 in Section D to get the lower bound for excess risk:

$$\inf_{\hat{f}_n} \sup_{f_\rho \in \mathcal{H}^\beta([0,1]^p, B_0)} \mathbb{E} \left[ \mathcal{R}^\rho(\hat{f}_n) - \mathcal{R}^\rho(f_\rho) \right] \geq C \times n^{-2\beta/(p+2\beta)}. \quad \square$$

### C. Proofs in Section 5

For the completeness of the proof, we present the definition of sequential covering number in the following (Kuznetsov and Mohri 2015).

**DEFINITION OA.3.** A  $\mathcal{Z}$ -valued complete binary tree  $z$  is a sequence  $(z_1, \dots, z_T)$  of  $T$  mappings  $z_t : \{\pm 1\}^{t-1} \rightarrow \mathcal{Z}, t \in [1, T]$ . A path in the tree is  $\sigma = (\sigma_1, \dots, \sigma_{T-1})$ . Simplify, we write  $z_t(\sigma)$  for  $z_t(\sigma_1, \dots, \sigma_{t-1})$ . A set  $V$  of  $\mathbb{R}$ -valued trees of the depth  $T$  is a sequential  $\alpha$  cover (with respect to  $\mathbf{q}$ -weighted  $\ell_p$  norm) of a function class  $\mathcal{G}$  on a tree  $z$  of the depth  $T$  if for all  $g \in \mathcal{G}$  and all  $\sigma \in \{\pm 1\}^T$ , there is  $v \in V$  such that

$$\left( \sum_{t=1}^T |v_t(\sigma) - g(\mathbf{z}_t(\sigma))|^p \right)^{\frac{1}{p}} \leq \|\mathbf{q}\|_q^{-1} \alpha,$$

where  $\|\cdot\|_q$  is the dual norm and  $\mathbf{q} = (q_1, \dots, q_T)$  is an arbitrary sequence. The (sequential) covering number  $\mathcal{N}_p(\alpha, \mathcal{G}, \mathbf{z})$  of a function class  $\mathcal{G}$  on a given tree  $\mathbf{z}$  is defined to be the size of the minimal sequential cover.

*Proof of Theorem 5.* We write  $L_f(z) = L(f(\mathbf{x}), d) := b(d - f(\mathbf{x}))^+ + h(f(\mathbf{x}) - d)^+ \leq b\bar{D} + h\mathcal{B}$  for any  $z = (\mathbf{x}, d) \in \mathbb{R}^{d+1}$  and  $f \in \mathcal{F}_{DNN}$ . We define the function class  $\mathcal{F}_L = \{L_f(\cdot) : f \in \mathcal{F}_{DNN}\}$ .

To prove the theorem, we essentially follow the idea of risk decomposition in Lemma 1, but the treatment of the stochastic error is slightly different. Recall that the stochastic error with dependent data is defined as

$$\sup_{f \in \mathcal{F}_{DNN}} |\mathcal{R}^\rho(f) - \mathcal{R}_T^\rho(f)|.$$

By definition, we know that  $\mathcal{F}_{DNN}$  contains networks with the parameter  $\phi$ , depth  $\mathcal{D}$ , width  $\mathcal{W}$ , size  $\mathcal{S}$ , and number of neurons  $\mathcal{U}$  so that  $\|f_\phi\|_\infty \leq \mathcal{B}$ . Also, it is obvious that the news vendor loss function  $L(y, y')$  is  $\max\{b, h\}$ -Lipschitz in both its two arguments. Then, by Corollary 2 in Kuznetsov and Mohri (2015), for any  $\delta > 0$ , with probability at least  $1 - \delta$ , for all  $\epsilon > 0$ ,

$$\sup_{f \in \mathcal{F}_{DNN}} |\mathcal{R}^\rho(f) - \mathcal{R}_T^\rho(f)| \leq 2\epsilon + \Delta + (b\bar{D} + h\mathcal{B}) \frac{\|\mathbf{q}\|_2}{\sqrt{T}} \sqrt{\frac{2 \log \mathbb{E}_{S_T} [\mathcal{N}_1(\epsilon, \mathcal{F}_L, S_T)] + \log(1/\delta)}{T}}, \quad (\text{OA.15})$$



where  $\mathcal{N}_1(\epsilon, \mathcal{F}_L, S_T)$  is the (sequential) covering number of the function class  $\mathcal{F}_L$  with radius  $\epsilon$  based on samples  $S_T$ ,  $\mathbf{q} = (q_1, \dots, q_T)$  is an arbitrary sequence, and  $\Delta$  is the discrepancy defined by

$$\Delta = \sup_{L \in \mathcal{F}_L} \left( \mathbb{E}[L(Z_{T+1}) \mid Z_1, \dots, Z_T] - \sum_{t=1}^T q_t \mathbb{E}[L(Z_t) \mid Z_1, \dots, Z_{t-1}] \right).$$

Recall that for any  $z = (x, d) \in \mathbb{R}^{d+1}$  and any  $f_1, f_2 \in \mathcal{F}_{DNN}$ ,  $L_{f_1}(z) = L_{f_1}(x, d)$  and  $L_{f_2}(z) = L_{f_2}(x, d)$ , and  $|L_{f_1}(z) - L_{f_2}(z)| \leq \max\{b, h\}|f_1(x) - f_2(x)|$ . For any  $\epsilon > 0$ , let  $\mathcal{F}_{DNN}^*$  be a  $(\epsilon/\max\{b, h\})$ -covering of  $\mathcal{F}_{DNN}$  with number  $\mathcal{N}_T(\epsilon/\max\{b, h\}, \mathcal{F}_{DNN}, \|\cdot\|_\infty)$ . Then it is easy to check that  $\mathcal{F}_L^* = \{L_f : f \in \mathcal{F}_{DNN}^*\}$  is a  $\epsilon$ -covering of  $\mathcal{F}_L$  with  $\mathbf{q} = (1, \dots, 1)$  (see Definition OA.3). Consequently, we have  $\mathcal{N}_1(\epsilon, \mathcal{F}_L, S_T) \leq \mathcal{N}_T(\epsilon/\max\{b, h\}, \mathcal{F}_{DNN}, \|\cdot\|_\infty)$  for any  $S_T$ . We choose  $\epsilon = 1/T$ , by Theorem OA.1 and Theorem 3 in Bartlett et al. (2019), we know that for  $T \geq \text{Pdim}(\mathcal{F}_{DNN})$ ,

$$\begin{aligned} \log \mathbb{E}_{S_T}[\mathcal{N}_1(\epsilon, \mathcal{F}_L, S_T)] &\leq \log \mathcal{N}_T(\epsilon/\max\{b, h\}, \mathcal{F}_{DNN}, \|\cdot\|_\infty) \\ &\leq \text{Pdim}(\mathcal{F}_{DNN}) \log \left( \frac{eT\mathcal{B} \max\{b, h\}}{\epsilon \text{Pdim}(\mathcal{F}_{DNN})} \right) \\ &\leq \text{Pdim}(\mathcal{F}_{DNN}) \log(eT^2\mathcal{B} \max\{b, h\}) \\ &\leq C\mathcal{B} \max\{b, h\} \mathcal{D}\mathcal{S} \log(\mathcal{S}) \log(T), \end{aligned}$$

where  $C > 0$  is some universal constant. Together with (OA.15), for a sufficient large  $T$  and any  $\delta > 0$ , we have, with probability at least  $1 - \delta$ ,

$$\begin{aligned} \sup_{f \in \mathcal{F}_{DNN}} |\mathcal{R}^\rho(f) - \mathcal{R}_T^\rho(f)| &\leq C[\max\{b, h\}(\bar{D}\mathcal{B})]^2 \sqrt{\frac{2\mathcal{D}\mathcal{S} \log(\mathcal{S}) \log(T)}{T}} \\ &\quad + (b\bar{D} + h\mathcal{B}) \sqrt{\frac{\log(1/\delta)}{T}} + \Delta, \end{aligned} \quad (\text{OA.16})$$

where  $C > 0$  is some universal constant. Then by Proposition OA.1 and the risk decomposition in Lemma 1, the following inequality holds with at least probability  $1 - \delta$ ,

$$\begin{aligned} \mathcal{R}^\rho(\hat{f}_{DNN}) - \mathcal{R}^\rho(f_\rho) &\leq C[\max\{b, h\}(\bar{D}\mathcal{B})]^2 \sqrt{\frac{2\mathcal{D}\mathcal{S} \log(\mathcal{S}) \log(T)}{T}} + 2(b\bar{D} + h\mathcal{B}) \sqrt{\frac{\log(1/\delta)}{T}} + 2\Delta \\ &\quad + 18 \max\{b, h\} B_0(\lfloor \beta \rfloor + 1)^2 p^{\lfloor \beta \rfloor + (\beta \vee 1)/2} (NM)^{-2\beta/p}, \end{aligned}$$

where  $T \geq C \cdot \mathcal{S}\mathcal{D} \log(\mathcal{S})$  for a large enough  $C > 0$  and  $M, N \in \mathbb{N}_+$ . Using the same arguments as in the proof of Theorem 2, we can reach the conclusion stated in Theorem 5.  $\square$

*Proof of Theorem 6.* The excess risk can again be decomposed into a stochastic error and an approximation error as stated in Lemma 1. Specifically, the stochastic error bound remains the same as in Theorem 1 since it is independent of the target function by definition in Lemma 1. Therefore, we only need to check the approximation error under this GLM setting.

We first notice that the target function can be represented in the following composite form:

$$f_\rho(\mathbf{x}) = g(\boldsymbol{\theta}^\top \mathbf{x}) = h_1 \circ h_0(\mathbf{x}),$$

where

$$h_1(y) = g(y) \text{ for } y \in \mathbb{R} \quad \text{and} \quad h_0(\mathbf{x}) = \boldsymbol{\theta}^\top \mathbf{x} \text{ for } \mathbf{x} \in \mathbb{R}^p.$$

Such a composite structure is indeed similar to the DNN structure (6) so that we can first use two sub-networks  $\tilde{h}_1$  and  $\tilde{h}_0$  to approximate  $h_1$  and  $h_0$ , respectively. Next, by stacking these two sub-networks, we can construct a new network in approximating  $f_\rho$ . Specifically, the domain of the univariate function  $h_1$  is  $[a, c]$ , and to apply Theorem 3.3 in Jiao et al. (2023) with a domain being  $[0, 1]$ , we first need an additional invertible linear layer  $A(\cdot) : [a, c] \rightarrow [0, 1]$  as the first layer in the sub-network  $\tilde{h}_1$  to finish the transformation of the domain. Indeed, this invertible layer can be easily established via  $A(y) = \sigma(\frac{1}{c-a}y - \frac{a}{c-a})$  where  $\sigma(\cdot)$  is the ReLU activation function. Then, by Theorem 3.3 in Jiao et al. (2023), there exists an  $\tilde{h}_1 \in \mathcal{F}_{DNN}$  with the width  $\mathcal{W} = 38(\lfloor \beta \rfloor + 1)^2 N \lceil \log_2(8N) \rceil$  and depth  $\mathcal{D} = 21(\lfloor \beta \rfloor + 1)^2 M \lceil \log_2(8M) \rceil + 1$  for  $M, N \in \mathbb{N}_+$ , such that

$$|\tilde{h}_1(y) - h_1(y)| \leq 18B_0(\lfloor \beta \rfloor + 1)^2 (NM)^{-2\beta}, \quad (\text{OA.17})$$

for  $y \in \mathbb{R}$  except a negligible set with an arbitrarily small Lebesgue measure.

On the other hand, for the construction of sub-network  $\tilde{h}_0$ , we know from Lemma 2 that there exists a one-layer network that can exactly represent a linear function. In other words, there is an  $\tilde{h}_0 \in \mathcal{F}_{DNN}$  with the width of each layer being  $(p, 2, 1)$ , such that

$$|\tilde{h}_0(\mathbf{x}) - h_0(\mathbf{x})| = 0, \quad (\text{OA.18})$$

for any  $\mathbf{x} \in \mathbb{R}^p$ .

Since the mappings  $A(\cdot)$  and  $\tilde{h}_0$  are both continuous, and the probability measure of  $\mathbf{X}$  is absolutely continuous with respect to the Lebesgue measure by Assumption 2(i), combining (OA.17) and (OA.18), we then have

$$\mathbb{E}|\tilde{h}_1 \circ \tilde{h}_0(\mathbf{x}) - h_1 \circ h_0(\mathbf{x})| \leq 18B_0(\lfloor \beta \rfloor + 1)^2 (NM)^{-2\beta}.$$

Therefore, the approximation error can be bounded as follows:

$$\begin{aligned} \inf_{f \in \mathcal{F}_{DNN}} [\mathcal{R}^\rho(f) - \mathcal{R}^\rho(f_\rho)] &\leq \mathcal{R}^\rho(\tilde{h}_1 \circ \tilde{h}_0) - \mathcal{R}^\rho(h_1 \circ h_0) \\ &\stackrel{(a)}{\leq} \max\{b, h\} \mathbb{E}|\tilde{h}_1 \circ \tilde{h}_0(\mathbf{x}) - h_1 \circ h_0(\mathbf{x})| \\ &\leq 18 \max\{b, h\} B_0(\lfloor \beta \rfloor + 1)^2 (NM)^{-2\beta}, \end{aligned}$$

where (a) holds because the newsvendor loss function is  $\max\{b, h\}$ -Lipschitz. Together with Lemma 1 and Theorem 1, the following inequality holds for at least probability  $1 - \delta$ ,

$$\begin{aligned} \mathcal{R}^\rho(\hat{f}_{DNN}) - \mathcal{R}^\rho(f_\rho) &\leq 2\sqrt{2}(b\bar{D} + h\mathcal{B}) \left( C_3 \sqrt{\frac{\mathcal{SD} \log(\mathcal{S}) \log(n)}{n}} + \sqrt{\frac{\log(1/\delta)}{n}} \right) \\ &\quad + 18 \max\{b, h\} B_0(\lfloor \beta \rfloor + 1)^2 (NM)^{-2\beta}. \end{aligned}$$

Using similar arguments as in the proof of Theorem 2, we choose  $MN = \lfloor n^{\frac{1}{4\beta+2}} \rfloor$  so that the convergence order in the sample size is optimized. Under this setting, we get

$$\mathcal{R}^\rho(\hat{f}_{DNN}) - \mathcal{R}^\rho(f_\rho) \leq 2\sqrt{2}(b\bar{D} + h\mathcal{B}) \left( C_3(\lfloor \beta \rfloor + 1)^4 (\log(n))^2 n^{-\frac{\beta}{2\beta+1}} + \sqrt{\frac{\log(1/\delta)}{n}} \right),$$

for  $n$  large enough. The stacked network consisting of  $\tilde{h}_1$  and  $\tilde{h}_0$  then has the width  $\tilde{W} = \max\{\mathcal{W}, 2p\}$  and depth  $\tilde{D} = D + 3$ .  $\square$

## D. Model Misspecification Issues

Ban and Rudin (2019) have made significant contributions by thoroughly exploring the importance of incorporating feature information into decision-making for the newsvendor problem, both theoretically and numerically. In particular, by adaptively integrating both the basic and nonlinearly transformed features into their decision models, they effectively address the model misspecification issues of the linear and kernel policies proposed in their work. In this section, we echo their insights by demonstrating that misspecified models can result in non-vanishing errors. In contrast, as shown in Section 4, the DNN method's excess risk can converge to zero for a large class of target functions, provided there is sufficient data. In practical implementations, a DNN with large enough depth and width should suffice to obtain a good decision with a small approximation error. In addition, there is no need to specify parametric forms of approximation rules, making it convenient in various practical scenarios. These advantages help mitigate the misspecification issues commonly found in learning problems. In our context, we consider the following definition of model misspecification.

**DEFINITION OA.4 (MODEL MISSPECIFICATION).** Let  $\{\mathcal{F}_n\}_{n=1}^\infty$  be the collection of hypothesis spaces and  $f_\rho$  be the *unknown* target function. The model is considered misspecified if  $f_\rho \notin \lim_{n \rightarrow \infty} \bigcup_{i=1}^n \mathcal{F}_i$ .

Notice that we allow the hypothesis set  $\mathcal{F}_n$  to expand with an increasing sample size to align with the formulation in Theorem 2.

**ASSUMPTION OA.1 (LOCAL MINIMAL SEPARATION).** *There exist  $\gamma \in (0, \bar{D}]$  and  $\kappa > 0$  such that for any  $|\zeta| \leq \gamma$ ,*

$$|F(f_\rho(\mathbf{x}) + \zeta|\mathbf{x}) - F(f_\rho(\mathbf{x})|\mathbf{x})| \geq \kappa|\zeta|$$

for any  $\mathbf{x} \in \mathcal{X}$  up to a zero-probability set under the probability measure of  $\mathbf{X}$ , where  $F(\cdot|\mathbf{x})$  is the conditional CDF of  $D$  given  $\mathbf{X} = \mathbf{x}$ .

Assumption OA.1 requires that the conditional density has a positive lower bound around the quantile function, which also warrants the strong convexity of the cost function in this region.

**THEOREM OA.4 (EXCESS RISK W.R.T. DECISION BIAS).** *Under Assumptions 1, 2, and OA.1, for any  $f : \mathcal{X} \rightarrow \mathbb{R}$ , we have*

$$\mathcal{R}^\rho(f) - \mathcal{R}^\rho(f_\rho) \geq \frac{\gamma\kappa(b+h)}{2(\bar{D} + \gamma)} \|f - f_\rho\|_{L^2(\mathbf{X})}^2.$$

Theorem OA.4 characterizes the lower bound for the excess risk caused by any suboptimal decision  $f$  in terms of its  $L^2$ -norm difference from the true optimal decision  $f_\rho$ . It is straightforward that if the decision bias is larger, this excess risk bound also gets larger. Generally speaking, we can arrive at the universal insight that the excess risk should increase with the deviation of  $f$  from  $f_\rho$ , even though we may not have an analytical expression for the latter. Therefore, parametric (misspecified) models will result in non-vanishing excess risk even with an infinite amount of data.

*Proof of Theorem OA.4.* We follow the idea of Steinwart and Christmann (2011) to construct a self-calibration function to finish the proof (see the proof of Theorem 2.7 therein). For any fixed  $\mathbf{x} \in \mathbf{X}$ , the self-calibration function is defined as

$$\varphi_L(\epsilon, \mathbf{x}) := \inf_{t \in \mathbb{R}: |t - f_\rho(\mathbf{x})| \geq \epsilon} \mathbb{E}_{D|\mathbf{x}}[L(t, D)] - \mathbb{E}_{D|\mathbf{x}}[L(f_\rho(\mathbf{x}), D)],$$

where  $\mathbb{E}_{D|\mathbf{x}}[\cdot]$  denotes the expectation taken with respect to the conditional distribution of  $D$  given  $\mathbf{X} = \mathbf{x}$  and  $L(t, d) := b(d - t)^+ + h(t - d)^+$ . By definition, the self-calibration function captures the sensitivity of  $L$ -risk around the minimizer  $f_\rho(\mathbf{x})$ , and it is named according to the property that

$$\varphi_L(|t - f_\rho(\mathbf{x})|, \mathbf{x}) \leq \mathbb{E}_{D|\mathbf{x}}[L(t, D)] - \mathbb{E}_{D|\mathbf{x}}[L(f_\rho(\mathbf{x}), D)], \quad \text{for any } t \in \mathbb{R}, \quad (\text{OA.19})$$

if we let  $\epsilon := |t - f_\rho(\mathbf{x})|$ . Since the newsvendor loss function  $L$  is convex, so does the map  $t \rightarrow \mathbb{E}_{D|\mathbf{x}}[L(t, D)] - \mathbb{E}_{D|\mathbf{x}}[L(f_\rho(\mathbf{x}), D)]$ , we then have

$$\varphi_L(\epsilon, \mathbf{x}) = \min\{\mathbb{E}_{D|\mathbf{x}}[L(f_\rho(\mathbf{x}) + \epsilon, D)], \mathbb{E}_{D|\mathbf{x}}[L(f_\rho(\mathbf{x}) - \epsilon, D)]\} - \mathbb{E}_{D|\mathbf{x}}[L(f_\rho(\mathbf{x}), D)]. \quad (\text{OA.20})$$

We then examine each term individually. First, for the first term, if  $\epsilon \in [0, \gamma]$ ,

$$\begin{aligned} \mathbb{E}_{D|\mathbf{x}}[L(f_\rho(\mathbf{x}) + \epsilon, D)] - \mathbb{E}_{D|\mathbf{x}}[L(f_\rho(\mathbf{x}), D)] &\stackrel{\text{(a)}}{=} (b+h) \int_{f_\rho(\mathbf{x})}^{f_\rho(\mathbf{x})+\epsilon} [F(y|\mathbf{x}) - \rho] dy \\ &= (b+h) \int_0^\epsilon [F(y + f_\rho(\mathbf{x})|\mathbf{x}) - F(f_\rho(\mathbf{x})|\mathbf{x})] dy \\ &\stackrel{\text{(b)}}{\geq} (b+h) \int_0^\epsilon \kappa y dy \\ &= \frac{1}{2}(b+h)\kappa\epsilon^2, \end{aligned}$$

where equation (a) follows from a standard integration-by-parts argument (see, e.g., Lemma A-1 of Besbes and Mouchtaki 2023); and inequality (b) holds due to Assumption OA.1. On the other hand, if  $\epsilon \in [\gamma, \bar{D}]$ ,

$$\begin{aligned} \mathbb{E}_{D|\mathbf{x}}[L(f_\rho(\mathbf{x}) + \epsilon, D)] - \mathbb{E}_{D|\mathbf{x}}[L(f_\rho(\mathbf{x}), D)] &= (b+h) \int_0^\epsilon [F(y + f_\rho(\mathbf{x})|\mathbf{x}) - F(f_\rho(\mathbf{x})|\mathbf{x})] dy \\ &\stackrel{(a)}{\geq} (b+h) \int_0^\gamma \kappa y dy + (b+h) \int_\gamma^\epsilon \kappa \gamma dy \\ &= \frac{1}{2}(b+h)\kappa\gamma^2 + (b+h)\kappa\gamma(\epsilon - \gamma) \\ &= (b+h)\kappa(\gamma\epsilon - \frac{1}{2}\gamma^2), \end{aligned}$$

where the inequality (a) applies Assumption OA.1 and also since  $F(y|\mathbf{x})$  is non-decreasing so that  $F(y|\mathbf{x}) \geq F(f_\rho(\mathbf{x}) + \gamma|\mathbf{x})$ . By Lemma OA.2 presented below, we know that

$$\mathbb{E}_{D|\mathbf{x}}[L(f_\rho(\mathbf{x}) + \epsilon, D)] - \mathbb{E}_{D|\mathbf{x}}[L(f_\rho(\mathbf{x}), D)] \geq \frac{\gamma\kappa(b+h)}{2(\bar{D} + \gamma)}\epsilon^2, \quad \text{for any } \epsilon \in [0, \bar{D}].$$

For the second term, we can also analogously show that

$$\mathbb{E}_{D|\mathbf{x}}[L(f_\rho(\mathbf{x}) - \epsilon, D)] - \mathbb{E}_{D|\mathbf{x}}[L(f_\rho(\mathbf{x}), D)] \geq \frac{\gamma\kappa(b+h)}{2(\bar{D} + \gamma)}\epsilon^2, \quad \text{for any } \epsilon \in [0, \bar{D}].$$

As a result, for any function  $f : \mathcal{X} \rightarrow \mathbb{R}$  and a fixed  $\mathbf{x} \in \mathcal{X}$ , by letting  $t := f(\mathbf{x})$  and  $\epsilon := |f(\mathbf{x}) - f_\rho(\mathbf{x})|$ , the self-calibration property (OA.19) and (OA.20) give

$$\begin{aligned} \mathbb{E}_{D|\mathbf{x}}[L(f(\mathbf{x}), D)] - \mathbb{E}_{D|\mathbf{x}}[L(f_\rho(\mathbf{x}), D)] &\geq \varphi_L(|f(\mathbf{x}) - f_\rho(\mathbf{x})|, \mathbf{x}) \\ &\geq \frac{\gamma\kappa(b+h)}{2(\bar{D} + \gamma)}|f(\mathbf{x}) - f_\rho(\mathbf{x})|^2. \end{aligned}$$

Taking expectation with respect to the distribution of  $\mathbf{X}$  on both sides, we obtain the desired inequality in Theorem OA.4.  $\square$

LEMMA OA.2. For  $\epsilon \in [0, \bar{D}]$  and the function  $h : [0, \bar{D}] \rightarrow [0, \infty)$  defined by

$$h(\epsilon) := \begin{cases} \frac{1}{2}(b+h)\kappa\epsilon^2, & \text{if } \epsilon \in [0, \gamma], \\ (b+h)\kappa(\gamma\epsilon - \frac{1}{2}\gamma^2), & \text{if } \epsilon \in [\gamma, \bar{D}], \end{cases}$$

we have

$$h(\epsilon) \geq \frac{\gamma\kappa(b+h)}{2(\bar{D} + \gamma)}\epsilon^2, \quad \text{for all } \epsilon \in [0, \bar{D}].$$

*Proof of Lemma OA.2.* When  $\epsilon \in [0, \gamma]$ , because  $\gamma \leq \bar{D}$ , it holds that

$$h(\epsilon) = \frac{1}{2}(b+h)\kappa\epsilon^2 = \frac{\gamma}{\gamma + \gamma}(b+h)\kappa\epsilon^2 \geq \frac{\gamma\kappa(b+h)}{\bar{D} + \gamma}\epsilon^2 \geq \frac{\gamma\kappa(b+h)}{2(\bar{D} + \gamma)}\epsilon^2.$$

When  $\epsilon \in [\gamma, \bar{D}]$ , we define

$$g(\epsilon) := h(\epsilon) - \frac{\gamma\kappa(b+h)}{2(\bar{D}+\gamma)}\epsilon^2 = (b+h)\kappa\left(\gamma\epsilon - \frac{1}{2}\gamma^2\right) - \frac{\gamma\kappa(b+h)}{2(\bar{D}+\gamma)}\epsilon^2,$$

whose first-order derivative is

$$g'(\epsilon) = (b+h)\kappa\gamma - \frac{\gamma\kappa(b+h)}{\bar{D}+\gamma}\epsilon = (b+h)\kappa\gamma\frac{\bar{D}+\gamma-\epsilon}{\bar{D}+\gamma} \geq 0.$$

Therefore,  $g(\epsilon)$  is non-decreasing on  $[\gamma, \bar{D}]$ , implying

$$g(\epsilon) \geq g(\gamma) = \frac{1}{2}(b+h)\kappa\gamma^2\frac{\bar{D}}{\bar{D}+\gamma} \geq 0,$$

from which we can claim the result in Lemma OA.2.  $\square$

## E. Supplementary Materials for Section 6

In this section, we present additional numerical experiments and results to supplement the analysis in Section 6. First, we examine the claim from Section 6.2 that the DNN method can achieve comparably good performance across a range of network structures, demonstrating its flexibility. Beyond Figure 5, this phenomenon holds robustly across different sample sizes (see Figures OA.1 and OA.2), various critical levels used (see Figures OA.3 and OA.4), as well as different model setups (as illustrated in the subplots of each figure).

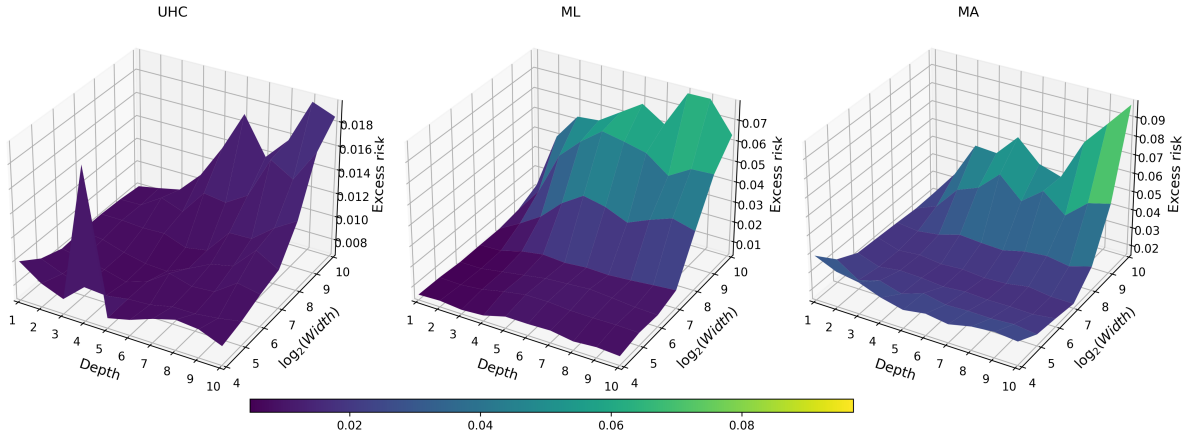


Figure OA.1 Excess risk against network depth and width when  $n = 256$  and  $\rho = 0.25$ .

As an interesting and independent trial, we further explore the impact of different activation functions on the performance of the DNN method. Specifically, we consider the Sigmoid and Tanh activation functions, defined respectively as

$$\sigma_{Sigmoid}(x) := \frac{1}{1 + e^{-x}} \quad \text{and} \quad \sigma_{Tanh}(x) := \frac{e^x - e^{-x}}{e^x + e^{-x}}.$$

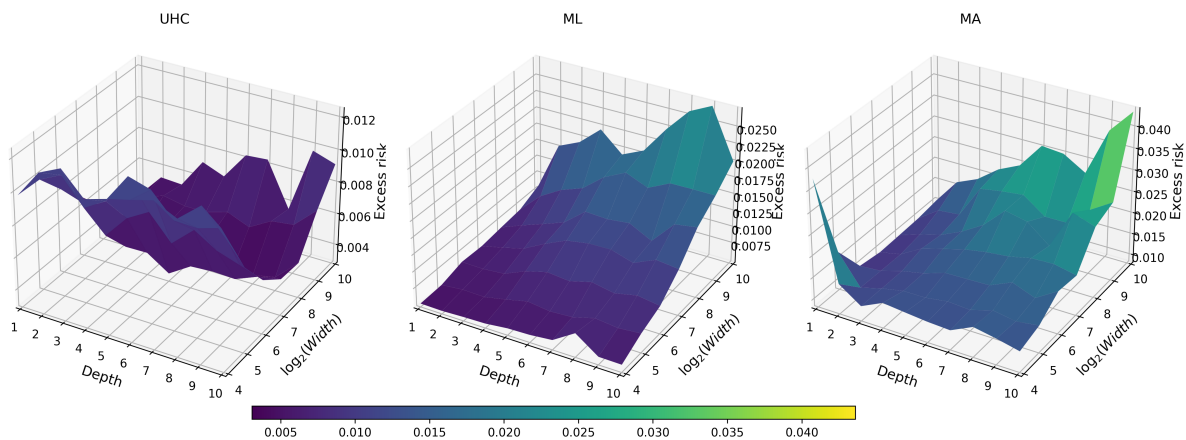


Figure OA.2 Excess risk against network depth and width when  $n = 512$  and  $\rho = 0.25$ .

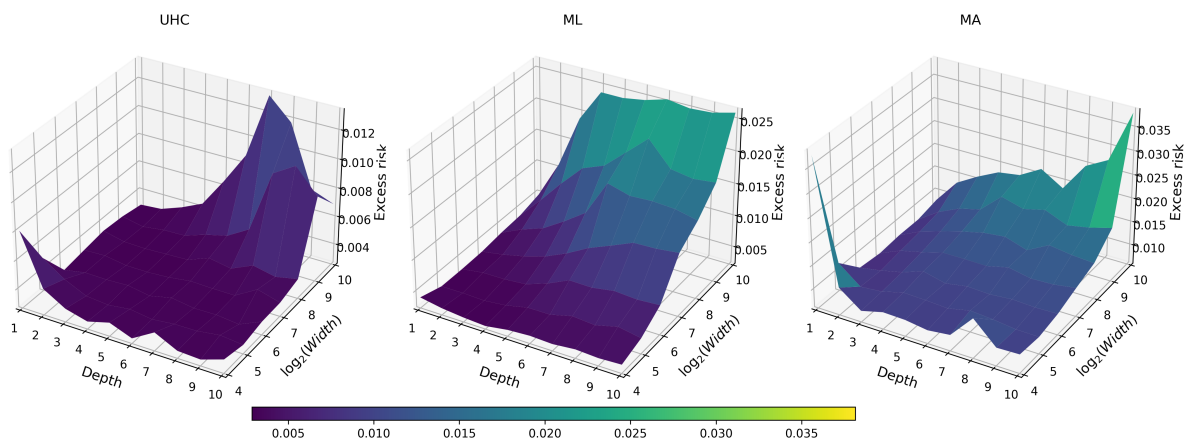


Figure OA.3 Excess risk against network depth and width when  $n = 1024$  and  $\rho = 0.5$ .

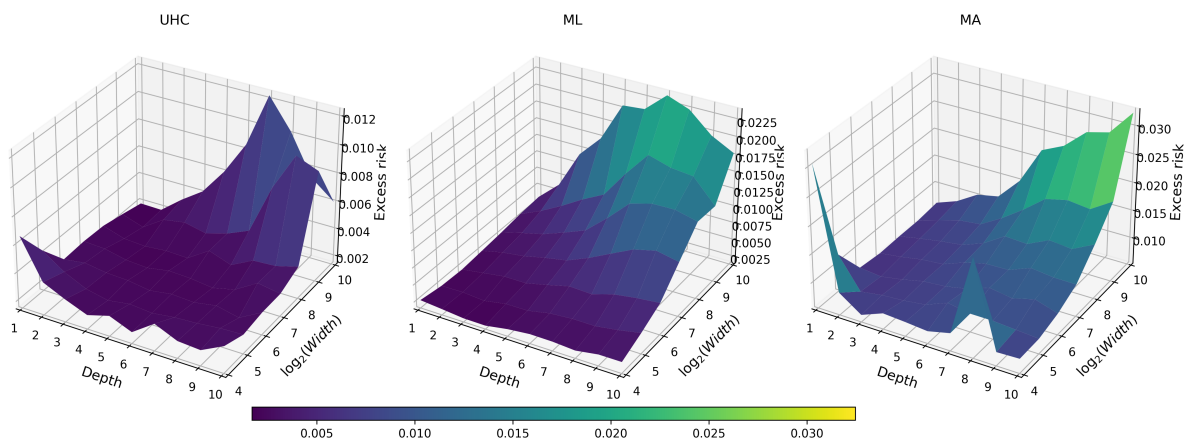
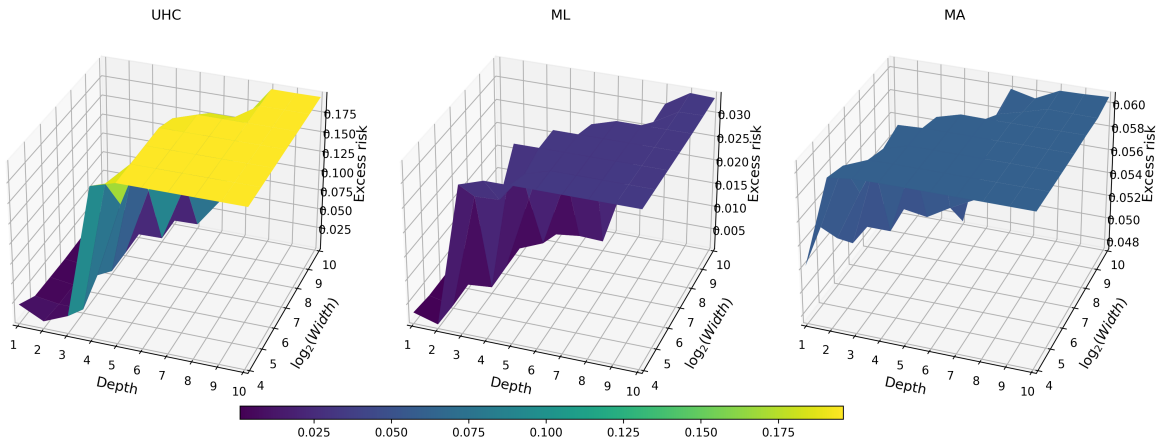


Figure OA.4 Excess risk against network depth and width when  $n = 1024$  and  $\rho = 0.75$ .

Compared to these alternatives, the ReLU activation function is simpler and often avoids vanishing gradients, even when inputs are large. Moreover, as noted in Section 3.2, ReLU networks have gained widespread popularity in deep learning applications due to their computational efficiency,

ease of training, and strong generalization performance (see, e.g., Nair and Hinton 2010, Krizhevsky et al. 2012).

For a brief comparison, we present the numerical performance of DNNs using these two activation functions in Figures OA.5 and OA.6, with other settings the same as those in Figure 5. We have the following observations. First, for the relatively simple tasks considered, the DNN method performs well with any of the activation functions once finely tuned, as the minimum loss across depth-width combinations remains consistently low. Second, Sigmoid and Tanh networks seem to be more sensitive to the network design, as their performance can deteriorate rapidly, evidenced by the wider range of errors across different figures. In particular, they perform relatively badly when the network gets deeper, which may be attributed to the vanishing gradient problem, as previously noted. Third, since both Sigmoid and Tanh activation functions introduce (more) nonlinearities, networks using these activation functions often require less depth to achieve a good approximation.



**Figure OA.5** Excess risk against network depth and width when using Sigmoid activation function ( $n = 1024, \rho = 0.25$ ).

## F. Supplementary Materials for Section 7

### F.1. Justification for the Selected Network Architecture

Here, we provide the rationale for selecting a three-layer network with 512 neurons per layer for our numerical experiments in Section 7. This choice is not made arbitrarily but is guided by the principles outlined in Section 6. Specifically, as suggested in Section 6.2, we first select a sufficiently wide network by setting the width to 512 and then progressively evaluate the performance of networks with varying depths. The final choice is based on achieving strong performance while avoiding unnecessary complexity in the number of layers. Following this principle, we conduct experiments on both the preliminary and full datasets, using a critical level of  $\rho = 0.7$  as a simple illustration. As shown in Figure OA.7, the three-layer network achieves the best performance



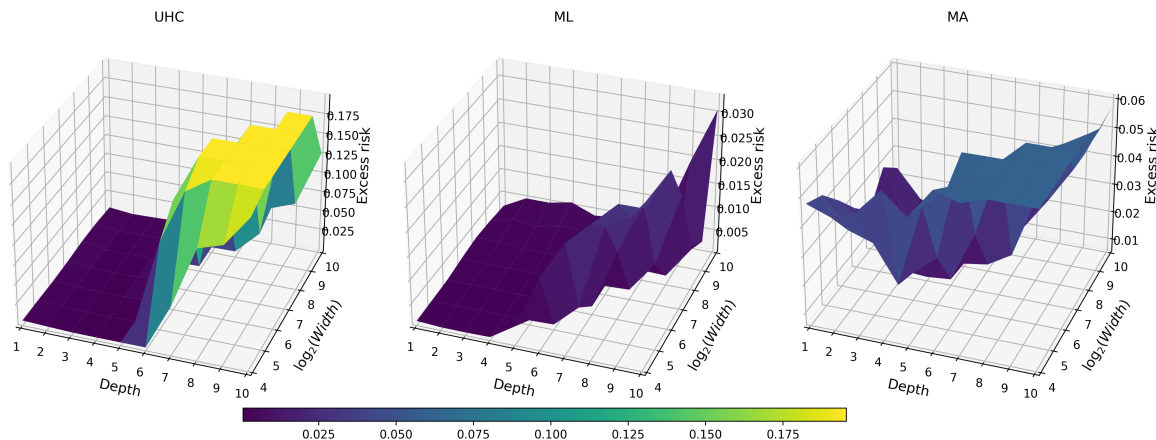


**Figure OA.6** Excess risk against network depth and width when using Tanh activation function ( $n = 1024, \rho = 0.25$ ).

on both the preliminary and full datasets among different depths. Additionally, the network's moderate depth makes implementation quite convenient. Based on these observations, we select the three-layer network with 512 neurons in each layer as the benchmark for the DNN method in all numerical experiments in Section 7.

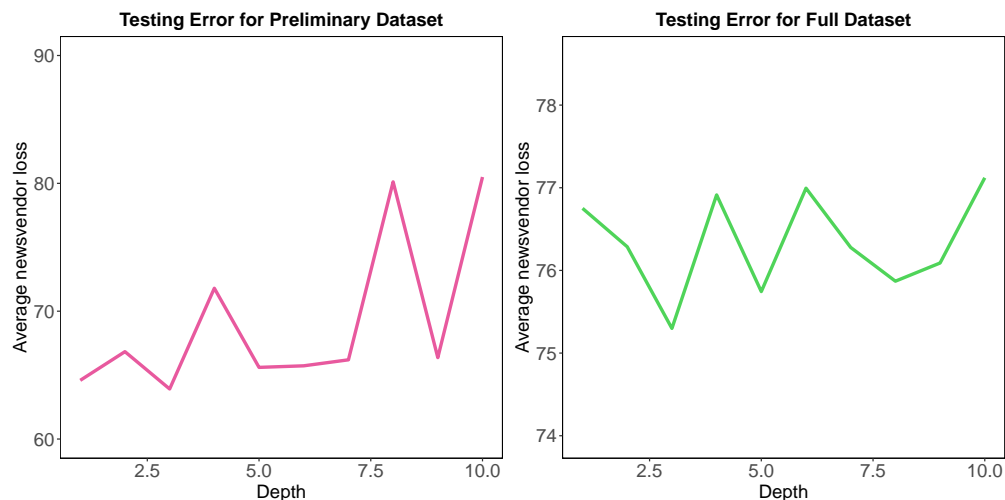


**Figure OA.7** Average newsvendor loss against network depth when width=512 and  $\rho = 0.7$ .

## F.2. Supplementary Experiment Outcomes

Based on Tables 1 and 2, Figures OA.8 and OA.9 present the relative average newsvendor loss of alternative methods compared to the DNN, for the small and full datasets, respectively.

Next, we present the training and execution times for each method on the full dataset (see Tables OA.1). All numerical experiments were conducted on a computer equipped with a 12th Gen Intel(R) Core(TM) i9-12900 CPU (2.40 GHz) and 128 GB of RAM. In particular, unlike in Ban

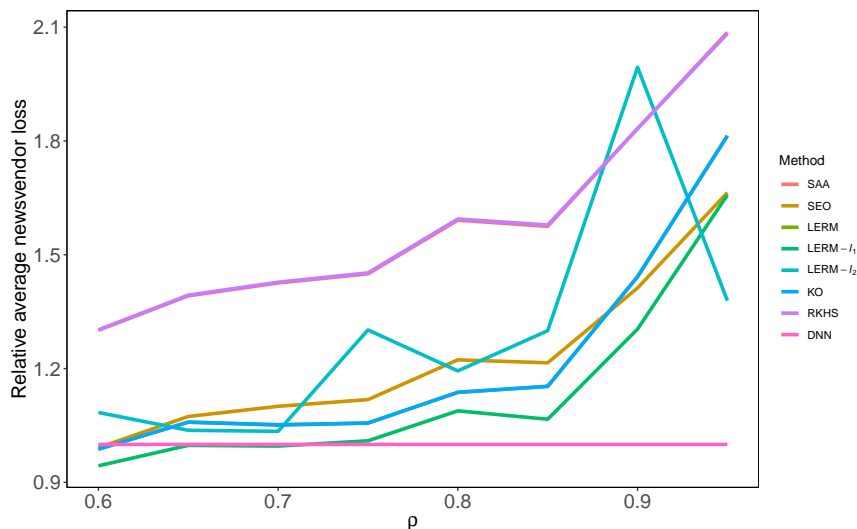


Figure OA.8 Relative average newsvendor loss (compared to DNN) for different methods on the small dataset.

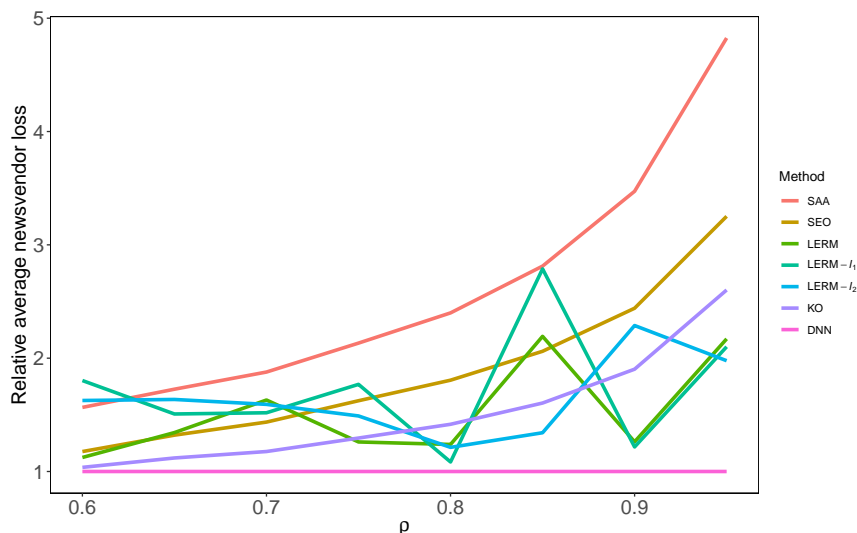


Figure OA.9 Relative average newsvendor loss (compared to DNN) for different methods on the full dataset. The performance of RKHS is not shown because it significantly increases the scale of the plot.

and Rudin (2019), the KO method in our setting requires a few seconds to implement, likely due to the significantly higher dimensionality and larger size of the training data, which increases the time needed to compute the distances for the kernel weights.

## G. Further Discussions

Although our main focus is on the single-product newsvendor problem for ease of exposition, our results naturally extend to the multi-product case. There are also many avenues for future research. We also anticipate that similar theoretical results would apply to other end-to-end stochastic optimization problems where the objective function is Lipschitz continuous and convex in the

**Table OA.1 Training and Execution times (in seconds) for different methods on the full dataset. Each cell displays the training time on the first line, followed by the execution time on the second line. A dash (“-”) indicates not applicable.**

$\rho$	0.6	0.65	0.7	0.75	0.8	0.85	0.9	0.95
SAA	- $\approx 0$	- $\approx 0$	- $\approx 0$	- $\approx 0$	- $\approx 0$	- $\approx 0$	- $\approx 0$	- $\approx 0$
SEO	0.14 0.002	0.09 0.002	0.08 0.003	0.08 0.002	0.25 0.002	0.08 0.002	0.08 0.003	0.34 0.003
LERM	6.10 0.001	6.17 0.002	6.23 0.001	6.20 0.001	6.10 0.001	6.29 0.001	6.17 0.001	6.07 0.001
LERM- $\ell_1$	6.21 0.001	6.07 0.001	6.13 0.001	6.17 0.001	6.14 0.001	6.22 0.001	6.20 0.001	6.13 0.001
LERM- $\ell_2$	8.85 0.001	13.96 0.001	7.35 0.001	6.27 0.001	6.31 0.001	6.36 0.001	6.42 0.001	6.44 0.001
KO	- 6.91	- 7.15	- 5.07	- 10.52	- 6.62	- 8.74	- 6.96	- 11.76
RKHS	368.26 0.10	367.55 0.14	433.51 0.12	430.40 0.12	430.60 0.15	387.65 0.12	364.89 0.11	362.15 0.10
DNN	13.96 0.01	13.83 0.01	14.41 0.01	14.29 0.01	14.43 0.01	14.38 0.01	13.93 0.01	13.50 0.01

decision variable. However, the same approach may not apply to the optimal pricing problem, where a mapping from prices to demand (or revenue) is usually learned from data, and then one needs to optimize the network function with respect to (some of) its inputs. In such cases, this additional optimization step requires other techniques, such as the gradient descent method (Chen et al. 2022). For some other examples, there is currently a theoretical gap between the expected risk bound in Theorem 3 and the high-probability risk bound in Theorem 2, where the convergence rate of the former is faster than that of the latter. As shown in the proof in Section B.2, the faster rate in Theorem 3 arises from a different yet tricky decomposition of the expected excess risk in Lemma OA.1, compared to the decomposition in Lemma 1. While the approximation error is similar in both cases, the definition of the stochastic error differs. To this end, a variant of Bernstein inequality (Györfi et al. 2002) is used to show that the stochastic error corresponding to the expected excess risk converges more rapidly in terms of the sample size, resulting in a faster convergence rate for the excess risk. While the high-probability bound offers strong probabilistic guarantees for the excess risk, the expectation bound only characterizes its behavior in the expected level. Therefore, improving the convergence rate of the high-probability bound, if possible, would likely require more advanced techniques for analyzing the stochastic error, such as the use of a more refined concentration inequality. In addition, it would be interesting to integrate various constraints on the DNN solution, addressing practical considerations such as capacity limitations (Elmachtoub et al. 2023). While this could potentially be tackled by implementing a penalized loss function that accounts for the relevant constraint, a thorough examination of the corresponding theoretical and

numerical performance is still required. Furthermore, we anticipate that the DNN method holds significant potential for solving other data-driven OM problems.

Finally, while we have established theoretical guarantees for using the DNN method in the considered newsvendor problem, there remains ample room for future research. To mention a few, first, we have mainly focused on analyzing worst-case error bounds so that the theory holds uniformly across a wide range of cases. However, maintaining such generality may suffer from the problem that the DNN method can perform better than what the worst-case bounds indicate in practical examples. For instance, in Section 6.3, we observe that the convergence rate of the excess risk in the sample size differs from the minimax optimal rate. Going beyond worst-case analysis, one can resort to other theoretical characterizations on helping explain why the DNN method generalizes so well. For instance, [Belkin \(2021\)](#) introduces the interpolation paradigm, showing that over-parameterized models can perfectly interpolate training data while still generalizing well. Another frequently employed method involves precise analyses of specific simple models, such as linear and ridge regressions ([Bartlett et al. 2020](#), [Hastie et al. 2022](#), [Tsigler and Bartlett 2023](#)). For a comprehensive review of various approaches explaining DNN’s generalization, readers can refer to [Bartlett et al. \(2021\)](#) and [Theisen \(2023\)](#). Second, one can possibly explore the optimization side of the DNN method in OM applications. As discussed in Section 6, providing a uniform theoretical analysis for the optimization error is highly challenging. Nevertheless, the success of DNNs is partially attributed to their optimization properties, which could be investigated both numerically and theoretically in simple setups. For example, [Neyshabur et al. \(2015\)](#) finds that the DNN optimization algorithm introduces a bias that favors simpler models, which contributes to the phenomenon of implicit regularization. Along similar lines, [Soudry et al. \(2018\)](#) and [Ji and Telgarsky \(2019\)](#) analyze the implicit bias of gradient descent on linearly separable and non-separable data, respectively, as well as its effects on model generalization. In particular, [Arora et al. \(2019\)](#) explores the connection between the optimization landscape and generalization performance in a two-layer network setting.

## References

- Arora S, Du S, Hu W, Li Z, Wang R (2019) Fine-grained analysis of optimization and generalization for overparameterized two-layer neural networks. *International Conference on Machine Learning*, 322–332.
- Bartlett PL, Long PM, Lugosi G, Tsigler A (2020) Benign overfitting in linear regression. *Proc. Natl. Acad. Sci. U. S. A.*, 117 (48), 30063–30070.
- Bartlett PL, Montanari A, Rakhlin A (2021) Deep learning: a statistical viewpoint. *Acta Numer.*, 30, 87–201.
- Belkin M (2021) Fit without fear: remarkable mathematical phenomena of deep learning through the prism of interpolation. *Acta Numer.*, 30, 203–248.

- Besbes O, Mouchtaki O (2023) How big should your data really be? Data-driven newsvendor: Learning one sample at a time. *Management Sci.*, 69 (10), 5848–5865.
- Elmachtoub AN, Lam H, Zhang H, Zhao Y (2023) Estimate-then-optimize versus integrated-estimation-optimization: A stochastic dominance perspective. arXiv:2304.06833
- Györfi L, Kohler M, Krzyzak A, Walk H (2002) *A Distribution-Free Theory of Nonparametric Regression*, Volume 1 (Springer).
- Hastie T, Montanari A, Rosset S, Tibshirani RJ (2022) Surprises in high-dimensional ridgeless least squares interpolation. *Ann. Statist.*, 50 (2), 949–986.
- Ji Z, Telgarsky M (2019) The implicit bias of gradient descent on nonseparable data. *Conference on learning theory*, 1772–1798.
- Lu Y, Chen H, Lu J, Ying L, Blanchet J (2021) Machine learning for elliptic PDEs: Fast rate generalization bound, neural scaling law and minimax optimality. arXiv:2110.06897
- Neyshabur B, Tomioka R, Srebro N (2015) In search of the real inductive bias: On the role of implicit regularization in deep learning. *International Conference on Learning Representations (ICLR) Workshop, 2015*
- Soudry D, Hoffer E, Nacson MS, Gunasekar S, Srebro N (2018) The implicit bias of gradient descent on separable data. *J. Mach. Learn. Res.*, 19 (70), 1–57.
- Steinwart I, Christmann A (2011) Estimating conditional quantiles with the help of the pinball loss. *Bernoulli*, 17 (1), 211–225.
- Theisen RC (2023) *Beyond Worst-Case Generalization in Modern Machine Learning*. University of California, Berkeley
- Tsigler A, Bartlett PL (2023) Benign overfitting in ridge regression. *J. Mach. Learn. Res.*, 24 (123), 1–76.